UNIVERSITY OF CAPE TOWN

IYUNIVESITHI YASEKAPA • UNIVERSITEIT VAN KAAPSTAD

Department of Chemical Engineering

Investigation of the Interactions Between Sea Ice Algae from the Marginal Ice Zone of Antarctica and Artificial Sea Ice.

DISSERTATION SUBMITTED TO THE UNIVERSITY OF CAPE TOWN IN FULFILMENT OF THE REQUIREMENTS FOR THE DEGREE OF MASTER OF SCIENCES IN CHEMICAL ENGINEERING

Prepared by: James Van Niekerk

Supervised by: Dr Tokoloho Rampai and Dr Emma Rocke

The copyright of this thesis vests in the author. No quotation from it or information derived from it is to be published without full acknowledgement of the source. The thesis is to be used for private study or non-commercial research purposes only.

Published by the University of Cape Town (UCT) in terms of the non-exclusive license granted to UCT by the author.

Plagiarism

I know that plagiarism is wrong. Plagiarism is to use another's work and pretend that it is my own. I have used the Harvard referencing system for citation and referencing. In this report, all contributions to, and quotation from, the work(s) of other people have been cited and referenced. This report is my own work, and it is in my own words (except where others are quoted). I have not allowed and will not allow anyone to copy my work with the intention of passing it off as their own work.

In addition, AI tools (such as Grammarly and ChatGPT) was used for refining and correcting of sentence structures and English. All outputs have been reviewed and edited appropriately. No AI was used in the generation of new content, all displayed work is my own work.

This thesis/dissertation has been submitted to the Turnitin module (or equivalent similarity and originality checking software) and I confirm that my supervisor has seen my report and any concerns revealed by such have been resolved with my supervisor.

Signed by candidate

James van Niekerk

January 2025

Acknowledgements

I would like to express my gratitude to those who have supported me throughout my academic journey.

First and foremost, I would like to thank my parents, Anne and Gerrie, for their unwavering support. To my brother, Tom, for your constant entertainment and support thought my masters.

A special thank you to my supervisors, Dr. Tokoloho Rampai and Dr. Emma Rocke, for their expert guidance, mentorship, and invaluable support throughout my project. A warm thank you to my colleagues and friends, Hayley and Safiyyah, whose support in work and life was great, and to my study friends Jen and Kyra, for sharing this journey and the study sessions that kept me going

I would also like to acknowledge Clint from the mechanical workshop for his assistance with my quirky and unorthodox design needs. To Egshaan and Curwin, thank you for your help in the lab and for making the building a fun place to work. Your presence made the tough times more bearable. To Klaus, thank you for your mentorship, assistance with my work and our always interesting conversations.

I am also grateful to the University of Cape Town for awarding me the merit award scholarship, and to the National Research Foundation for their generous scholarship support. Lastly, my sincere thanks to the Marine and Antarctic Research for Innovation and Sustainability for letting me be part of the team and for providing a platform to showcase my work.

This thesis would not have been possible without the support of each of you. Thank you.

Abstract

Sea ice is multi-phase system that plays a major role in the Earth's climate system. Sea ice algae act as primary producers of organic carbon, forming the building blocks of the aquatic food web. In addition to the ecological function, sea ice algae aid in the earth's carbon cycle playing a role in mitigating global warming. Understanding the dynamics of sea ice algae under changing environmental conditions is important for developing predictive models for marine ecosystems and climate systems. Sea ice and algae are under researched in the Marginal Ice Zone (MIZ) of the Southern Ocean. The logistical difficulties of *in situ* research have favoured the shift towards *ex situ* research in land-based laboratories, typically performing artificial experiments in sub-zero polar laboratories. However, access to sub-zero laboratories geared for polar experiments facilitating artificial sea ice experiments is limited to MARiS (Marine and Antarctic Research for Innovation and Sustainability) at the University of Cape Town.

A cold finger apparatus was designed to grow artificial sea ice, at -5°C -10°C and -15°C, in 1-litre aquaria containing sea ice algae. Key design considerations include materials of construction, size and shape of the cold finger. A thermodynamic model of ice growth using the cold finger was developed to mitigate wall effects of the aquaria on growth dynamics. In contrast to top-down growth of natural sea ice, ice growth induced by the cold finger occurred radially, with ice crystals orientated horizontally and brine inclusions slanted downward. The development of a methodology followed an iterative process, involving adjustments to sampling protocols, ice sectioning, and analytical methods. Sea ice algae were subjected to acclimatisation (10-day growth period) and cold finger procedure (ice growth).

The results of acclimatisation supported that light and ocean temperatures significantly influenced the growth of sea ice algae. In the uptake experiments, the sea ice algae were subjected to different ice inducing temperatures under the same light and ocean temperatures in the acclimatisation period. The results indicated that atmospheric temperature, irradiance and ocean warming had no significant effects on sea ice algae uptake. The distribution of algae uptake into the ice was dictated by algae settling (gravity) and natural convention in brine inclusions.

Contents

Plagiarism ..... *i*

Acknowledgements ..... *ii*

Abstract ..... *iii*

Contents ..... *iv*

Figures: ..... *vii*

Tables: ..... *xiii*

Glossary ..... *xxi*

Abbreviations ..... *xxi*

1. Introduction *1*

1.1. Background Information **1**

1.2. Problem Statement **2**

1.3. Scope and Limitations **2**

2. Literature Review *3*

2.1. Considerations of Sea Ice Algae **4**

2.1.1. Sea Ice Algae Communities 4

2.1.2. Factors Affecting the Growth of Sea-ice Algae 5

2.2. Sea Ice Dynamics, Texture and Structure **8**

2.2.1. Sea Ice Dynamics 8

2.2.2. Sea Ice Texture and Structure 9

2.3. Algae Incorporation into Sea Ice **12**

2.4. Extracellular Polymeric Substances (EPS) **13**

2.4.1. Composition and Concentration Profiles 13

2.4.2. EPS Impact on Ice Structures and Textures 16

2.5. Artificial Sea Ice Experiments **19**

2.6. Rationale of Study **23**

3. Aims, Objectives and Key Questions *25*

4. Design and Optimisation of Cold Finger 26

4.1. Design Considerations 27

4.1.1. Materials of Construction 28

4.1.2. Shape and Size 31

4.2. Growth Dynamics 33

4.2.1. Development of a Thermodynamic Model 33

4.2.2. Thermodynamic Model Application: 34

4.3. Comparing Natural Sea Ice and Cold Finger Growth Dynamics 35

4.3.1. Experimental Methodology for Growth Dynamics Evaluation 35

4.3.2. Results of Growth Dynamics 37

4.3.3. Discussion Cold finger Growth Dynamics 41

5. Design and Optimisation of Cold Finger Experiment Methodology 43

5.1. Experimental Procedure 45

***5.2.* Analytical Methods 49**

5.2.1. Flow Cytometry 50

5.2.2. Microscopy 53

6. Impacts of Changing Environmental Conditions on Sea Ice Algae 55

6.1. Comparison of Flow Cytometry and Microscopy 55

6.2. Comparing The Effect of Different Environmental Conditions on Sea Ice Algae Growth . 58

6.2.1. Acclimatisation 59

6.2.2. Investigation of Algae Uptake Dynamics into Sea Ice Using the Cold Finger 64

6.3. Summary of Key Findings 75

7. Overall Discussion 76

8. Conclusions and Recommendations 78

References 81

Appendices: ..... A

A. Cold Finger Engineering Drawings ..... A

B. Thermodynamic Model and Ice Growth Dynamics ..... D

B.1. Thermodynamic Model Development ..... D

B.2. Thermodynamic Model Code ..... G

B.3. Experimental Output of Thermodynamic Model Performance ..... H

C. Preliminary Output of the Optimisation of the Experimental Methodology L

D. Experimental Output of Fully Optimised Experiment ..... O

D.1. Light Data ..... O

D.2. Growth Dynamics ..... Q

D.3. Physical Properties ..... Q

D.4. Graphs Displaying Normalised Cell Concentrations ..... T

E. Parametric Statistical Testing Output ..... HH

F. Ethics Clearance VV

Figures:

Figure 2-1: Comparison of PAR (400–700 nm) at three locations in Greenland over 12 months: (A) Villum Research Station (81ℕ), (B) Zackenberg (74ℕ), and (C) Kobbefjord (64ℕ). (D) shows how light transmittance of different wavelengths with and without snow cover. (E) shows the attenuation of PAR through ice as percentage of surface irradiance (Lund-Hansen et al., 2024). 7
Figure 2-2: Schematic representation of ice growth process for Antarctic and Arctic conditions adapted from European Space Agency (2016). 9
Figure 2-3: Structure of ice Ih, illustrating the highly ordered hydrogen-bonding network between water molecules that results in a unique hexagonal crystal lattice (Weeks & Ackley, 1982)..... 10
Figure 2-4: Cross polarised images of different sea ice texture (A) granular, (B) columnar, (C) transitional (Johnson et al., 2023). 11
Figure 2-5: Schematic summarising ice textures (red) granular, (purple) transitional and (green) columnar. The schematic includes growth conditions, typical winter temperatures and salinity profiles for first-year sea ice (Petrich & Eicken, 2017). 11
Figure 2-6: Schematic distribution of ice algae in pack sea ice. Adapted from (Arrigo & Thomas, 2004; Tedesco & Vichi, 2014) 13
Figure 2-7: Vertical distributions across different sampling days of A) carbohydrate, B) proteins, C) lipids concentration and D) their contribution in sea ice (Kim et al., 2023). 14
Figure 2-8: Monosaccharide compositions of bulk ice in A) the North-western Weddell Sea and B) Western Weddell Sea. Adapted from Underwood et al. (2010). 15
Figure 2-9: Microscope images of artificial ice grown at -10 °C with EPS (right) and without EPS (left) with A and B show ice texture at low magnification under polarised light, C and D with contrast staining, and E and F showing pore structure at high magnification (Krembs, Eicken & Deming, 2011). 18
Figure 2-10: Stratigraphy diagrams for ice grown from solutions of starting artificial ocean salinity of 30 psu at -10°C with and without EPS (Matlakala, 2022). 18
Figure 2-11: Micro-CT scan visuals for the top part of ice grown at -10°C from solutions of starting artificial ocean salinity of 30 psu (A) without EPS, (B) with EPS (Matlakala, 2022). .. 19

Figure 2-12: Schematic diagram of a freezing tank experimental set up with includes axillary equipment (Weeks, 1962). 20
Figure 2-13: (A) Cold plate internals and (B) cold plate set up used for direct cooling of saline solution (Schulson, Renshaw & Snyder, 2012). 21
Figure 2-14: Schematic diagram of a cold finger (left) and experimental set up with water bath, magnetic stirrer and chiller (right) (Kuiper et al., 2003). 22
Figure 2-15: Photographs of ice formed using cold finger apparatus with (A) photographed from the top, with axis perpendicular to underlying surface; (B) the ice photographed from the side, with axis parallel to underlying surface and (C) the ice photographed from the side after a 90°C rotation. Bars indicate 1.25cm. Adapted from (Ewert & Deming, 2011). 23
Figure 4-1: Schematic diagram and annotated image of environmental chamber with four 1L aquaria, illustrating insulation, 1-litre aquaria, light source and light measurement devices. 26
Figure 4-2: Schematic diagram of cold finger in 1-litre aquaria with basic dimensions. 32
Figure 4-3: Plot of radial ice growth with time at a cold finger operating temperature of -5°C, -10°C and -15°C. 34
Figure 4-4: Schematic of ice sectioning for ice growth dynamic analysis, which includes samples for cross polarisation, Micro-CT scanning, salinity measurements and back up samples. 36
Figure 4-5: Cross polarised images of ice grown from the cold finger at differing EPS concentrations A) 0 mg/l, B) 1 mg/l, C) 10 mg/l, D) 100 mg/l and E) 1000 mg/l. 38
Figure 4-6: Stratigraphy diagram of ice grown from the cold finger at varying EPS concentrations (0, 1, 10, 1000 mg/l). 39
Figure 4-7: Grey scale image slice from CT scan at different EPS concentration of 0 mg/l (left) and 1000 mg/l (right). 40
Figure 4-8: Summary of air and brine inclusion characteristics at differing EPS concentrations (0, 1, 10, 1000 mg/l) with (Left) illustrating ice porosity and (right) illustrating inclusion number density. The figure indicates EPS has no effect on inclusion characteristics. 41
Figure 5-1: Microscope photograph illustrating size ranges of Cocconeis sp. and Pseudo-Nitzchia sp. 44
Figure 5-2: Flow chart of the basic experimental skeleton of the cold finger experiments. 45
Figure 5-3: Schematic diagram of (A) initial and (B) optimised ice sectioning for cold finger experiments. 48

Figure 5-4: Flow cytometry plot for a sample during acclimatisation comparing scatter of data on yellow green wavelength and forward scatter. 52
Figure 5-5: Flow cytometry plot of sample from ice comparing scatter of data on yellow green wavelength and forward scatter. 52
Figure 5-6: Microscopy images illustrating cell density A) before dilution and B) after dilution. 54
Figure 6-6-1: Normalised cell concentrations in the -10°C tank comparing flow cytometry and microscopy during acclimatisation with no light and ocean temperature of -1.8°C. 57
Figure 6-2: Normalised cell concentrations for atmospheric temperature of -10°C comparing flow cytometry and microscopy uptake dynamics with no light and ocean temperature of -1.8°C. 57
Figure 6-3: Averaged normalised cell concentrations comparing different light conditions and ocean temperatures during acclimatisation for flow cytometry. 59
Figure 6-4: Normalised cell concentrations comparing different light conditions and ocean temperatures during acclimatisation for microscopy. 60
Figure 6-5: Normalised cell concentrations comparing atmospheric temperatures for different light conditions and ocean temperatures during uptake dynamics for flow cytometry. 66
Figure 6-6: Normalised cell concentrations comparing atmospheric temperatures with no light conditions and ocean temperature of -1.8°C during uptake dynamics for microscopy. 66
Figure 6-7: Averaged normalised cell concentrations comparing different light conditions during uptake dynamics for flow cytometry. 69
Figure 6-8: Averaged normalised cell concentrations comparing different light conditions during uptake dynamics for microscopy. 69
Figure 6-9: Averaged normalised cell concentrations comparing different ocean temperatures during uptake dynamics for flow cytometry. 71
Figure 6-10: Averaged normalised cell concentrations comparing different ocean temperatures during uptake dynamics for microscopy. 71
Figure 6-11: Averaged normalised cell concentrations comparing different sampling positions during uptake dynamics for flow cytometry. 73
Figure 6-12: Averaged normalised cell concentrations comparing different sampling positions during uptake dynamics for microscopy. 73

Figure A-1: Cold finger internal and external drawings with dimensions. ..... A
Figure A-2: Cold finger scaffolding design with dimensions part 2. ..... B
Figure A-3: Cold finger scaffolding design with dimensions part 2. C
Figure B-1: Radial conduction through a semi-hollow cylinder adapted from Bejan & Kraus (2003). ..... D
Figure C-1: Preliminary results for the initial experiment. L
Figure C-2: Preliminary flow cytometry results for the first optimisation experiment. ..... M
Figure C-3: Preliminary microscopy results for the first optimisation experiment. ..... N
Figure D-1: Daily averaged par sensor data for the experiment conducted with no light and an ocean temperature of -1.8C. ..... O
Figure D-2: Daily averaged par sensor data for the experiment conducted with light and an ocean temperature of -1.8°C. ..... P
Figure D-3: Daily averaged par sensor data for the experiment conducted with light and an ocean temperature of 0°C. ..... P
Figure D-4: Normalised cell concentrations in the -5°C tank comparing flow cytometry and microscopy during acclimatisation with no light and ocean temperature of -1.8°C. ..... T
Figure D-5: Normalised cell concentrations for atmospheric temperature of -5°C comparing flow cytometry and microscopy uptake dynamics with no light and ocean temperature of -1.8°C. ..... T
Figure D-6: Normalised cell concentrations in the -15°C tank comparing flow cytometry and microscopy during acclimatisation with no light and ocean temperature of -1.8°C. ..... U
Figure D-7: Normalised cell concentrations for atmospheric temperature of -15°C comparing flow cytometry and microscopy uptake dynamics with no light and ocean temperature of -1.8°C. ..... U
Figure D-8: Normalised cell concentrations in the -5°C tank comparing flow cytometry and microscopy during acclimatisation with light and ocean temperature of -1.8°C. V
Figure D-9: Normalised cell concentrations for atmospheric temperature of -5°C comparing flow cytometry and microscopy uptake dynamics with light and ocean temperature of -1.8°C. V
Figure D-10: Normalised cell concentrations in the -10°C tank comparing flow cytometry and microscopy during acclimatisation with light and ocean temperature of -1.8°C. ..... W

Figure D-11: Normalised cell concentrations for atmospheric temperature of -10°C comparing flow cytometry and microscopy uptake dynamics with light and ocean temperature of -1.8°C. ..... W
Figure D-12: Normalised cell concentrations in the -15°C tank comparing flow cytometry and microscopy during acclimatisation with light and ocean temperature of -1.8°C. X
Figure D-13: Normalised cell concentrations for atmospheric temperature of -15°C comparing flow cytometry and microscopy uptake dynamics with light and ocean temperature of -1.8°C. X
Figure D-14: Normalised cell concentrations in the -5°C tank comparing flow cytometry and microscopy during acclimatisation with light and ocean temperature of 0°C..... Y
Figure D-15: Normalised cell concentrations for atmospheric temperature of -5°C comparing flow cytometry and microscopy uptake dynamics with light and ocean temperature of 0°C.. Y
Figure D-16: Normalised cell concentrations in the -10°C tank comparing flow cytometry and microscopy during acclimatisation with light and ocean temperature of 0°C..... Z
Figure D-17: Normalised cell concentrations for atmospheric temperature of -10°C comparing flow cytometry and microscopy uptake dynamics with light and ocean temperature of 0°C.. Z
Figure D-18: Normalised cell concentrations in the -15°C tank comparing flow cytometry and microscopy during acclimatisation with light and ocean temperature of 0°C..... AA
Figure D-19: Normalised cell concentrations for atmospheric temperature of -15°C comparing flow cytometry and microscopy uptake dynamics with light and ocean temperature of 0°C. ..... AA
Figure D-20: Normalised cell concentrations comparing atmospheric temperatures with no light conditions and ocean temperature of -1.8°C during the cold finger procedure for microscopy (including underlying seawater solution). ..... BB
Figure D-21: Normalised cell concentrations comparing atmospheric temperatures with light conditions and ocean temperature of -1.8°C during the cold finger procedure for microscopy (including underlying seawater solution). CC
Figure D-22: Normalised cell concentrations comparing atmospheric temperatures with light conditions and ocean temperature of 0°C during the cold finger procedure for microscopy (including underlying seawater solution). ..... DD

Figure D-23: Normalised cell concentrations comparing atmospheric temperatures for different light conditions and ocean temperatures during the cold finger procedure for flow cytometry (including underlying brine solution). ..... EE
Figure D-24: Averaged normalised cell concentrations comparing different light conditions during the cold finger procedure for flow cytometry (including underlying brine solution).. FF
Figure D-25: Averaged normalised cell concentrations comparing different light conditions during the cold finger procedure for microscopy (including underlying brine solution). ..... FF
Figure D-26: Averaged normalised cell concentrations comparing different ocean temperatures during the cold finger procedure for flow cytometry (including underlying brine solution)..... GG
Figure D-27: Averaged normalised cell concentrations comparing different ocean temperatures during the cold finger procedure for microscopy (including underlying brine solution)..... GG

Tables:

Table 2-1: Vertical distribution of EPS in the bottom 10 cm of natural sea ice and artificial sea ice using Melosira EPS (Krembs, Eicken & Deming, 2011). 16
Table 4-1: Key Design considerations for material of construction of the cold finger in saline and algal environment. 30
Table 4-2: Overall ice growth and performance of thermodynamic model. 35
Table 4-3: Summary of key finding on normalised growth dynamics at differing EPS concentrations. 37
Table 5-1: Ice growth dimensions and times for optimisation experiments. 47
Table 6-1: Summary of p-values from both F-tests and t-test comparing flow cytometry and microscopy normalised cell concentrations. 56
Table 6-2: Summary of p-values from single-factor ANOVA tests comparing normalised cell concentrations across sampling days for different light and ocean temperatures during acclimatisation. 60
Table 6-3: Summary of p-values from single-factor ANOVA tests comparing normalised cell concentrations for different light conditions during acclimatisation. 61
Table 6-4: Summary of p-values from single-factor ANOVA tests comparing normalised cell concentrations for different ocean temperatures during acclimatisation. 63
Table 6-5: Summary of p-values from single-factor ANOVA tests comparing normalised cell concentrations for differing atmospheric temperature with various light and ocean temperatures. 64
Table 6-6: Summary showing the relationship between atmospheric temperature and average normalised percentage uptake with flow cytometry data 65
Table 6-7: Summary showing the relationship between atmospheric temperature and average normalised percentage uptake with microscopy data. 65
Table 6-8: Summary of p-values from single-factor ANOVA tests comparing normalised cell concentrations for differing light conditions on uptake dynamics. 68
Table 6-9: Summary of p-values from single-factor ANOVA tests comparing normalised cell concentrations for ocean temperatures on uptake dynamics. 70

Table 6-10: Summary of p-values from single-factor ANOVA tests comparing normalised cell concentrations for different sampling positions within the ice. 72
Table 6-11: A summary of key findings from the results of varying environmental conditions on sea ice algae growth and uptake dynamics. 75
Table B-1: Theoretical and experimental ice growth measurements at different experimental durations. .....H
Table B-2: Fraction of each ice texture and corresponding crystal size with varying EPS concentrations. .....H
Table B-3: Comparison of EPS concentrations, salinity (initial, underlying, and ice), and ice growth parameters (diameter and rate) across samples..... I
Table B-4: Cross polarised image of all sea ice sample replicates at different EPS concentrations. .....J
Table B-5: Visual output from Micro-CT scanning analysis at varying EPS concentrations. ..... K
Table D-1: Summary of growth times for each experiment. ..... Q
Table D-2: Summary of ice diameters for each experiment. ..... Q
Table D-3: Summary of measured ice volumes for the experiment conducted with no light and an ocean temperature of -1.8°C. ..... Q
Table D-4: Summary of measured ice volumes for the experiment conducted with light and an ocean temperature of -1.8°C. ..... R
Table D-5: Summary of measured ice volumes for the experiment conducted with light and an ocean temperature of 0°C. ..... R
Table D-6: Summary of measured ice salinities for the experiment conducted with no light and an ocean temperature of -1.8°C. ..... R
Table D-7: Summary of measured ice salinities for the experiment conducted with light and an ocean temperature of -1.8°C. ..... S
Table D-8: Summary of measured ice salinities for the experiment conducted with light and an ocean temperature of 0°C. ..... S
Table E-1: Summary of F-test comparing variances between microscopy and flow cytometry cell concentrations during acclimatisation. ..... HH
Table E-2: Summary of t-test comparing variances between microscopy and flow cytometry cell concentrations during acclimatisation. ..... HH

Table E-3: Summary of F-test comparing variances between microscopy and flow cytometry cell concentrations during the cold finger procedure..... HH
Table E-4: Summary of t-test comparing variances between microscopy and flow cytometry cell concentrations during the cold finger procedure..... II
Table E-5: Summary of statistics used in single factor ANOVA comparing flow cytometry cell concentrations on different sampling days with no light and ocean temperature of -1.8°C.... II
Table E-6: Summary of single factor ANOVA results comparing flow cytometry cell concentrations on different sampling days with no light and ocean temperature of -1.8°C.... II
Table E-7: Summary of statistics used in single factor ANOVA comparing flow cytometry cell concentrations on different sampling days with light and ocean temperature of -1.8°C..... II
Table E-8: Summary of single factor ANOVA results comparing flow cytometry cell concentrations on different sampling days with light and ocean temperature of -1.8°C.....JJ
Table E-9:Summary of statistics used in single factor ANOVA comparing flow cytometry cell concentrations on different sampling days with light and ocean temperature of 0°C. .....JJ
Table E-10: Summary of single factor ANOVA results comparing flow cytometry cell concentrations on different sampling days with light and ocean temperature of 0°C .....JJ
Table E-11: Summary of statistics used in single factor ANOVA comparing Cocconeis microscopy cell concentrations on different sampling days with no light and ocean temperature of -1.8°C. .....JJ
Table E-12: Summary of single factor ANOVA results comparing Cocconeis microscopy cell concentrations on different sampling days with no light and ocean temperature of -1.8°C....JJ
Table E-13:Summary of statistics used in single factor ANOVA comparing Cocconeis microscopy cell concentrations on different sampling days with light and ocean temperature of -1.8°C..... KK
Table E-14: Summary of single factor ANOVA results comparing Cocconeis microscopy cell concentrations on different sampling days with light and ocean temperature of -1.8°C..... KK
Table E-15: Summary of statistics used in single factor ANOVA comparing Cocconeis microscopy cell concentrations on different sampling days with light and ocean temperature of -0°C..... KK
Table E-16: Summary of single factor ANOVA results comparing Cocconeis microscopy cell concentrations on different sampling days with light and ocean temperature of 0°C. ..... KK

Table E-17: Summary of statistics used in single factor ANOVA comparing Pseudo-Nitzchia microscopy cell concentrations on different sampling days with no light and ocean temperature of -1.8°C. ..... KK
Table E-18: Summary of single factor ANOVA results comparing Pseudo-Nitzchia microscopy cell concentrations on different sampling days with no light and ocean temperature of -1.8°C. ..... KK
Table E-19: Summary of statistics used in single factor ANOVA comparing Pseudo-Nitzchia microscopy cell concentrations on different sampling days with light and ocean temperature of -1.8°C. LL
Table E-20: Summary of single factor ANOVA results comparing Pseudo-Nitzchia microscopy cell concentrations on different sampling days with light and ocean temperature of -1.8°C. LL
Table E-21: Summary of statistics used in single factor ANOVA comparing Pseudo-Nitzchia microscopy cell concentrations on different sampling days with light and ocean temperature of 0°C. LL
Table E-22: Summary of single factor ANOVA results comparing Pseudo-Nitzchia microscopy cell concentrations on different sampling days with light and ocean temperature of 0°C..... LL
Table E-23: Summary of statistics used in single factor ANOVA comparing flow cytometry cell concentrations at different light conditions during acclimatisation. LL
Table E-24: Summary of single factor ANOVA results comparing flow cytometry cell concentrations at different light conditions during acclimatisation. LL
Table E-25: Summary of statistics used in single factor ANOVA comparing Cocconeis microscopy cell concentrations at different light conditions during acclimatisation..... MM
Table E-26: Summary of single factor ANOVA results comparing Cocconeis microscopy cell concentrations at different light conditions during acclimatisation. ..... MM
Table E-27: Summary of statistics used in single factor ANOVA comparing Pseudo-Nitzchia microscopy cell concentrations at different light conditions during acclimatisation..... MM
Table E-28: Summary of single factor ANOVA results comparing Pseudo-Nitzchia microscopy cell concentrations at different light conditions during acclimatisation. ..... MM
Table E-29: Summary of statistics used in single factor ANOVA comparing flow cytometry cell concentrations at different ocean temperatures during acclimatisation. ..... MM

Table E-30: Summary of single factor ANOVA results comparing flow cytometry cell concentrations at different ocean temperatures during acclimatisation. ..... MM
Table E-31: Summary of statistics used in single factor ANOVA comparing Cocconeis microscopy cell concentrations at different ocean temperatures during acclimatisation. .... NN
Table E-32: Summary of single factor ANOVA results comparing Cocconeis microscopy cell concentrations at different ocean temperatures during acclimatisation. ..... NN
Table E-33: Summary of statistics used in single factor ANOVA comparing Pseudo-Nitzchia microscopy cell concentrations at different ocean temperatures during acclimatisation. .... NN
Table E-34: Summary of single factor ANOVA results comparing Pseudo-Nitzchia microscopy cell concentrations at different ocean temperatures during acclimatisation. ..... NN
Table E-35: Summary of statistics used in single factor ANOVA comparing flow cytometry cell concentrations at different atmospheric temperatures with no light and ocean temperature of -1.8°C. ..... NN
Table E-36: Summary of single factor ANOVA results comparing flow cytometry cell concentrations at different atmospheric temperatures with no light and ocean temperature of -1.8°C ..... NN
Table E-37: Summary of statistics used in single factor ANOVA comparing flow cytometry cell concentrations at different atmospheric temperatures with light and ocean temperature of -1.8°C. ..... OO
Table E-38: Summary of single factor ANOVA results comparing flow cytometry cell concentrations at different atmospheric temperatures with light and ocean temperature of -1.8°C ..... OO
Table E-39: Summary of statistics used in single factor ANOVA comparing flow cytometry cell concentrations at different atmospheric temperatures with light and ocean temperature of 0°C. ..... OO
Table E-40: Summary of single factor ANOVA results comparing flow cytometry cell concentrations at different atmospheric temperatures with light and ocean temperature of 0°C. ..... OO
Table E-41: Summary of statistics used in single factor ANOVA comparing Cocconeis microscopy cell concentrations at different atmospheric temperatures with no light and ocean temperature of -1.8°C. ..... OO

Table E-42: Summary of single factor ANOVA results comparing Cocconeis microscopy cell concentrations at different atmospheric temperatures with no light and ocean temperature of -1.8°C..... OO
Table E-43: Summary of statistics used in single factor ANOVA comparing Cocconeis microscopy cell concentrations at different atmospheric temperatures with light and ocean temperature of -1.8°C. ..... PP
Table E-44: Summary of single factor ANOVA results comparing Cocconeis microscopy cell concentrations at different atmospheric temperatures with light and ocean temperature of -1.8°C ..... PP
Table E-45: Summary of statistics used in single factor ANOVA comparing Cocconeis microscopy cell concentrations at different atmospheric temperatures with light and ocean temperature of 0°C..... PP
Table E-46: Summary of single factor ANOVA results comparing Cocconeis microscopy cell concentrations at different atmospheric temperatures with light and ocean temperature of 0°C. ..... PP
Table E-47: Summary of statistics used in single factor ANOVA comparing Pseudo-Nitzchia microscopy cell concentrations at different atmospheric temperatures with no light and ocean temperature of -1.8°C. ..... PP
Table E-48: Summary of single factor ANOVA results comparing Pseudo-Nitzchia microscopy cell concentrations at different atmospheric temperatures with no light and ocean temperature of -1.8°C ..... QQ
Table E-49: Summary of statistics used in single factor ANOVA comparing Pseudo-Nitzchia microscopy cell concentrations at different atmospheric temperatures with light and ocean temperature of -1.8°C. ..... QQ
Table E-50: Summary of single factor ANOVA results comparing Pseudo-Nitzchia microscopy cell concentrations at different atmospheric temperatures with light and ocean temperature of -1.8°C..... QQ
Table E-51: Summary of statistics used in single factor ANOVA comparing Pseudo-Nitzchia microscopy cell concentrations at different atmospheric temperatures with light and ocean temperature of 0°C..... QQ

Table E-52: Summary of single factor ANOVA results comparing Pseudo-Nitzchia microscopy cell concentrations at different atmospheric temperatures with light and ocean temperature of 0°C. ..... QQ
Table E-53: Summary of statistics used in single factor ANOVA comparing flow cytometry cell concentrations at different light conditions during the cold finger procedure. ..... QQ
Table E-54: Summary of single factor ANOVA results comparing flow cytometry cell concentrations at different light conditions during the cold finger procedure. ..... RR
Table E-55: Summary of statistics used in single factor ANOVA comparing Cocconeis microscopy cell concentrations at different light conditions during the cold finger procedure. ..... RR
Table E-56: Summary of single factor ANOVA results comparing Cocconeis microscopy cell concentrations at different light conditions during the cold finger procedure. ..... RR
Table E-57: Summary of statistics used in single factor ANOVA comparing Pseudo-Nitzchia microscopy cell concentrations at different light conditions during the cold finger procedure. ..... RR
Table E-58: Summary of single factor ANOVA results comparing Pseudo-Nitzchia microscopy cell concentrations at different light conditions during the cold finger procedure. ..... RR
Table E-59: Summary of statistics used in single factor ANOVA comparing flow cytometry cell concentrations at different ocean temperatures during the cold finger procedure..... RR
Table E-60: Summary of single factor ANOVA results comparing flow cytometry cell concentrations at different ocean temperatures during the cold finger procedure..... SS
Table E-61: Summary of single factor ANOVA results comparing Cocconeis microscopy cell concentrations at different ocean temperatures during the cold finger procedure..... SS
Table E-62: Summary of statistics used in single factor ANOVA comparing Pseudo-Nitzchia microscopy cell concentrations at different ocean temperatures during the cold finger procedure. ..... SS
Table E-63: Summary of single factor ANOVA results comparing Pseudo-Nitzchia microscopy cell concentrations at different ocean temperatures during the cold finger procedure. ..... SS
Table E-64: Summary of statistics used in single factor ANOVA comparing flow cytometry cell concentrations at different horizontal positions during the cold finger procedure..... SS
Table E-65: Summary of single factor ANOVA results comparing flow cytometry cell concentrations at different horizontal positions during the cold finger procedure..... SS

Table E-66: Summary of statistics used in single factor ANOVA comparing Cocconeis microscopy cell concentrations at different horizontal positions during the cold finger procedure. ..... TT
Table E-67: Summary of single factor ANOVA results comparing Cocconeis microscopy cell concentrations at different horizontal positions during the cold finger procedure..... TT
Table E-68: Summary of statistics used in single factor ANOVA comparing Pseudo-Nitzchia microscopy cell concentrations at different horizontal positions during the cold finger procedure. ..... TT
Table E-69: Summary of single factor ANOVA results comparing Pseudo-Nitzchia microscopy cell concentrations at different horizontal positions during the cold finger procedure. ..... TT
Table E-70: Summary of statistics used in single factor ANOVA comparing flow cytometry cell concentrations at different vertical positions during the cold finger procedure. ..... TT
Table E-71: Summary of single factor ANOVA results comparing flow cytometry cell concentrations at different vertical positions during the cold finger procedure. ..... TT
Table E-72: Summary of statistics used in single factor ANOVA comparing Cocconeis microscopy cell concentrations at different vertical positions during the cold finger procedure. ..... UU
Table E-73: Summary of single factor ANOVA results comparing Cocconeis microscopy cell concentrations at different vertical positions during the cold finger procedure. ..... UU
Table E-74: Summary of statistics used in single factor ANOVA comparing Pseudo-Nitzchia microscopy cell concentrations at different vertical positions during the cold finger procedure. ..... UU
Table E-75: Summary of single factor ANOVA results comparing Pseudo-Nitzchia microscopy cell concentrations at different vertical positions during the cold finger procedure..... UU

Glossary

Frazil Ice	Small needle like ice crystals
Pancake Ice	Disk-like ice floes
Grease Ice	Thin viscous layer of frazil ice crystal clumped together
Nilas Ice	Thin and elastic crust of ice
Conduction	Transfer of heat energy through solids
Convection	Transfer of heat energy through fluids
Brine Inclusions	Pockets and/or channels in sea ice containing brine
Sympagic	Ice associated
Benthic	Associated with the bottom of a body of water
Pelagic	Relating to open ocean
Sea Ice Algae	Microalgal species found in sea ice
Flagellates	Unicellular organism with one or more flagella
Dinoflagellates	Single-cell organism with two flagella
Diatoms	Single-celled algae with silica cell walls
Centric Diatoms	Diatoms with radial symmetry
Pennate Diatoms	Diatoms with bilateral symmetry
F2 Medium	Enriched sea water for growing diatoms
Cold Finger	An apparatus used to induce a localised cold surface
In situ	In the original place
Ex situ	Away from original place

Abbreviations

MIZ	Marginal Ice Zone
EPS	Extracellular Polymeric Substances
EC	Environmental Chamber
CF	Cold Finger

1. Introduction

1.1. Background Information

Sea ice is a major component of the cryosphere and is extensively connected to key Earth systems, influencing the hydrosphere, biosphere and atmosphere. Sea ice plays a major role in maintaining the regional and global climate through several mechanisms. One such mechanism is sea ice's high albedo effect, which allows it to reflect a signification portion of solar radiation, with studies showing snow free ice reflecting up to 70% and up to 90% for snow covered ice for specific wavelengths (Brandt et al., 2005). Additionally, the insulative properties of sea ice help reduce heat exchange between the ocean and atmosphere. This is important, given that ocean water can store about 3,600 times more heat than air (Vihma, 2014). This makes the temperature increase per unit of heat added much smaller for the ocean compared to the atmosphere. Sea ice forms one of the largest biomes on the earth and is therefore integral to maintaining marine ecosystems (van Leeuwe et al., 2020). Sea ice supports life from a microscopic level to large marine animals. Sea ice algae, which typically inhabit the bottom layers of the ice, serving as the building blocks of this food web (Fenchel, 1988). Sea ice algae are pivotal for maintaining higher trophic levels and are often most concentrated in the ice relative to the ocean. In addition, algae act as a carbon sink, absorbing carbon equivalent to forests and other land plants (Lindsey & Scott, 2010).

Human consumption of fossil fuels has caused over 90% of excess heat produced by greenhouse gasses to be absorbed by the ocean (Abraham et al., 2013). This has led to an increase in average ocean temperature by 0.88°C from 1850 to 2020, with 0.6°C of ocean warming occurring in the last 40 years (Venegas, Acevedo & Treml, 2023). Forecasts suggest ocean temperatures will increase by 0.6-2°C by the end of the century (Venegas, Acevedo & Treml, 2023). Global warming is driven by rising greenhouse gas emissions and is the primary cause of the retreating sea ice extent and thickness in the Arctic and Antarctic (Maksym, 2025). In the Arctic, sea ice thickness has declined by around 65% between 1975 and 2012, and the sea ice extent is significantly decreasing, with reductions of -12.8% per decade ± 2.3% in summer and -2.7% per decade ± 0.5% in winter (Meredith et al., 2022). In contrast, limited

data on Antarctic sea ice thickness precludes the identification of long-term trends. Similarly, no significant long-term change in sea ice extent has been observed, primarily due to substantial regional and seasonal variability (Meredith et al., 2022). The accelerated warming effects is aggravated by sea ice positive feedback loop, where decreasing ice extent and thickness reduces the ice's albedo and insulative capabilities, further driving global warming. Additionally, the decreasing ice extent and thickness reduces the habitat available for sea ice algae, potentially significantly impacting the Earth's carbon cycling and marine food webs.

1.2. Problem Statement

Ideally research would be done *in situ* in the Marginal Ice Zone (MIZ) of Antarctica, however *in situ* research incurs high costs and logistical difficulties. The challenges include finite lab resources and limited time available for testing. This has favoured the shift towards *ex situ* research in artificial environments in land-based laboratories. *Ex situ* research requires transportation of the algae from the MIZ of Antarctica to land-based laboratories. However, transportation systems have struggled to preserve species community composition and maintain species concentration. This results in limited research being conducted on algae communities that mimic those found in the MIZ. Additionally, *ex situ* research favours the use of sub-zero laboratories to simulate natural ice growth using atmospheric cooling.

1.3. Scope and Limitations

The focus of this project was to develop a method to facilitate algae uptake into artificial sea ice. In the absence of pumps or shake tables to simulate Antarctic turbulence, sea ice was grown under Arctic-like conditions. Turbulence was excluded as an additional variable to allow isolation of key factors and maintain a simplified system. The study involved two algae strains, limiting understanding of full community interactions in response to environmental changes. Furthermore, the experiments focused on two light intensities and ocean temperatures, restricting the range of environmental parameters investigated

.

2. Literature Review

Algae refers to a diverse range of eukaryotic organisms with various morphologies. These photosynthesising microorganisms aid in the earth's carbon cycle by absorbing carbon from the atmosphere. Through photosynthesis, algae use sunlight and atmospheric/dissolved carbon to produce oxygen (Forgereau, Lange & Campbell, 2023). Additionally, algae transfer the carbon to higher trophic levels or retain the carbon when they die (Forgereau, Lange & Campbell, 2023). The dead algae sink to the ocean floor, sequestering the carbon deep into the ocean bed.

Sea ice algae primarily inhabit the sea ice, with their survival and development through the secretion of extracellular polymeric substances (EPS) (Costa, Raaijmakers & Kuramae, 2018). EPS is comprised of macromolecules that include polysaccharides, proteins, and DNA. These macromolecules help form a protective layer around the algal cell, which protects the cell from external interferences such as low temperature and high salinity environments (Costa, Raaijmakers & Kuramae, 2018). The production of EPS facilitates the locomotion and the adhesion of the algae cells to surfaces by altering the physiochemical characteristics of the surface and hence is fundamental for the development of a biofilm (Demir-Yilmaz et al., 2023). Additionally, EPS is important for the retention of nutrients and water within the cells, which is important for growth and survival of the cell, especially in winter conditions (Costa, Raaijmakers & Kuramae, 2018). Studies have supported that EPS influences the sea ice microstructure during ice formation (Krembs, Eicken & Deming, 2011; Matlakala, 2022). Understanding the impacts of EPS on artificial ice growth dynamics can improve the design of more accessible equipment and on-land algal research.

Sea ice algae communities' growth and survival is dictated by several key parameters, including temperature, salinity, irradiance, and nutrients. These key factors undergo significant changes during sea ice formation. Thus, to predict alterations to biological ecosystems, the effect of sea ice on algae is required input to successfully model the system.

2.1. Considerations of Sea Ice Algae

2.1.1. Sea Ice Algae Communities

Sea ice algae include various groups of marine species such diatoms, flagellates and dinoflagellates (Forgereau, Lange & Campbell, 2023). Diatoms, the dominant group of sea ice algae found in Antarctic sea ice, are primarily categorised as either benthic or pelagic (Majewska et al., 2013; Louw, Walker & Fawcett, 2022). Pelagic diatoms refer to free-floating and swimming species in the water column, while benthic diatoms refer to species that attach to substrates in water or at depth (Lu et al., 2022).

Sea ice studies in the Southern Ocean observed common taxa of diatom, including *Cylindrotheca spp*., *Fragilariopsis spp*., *Coscinodiscus spp., Dactyliosen spp., Nitzchia spp., Pseudo-nitzchia spp. Cocconies spp.* and *Chaetoceros spp.* (Beans et al., 2008; Majewska et al., 2013a; Louw, Walker & Fawcett, 2022). Diatoms are divided into two main subgroups: centric and pennate diatoms (Louw, Walker & Fawcett, 2022). Centric diatoms are characterised by radial symmetry, while pennate diatoms are characterised by bilateral symmetry (Morrow, n.d.) Although, pennate and centric diatoms are abundant in sea ice algae communities, observations in the Antarctic Marginal Ice Zone have shown that pennate diatoms are the most dominant subgroup (Louw, Walker & Fawcett, 2022).

Although certain species can inhabit multiple environments, not all diatoms present in sea ice are typically associated with sympagic environments. Some species that are not primarily associated with sympagic environments may still be incorporated into the ice matrix through various ecological processes (Cefarelli, Ferrario & Vernet, 2016). This is particularly evident for *Cocconeis spp.*, which are primarily benthic marine and freshwater diatoms (Kingston, 2003). Studies in the Ross Sea and Weddell Sea observe *Cocconeiss spp.,* with relatively low abundance found in sea ice (Romero, 2011; Majewska et al., 2013). Pesjak et al. (2023) found low abundance of *Cocconeis spp.* found in sea ice samples from the Southern Ocean in the Eastern Antarctic. Similarly to *Coccoenis spp.*, P*seudo-nitzchia spp.* are primarily pelagic species that have been associated with sympagic environments (Tetzner, Allen & Thomas,

2022). Many studies have reported observations of *Pseudo-nitzchia spp.* in the Southern Ocean around the Antarctic (Almandoz et al., 2008; Tetzner, Allen & Thomas, 2022; Lundholm et al., 2024).

2.1.2. Factors Affecting the Growth of Sea-ice Algae

Temperature, irradiance, nutrients and salinity are keys drivers that influences sea ice algae survival and development. Sea ice algae are adaptable species, acclimatising to different seasonal conditions and environments specifically in the Marginal Ice zone of the Antarctic.
Sea ice algae growth shows a linear relationship with temperature, with significant importance of temperature on metabolic pathways (Montagnes & Franklin, 2001; Anderson, 2019). Montagnes & Franklin (2001) observed increases with specific growth rates of sea ice algae species with increasing temperature. However, increasing specific growth rates declined once species-specific threshold temperatures were reached. Research has demonstrated that cell size decreases with increasing temperatures due to cell divisions occurring in the cell life cycle (Montagnes & Franklin, 2001). Campbell et al. (2019) suggests the most favourable temperature for sea ice algae carbon fixing occurs between 4°C and 14°C, while Montagnes & Franklin (2001) suggest decline in specific growth rates occurred between 12.0°C and 25.0°C. The environmental temperatures sea ice algae are exposed to are below these optimal temperatures for much of the year. Typical Antarctic Spring conditions are between -20°C and -2°C and winter temperatures can decrease to below -20°C (Stoecker et al., 1997).

Salinity, a key factor dictating algae development is primarily controlled by temperature. Temperature and salinity share an inverse relationship. As temperature rises, the brine volume increases, expanding the brine inclusions. This expansion reduces the salt concentration, thereby decreasing the local salinity within brine inclusions (Ackley & Sullivan, 1994). Similarly, as with temperature, sea ice algae adapt to abroad spectrum of salinities, however rapid changes in salinity causes osmotic stress (Forgereau et al., 2023). Salinity of brine within the ice can reach magnitudes greater than 140 PSU (Krembs, Gradinger & Spindler, 2000). Campbell et al. (2019) suggest that optimised algal growth occurs during salinities of 30-50 PSU. Generally higher salinity inhibits algae growth and survival by limiting nutrient uptake

and causing damage to the cell membranes, which leaves the cell susceptible to damage (Campbell et al., 2019).

Sea ice algae are photosynthesising microorganisms which means that they require light to grow and survive. The Antarctic has varying light conditions across differing seasons. Winter has almost no light while summer has an abundance of light available. A gradient of light exposure can be found throughout ice structures. According to Ackley & Sullivan (1994), the intensity of light exposure is influenced by factors such as the depth of the ice, the amount of snow covering the ice and the amount of flooding present (Figure 2-1). These factors also influence the wavelengths of light transmitted through the ice, with the under-ice light spectrum typically dominated by wavelengths around 500 nm, as shown in Figure 2-1 (Lund-Hansen et al., 2024). Similarly, Lund-Hansen et al. (2024) found that light intensity is influenced by latitude, with regions closer to the equator experiencing higher irradiance levels (Figure 2-1).

Surface irradiance can reach irradiance levels as high as 1300 µmol.photons.m^{-2}.s^{-1}, while under ice irradiance can be a low as 0.5 µmol.photons.m^{-2}.s^{-1} (Rajanahally et al., 2014). Typical optimal light intensity for the growth of microalgae occurs between 26-400 µmol.photons.m^{-2}.s^{-1}(Maltsev et al., 2021). However, Rajanahally et al. (2014) reported that algae can grow at irradiance levels of 1-100 µmol.photons.m^{-2}.s^{-1} in temperature environments lower than 5°C. As illustrated in Figure 2-1, the transmittance of light intensity decreases with increasing ice depth, a trend that aligns with findings from other studies, including Rajanahally et al. (2014) which highlight the inverse relationship between ice depth and light availability (Lund-Hansen et al., 2024). Research has shown that sea ice algae communities must receive a certain amount of light in order to grow and is referred to as the compensation irradiance. The compensation irradiance refers to the rate of respiration equalling the rate of photosynthesis, which requires the photon flux range of 2-9 µmol.photons.m^{-2}.s^{-1} (Hancke et al., 2018). However, Hancke et al. (2018) report that growth of sea ice algae can occur below compensation irradiance with initial growth occurring as low as 0.17 µmol.photons.m^{-2}.s^{-1} in extreme cases. Conversely, observations from previous studies suggest that photo-inhibition occurs between 20-25 µmol.photons.m^{-2}.s^{-1} (Mangoni et al., 2009; Rajanahally et al., 2014). The wavelength of light is critical for sea ice algae photosynthesis, as algae use light within the

Photosynthetically Active Radiation (PAR) range, typically from 400 to 700 nm (Maltsev et al., 2021). Different wavelengths of light impact the efficiency of photosynthesis and, consequently, the growth of algae. However, the optimal wavelengths for growth are species specific, as different species have different light absorption characteristics (Zwaan, Jacobs & Van Houcke, 2023). However in the general trend indicate that algae tend to perform best under light at the blue (approximately 400-500 nm) and red (approximately 600-700 nm) wavelengths (Zwaan, Jacobs & Van Houcke, 2023).

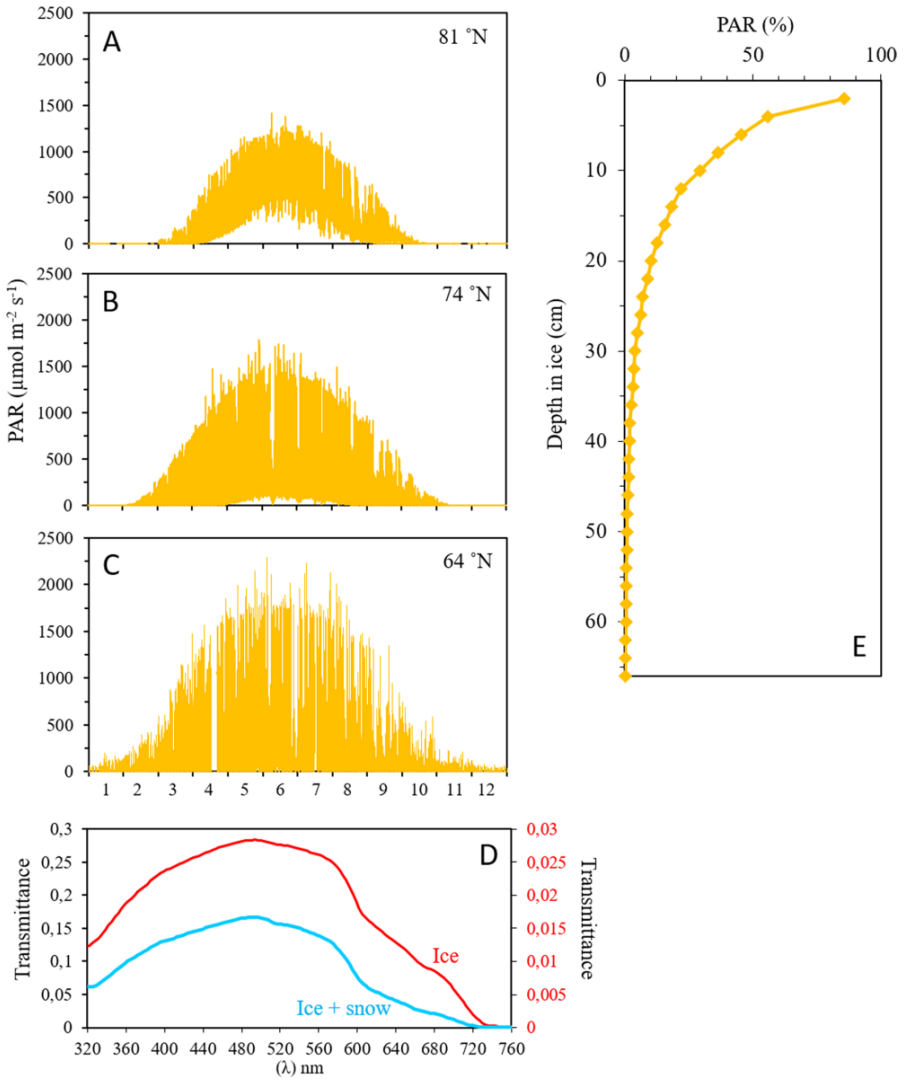

Figure 2-1: Comparison of PAR (400–700 nm) at three locations in Greenland over 12 months: (A) Villum Research Station (81˚N), (B) Zackenberg (74˚N), and (C) Kobbefjord (64˚N). (D) shows how light transmittance of different wavelengths with and without snow cover. (E) shows the attenuation of PAR through ice as percentage of surface irradiance (Lund-Hansen et al., 2024).

Nutrients are essential to the survival of all living organisms. Sea ice algae nutrient requirements consist of macro and micro-nutrients. The macronutrients include nitrogen, phosphorous, carbon and silicone (Sunda, 2012). Their micronutrient requirements are trace metals such as iron, zinc, cobalt, manganese, copper, and cadmium (Morel, Milligan & Saito, 2003; Sunda, 2012). Morel, Milligan & Saito (2003) report higher concentrations of manganese, cobalt, and cadmium in diatoms. These trace metals are important in facilitating key cell process such as photosynthesis and respiration (Morel, Milligan & Saito, 2003). Studies have shown that algae growth is proportional to the nutrient distribution, with the largest sea ice algae communities are where nutrient concentrations are the highest (Swadling et al., 2023).

2.2. Sea Ice Dynamics, Texture and Structure

2.2.1. Sea Ice Dynamics

Sea ice formation begins due to changing seasonal conditions. The formation process is governed by heat transfer which is defined as the exchange of energy across a system's boundary driven by temperature differentials (Himmelblau & Riggs, 2013). It is commonly categorised into three modes: conduction, convection, and radiation (Himmelblau & Riggs, 2013). Convection is the primary heat transfer for ocean-atmosphere interactions, however when the initial ice layer forms, conduction becomes the dominant mechanism of heat transfer (Gow & Iii, 1991).

Frazil ice forms in the upper region of the water column when the temperature of the ocean drops below freezing due to the cold atmospheric temperatures (Ewert & Deming, 2013). The freezing point of sea water is -1.8°C due to freeze point depression (Petrich & Eicken, 2017). The frazil ice forming in the upper region of the water column begin to rise to the ocean surface due to the density differences between the phases (Petrich & Eicken, 2017).

The growth and development of sea ice into a continuous ice sheet is influenced by the environmental conditions in which the ice forms. Loose frazil ice crystals initially form a viscous

layer near the ocean surface (Petrich & Eicken, 2017). The gradual consolidation of frazil crystals in turbulent ocean conditions leads to the formation of disk-like floes of ice called pancake ice (Doble, Coon & Wadhams, 2003). The dynamic wind and wave actions cause ridging and rafting of the pancake ice that eventually consolidate to form a continuous ice sheet with varying ice depth (rough-bottomed) shown Figure 2-2 (Gow & Iii, 1991; Ewert & Deming, 2013; Petrich & Eicken, 2017). In contrast, calm ice growth conditions allow for the frazil ice to consolidate as a smooth thin ice sheet at the ocean surface known as nilas ice (Naumann et al., 2012). Nilas ice allows for the development of congelation ice growth forming a smooth-bottomed continuous ice sheet (Figure 2-2) (Wolfenbarger et al., 2022).

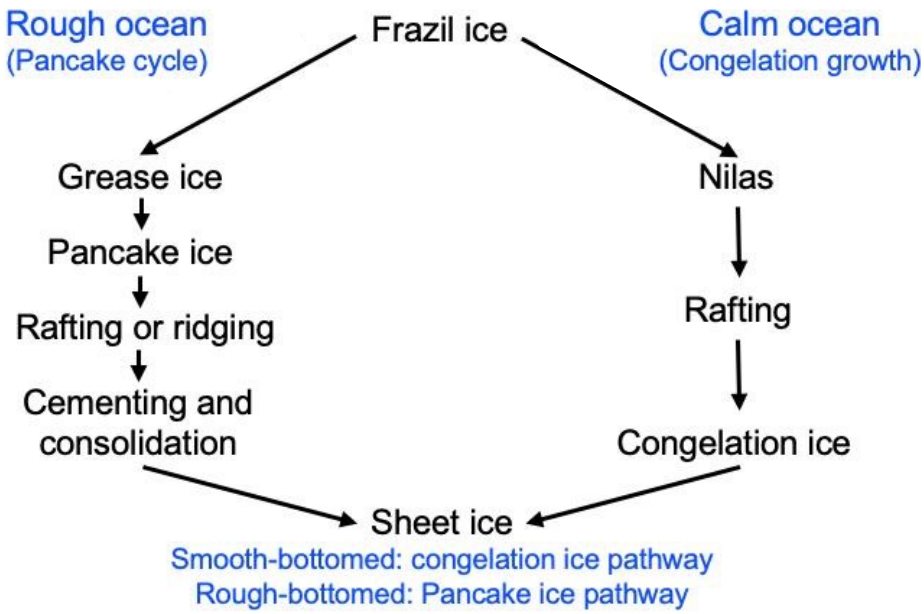

Figure 2-2: Schematic representation of ice growth process for Antarctic and Arctic conditions adapted from European Space Agency (2016).

2.2.2. Sea Ice Texture and Structure

Sea ice structure refers to the physical arrangement of ice crystals, brine and air inclusions. Sea ice texture pertains to the shape, size and geometry of ice crystals (Lange and Eicken, 1991). During the freezing process the water molecules form a unique crystal lattice structure (Ih) that is highly ordered in a hexagonal arrangement (Figure 2-3). The Ih lattice is particularly selective and rejects large salt ions from the crystal lattice structure (Petrich & Eicken, 2017). Salt ions that are not rejected into the underlying ocean are incorporated into pockets of

highly liquid inclusions within the sea ice, resulting in multiphase material. The brine inclusions form along the grain boundaries of ice crystals (Morawetz, Thoms & Kutschan, 2017). The ice crystal formation and growth are influenced by temperature, salinity and turbulent climate conditions (Morawetz, Thoms & Kutschan, 2017). The arrangement of ice crystals, brine and air inclusions within sea ice effects the optical and physical properties of sea ice (Perovich & Grenfell, 1981; Crabeck et al., 2014).

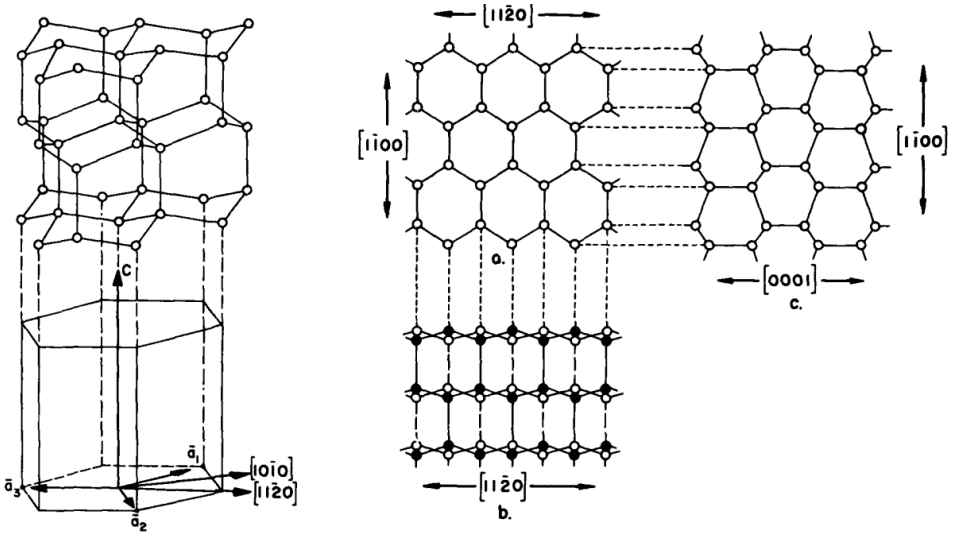

Figure 2-3: Structure of ice Ih, illustrating the highly ordered hydrogen-bonding network between water molecules that results in a unique hexagonal crystal lattice (Weeks & Ackley, 1982).

Sea ice is predominantly categorised as granular or columnar ice as shown in Figure 2-4 (Lange et al., 1989). The granular-textured zone as shown by the red in Figure 2-4 and Figure 2-5, forms from slush ice generally consisting of snow-ice and frazil ice (Weeks & Ackley, 1982). Granular texture is characterised by randomly orientated, isomeric or prismatic crystals (Petrich & Eicken, 2017). In calm conditions, once the surface layer of loose ice crystals has solidified to form a solid ice sheet, ice crystals with horizontally orientated c-axis are favoured (Weeks & Ackley, 1982; Gow & Iii, 1991). This geometric selection is a result of ice growth being fastest in the basal plane (Weeks & Ackley, 1982). The downward growth of ice crystals results in elongated crystals termed columnar textured ice shown by green within Figure 2-4 and Figure 2-5 (Gow & Iii, 1991; Petrich & Eicken, 2017). A transition layer shown by the purple in Figure 2-4 and Figure 2-5, occurs due to the transition from granular to columnar textured ice.

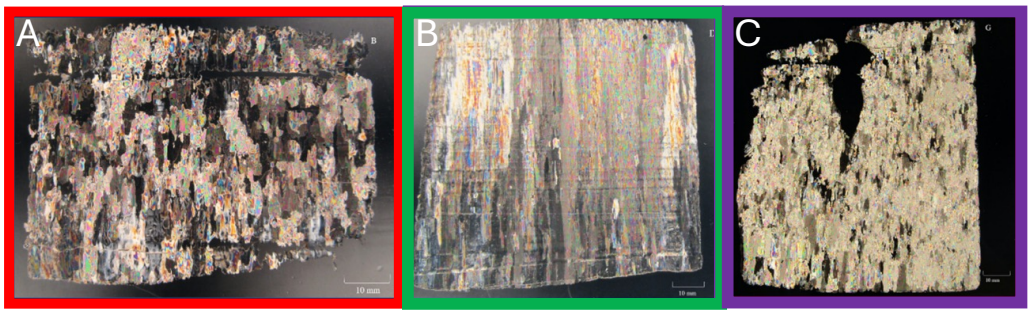

Figure 2-4: Cross polarised images of different sea ice texture (A) granular, (B) columnar, (C) transitional (Johnson et al., 2023).

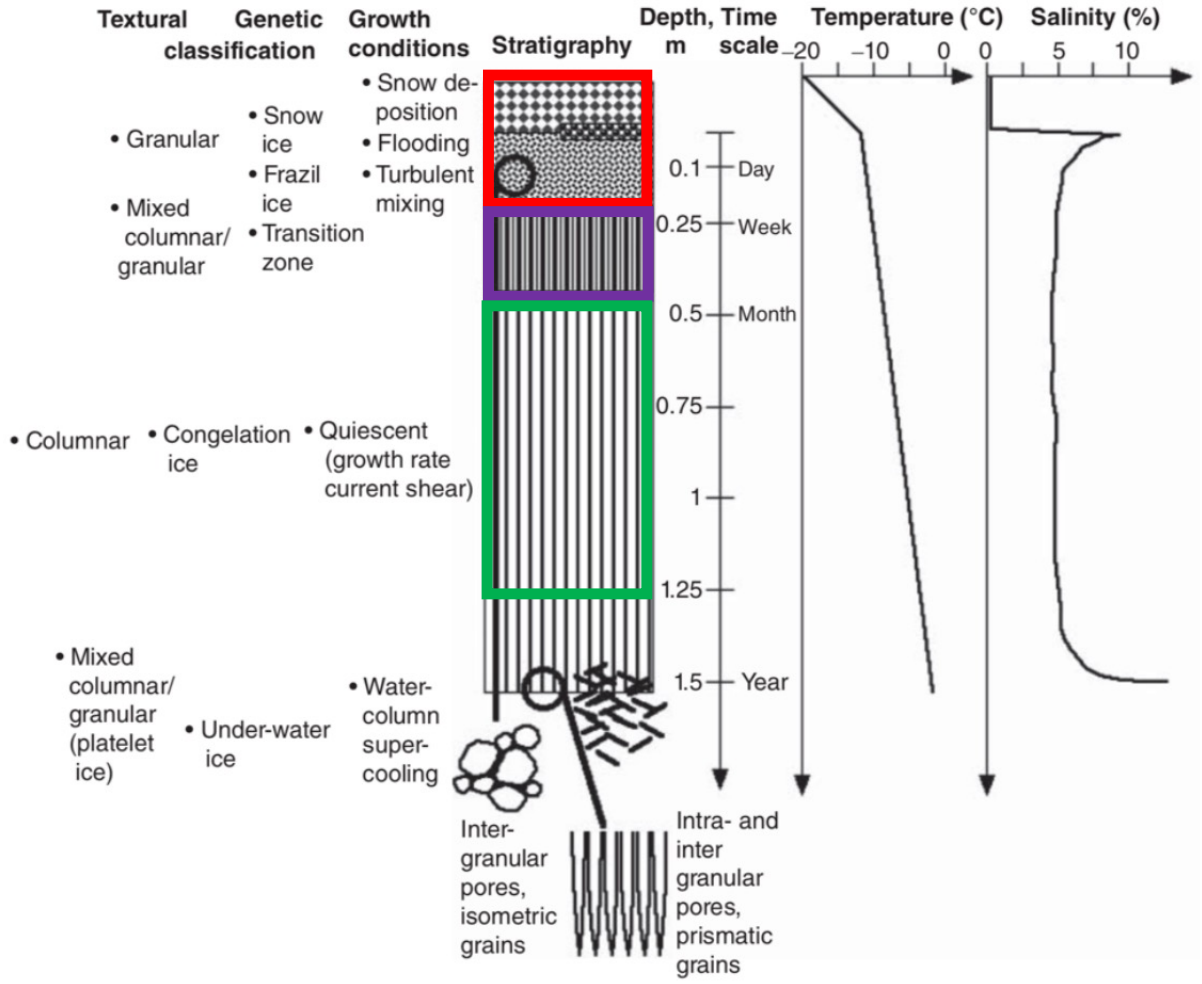

Figure 2-5: Schematic summarising ice textures (red) granular, (purple) transitional and (green) columnar. The schematic includes growth conditions, typical winter temperatures and salinity profiles for first-year sea ice (Petrich & Eicken, 2017).

Lange & Eicken (1991) investigated sea ice textures found in the Weddel Sea of Antarctica and compared it to ice texture found in the Arctic. Sea ice texture compositions in the Arctic

consists of 75% columnar-textured ice and 25% granular-textured ice. However, in the Antarctic, Lange & Eicken (1991) found a mean distribution of ice to be 56.9% granular-textured ice and 43.1% columnar-textured ice. Thus, indicating that sea ice in the Antarctic is dominated by granular ice textures due to the dynamic nature of the ice growth.

2.3. Algae Incorporation into Sea Ice

Sea ice algae and other microorganisms exist within the ocean in the upper region of the water column. Different physical processes caused by turbulent conditions in the Antarctic MIZ and low temperature are the primary drivers that lead to the inclusion of microorganisms and other organic substances in the upper region of the water column. These microorganisms are then incorporated into the ice structures during ice growth within this region. As shown in Figure 2-6, sea ice algae communities exist within the surface layer of the ice, the bulk of the ice and the bottom layer of the ice (skeletal layer). As discussed in Section 2.2.2, during the consolidation of frazil ice, microorganisms, nutrients salts and other impurities in the sea water are rejected from the growing ice lattice (Ewert & Deming, 2013). This results in sea ice algae being entrapped within the brine inclusions of sea ice microstructure.

One of these techniques for algae incorporation into sea ice is through scavenging of frazil ice, where frazil ice crystals rise to the ocean surface, dragging along algal cells (Ewert & Deming, 2013). Ewert & Deming (2013) postulated that algal cells may act as nucleation points for ice crystals in the sea ice algae immediate environment that can bring them to the surface.

Another technique is through the desalination of sea ice. The primary mechanism of sea ice desalination is known as gravity drainage and involves the convective overturing of brine in the mushy layer and the underlying ocean (Figure 2-6) (Notz & Worster, 2009). The convective overturning facilitates the incorporation of sea ice algae and other organic matter into the mushy layer. Alternatively, brine in the upper layer of consolidating sea ice is expelled towards the ice-atmosphere interface. The upward expulsion of brine in addition to wind and wave action, contributes to the population of microorganisms on the upper surface of the ice forming the surface communities (Figure 2-6) (Ewert & Deming, 2013).

As per Section 2.1.2, factors including temperature, salinity, irradiance and nutrients affect the survival and development of sea ice algae. Thus, the sea ice algal communities thrive where conditions are favourable. The largest portions of sea ice algal communities are found from skeletal layer shown in Figure 2-6 to 20cm above the ice-ocean interface (Arrigo, 2016). Although light availability is lowest at the bottom of the pack ice, environmental conditions are more stable and a constant influx of fresh nutrients occurs due to the convective overturning of brine in this layer (Arrigo, 2016). The upward distribution of sea ice algae to the internal communities shown in Figure 2-6, are limited by the nutrient availability and the high fluctuations in environmental conditions. Generally, internal communities are found in the freeboard layer of the granular ice portion of pack ice as shown in Figure 2-6 due to the influx of sea water and hence fresh nutrients due to ocean wave action (Arrigo, 2016).

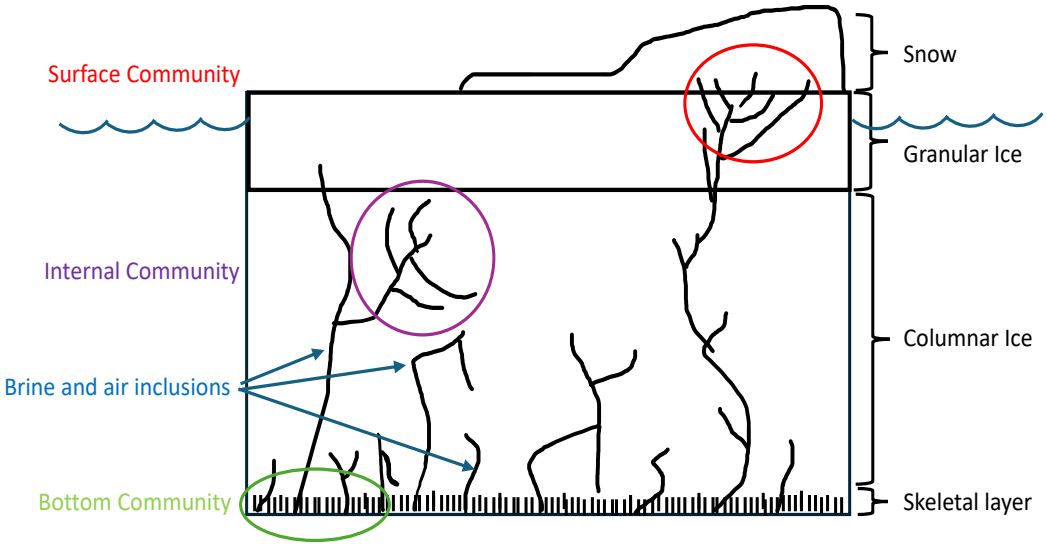

Figure 2-6: Schematic distribution of ice algae in pack sea ice. Adapted from (Arrigo & Thomas, 2004; Tedesco & Vichi, 2014) .

2.4. Extracellular Polymeric Substances (EPS)

2.4.1. Composition and Concentration Profiles

EPS macromolecules are comprised of DNA, polysaccharides and proteins (Jiao et al., 2010). However, the distribution and composition of EPS in sea ice is not uniform and is largely dependent on microorganism concentration (Kim et al., 2023). Kim et al. (2023) investigated

the vertical distribution of organic components in sea ice, with Figure 2-7 D illustrating the contribution of three of the main organic components in sea ice and the underlying water. Carbohydrates are the primary constituent across all ice depths, followed by lipids. Protein contributions were negligible across most ice depths excluding the bottom 10cm (Kim et al., 2023). Figure 2-7 A, B and C indicate that the highest concentrations of organic components are present in the bottom 10cm, which is supportive of the largest sea ice algal communities as discussed in Section 2.3. Kim et al. (2021) found monthly variations of lipids, carbohydrates and proteins. Carbohydrates dominated the contributions, followed by lipids and then proteins (Kim et al., 2023). The average ice concentrations for particulate organic matter (>0.7 µm) reported by Kim et al. (2021) were 89.0 ± 23.0, 7.4 ± 7.8, and 24.7 ± 4.6 µg/L for carbohydrates, proteins and lipids respectively.

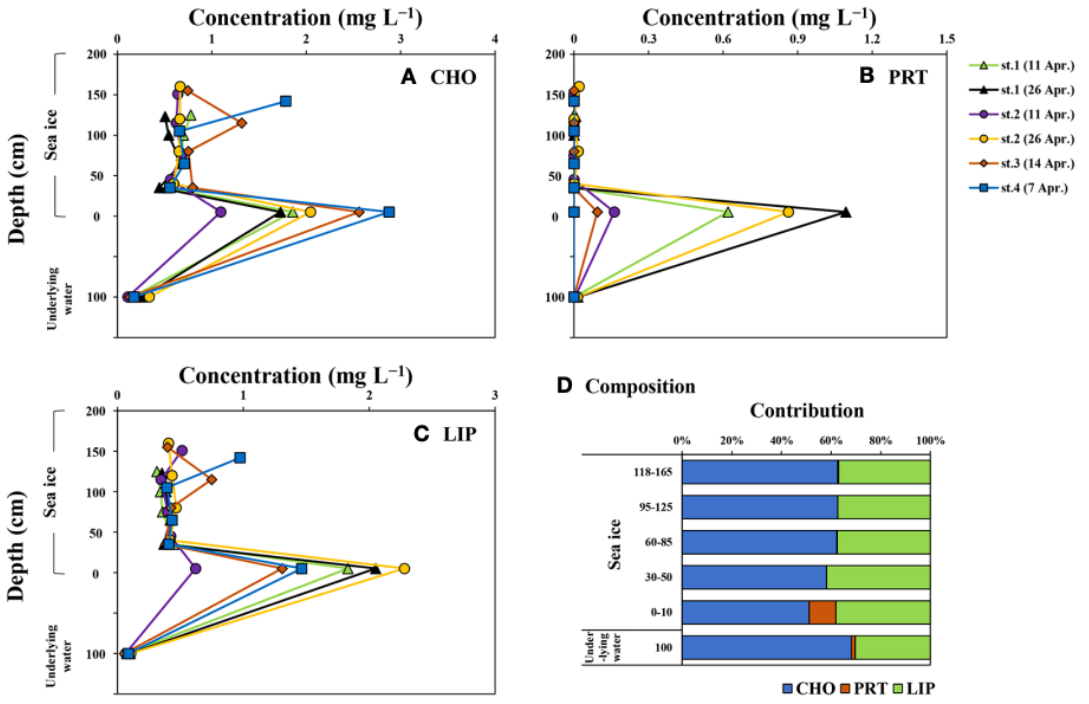

Figure 2-7: Vertical distributions across different sampling days of A) carbohydrate, B) proteins, C) lipids concentration and D) their contribution in sea ice (Kim et al., 2023).

The carbohydrates found in bulk ice cores consists mainly of EPS with Underwood et al. (2010) reporting that 83% of total carbohydrates are composed of EPS. EPS is largely composed of polysaccharides which are long chains of monosaccharides (Underwood et al., 2010). Underwood et al. (2010) found statistically significant differences between the contributions of different monosaccharides in different locations within the sea ice environment. Figure 2-8

shows that the distribution of the monosaccharides is largely similar between North and North-western Weddell Sea monosaccharide compositions The noticeable differences between testing location is the exclusion of rhamnose and fucose in the Western Weddell Sea samples, although the North-western Weddell Sea sample has small amounts of 0.8% and 1.3%, respectively (Underwood et al., 2010). Glucose dominates the composition of bulk ice with over 50.0% in both locations with mannose also featuring prominently at an average composition of 25.3% (Underwood et al., 2010). Relative to the remaining monosaccharides, xylose and galactose are found in larger quantities (Figure 2-8).

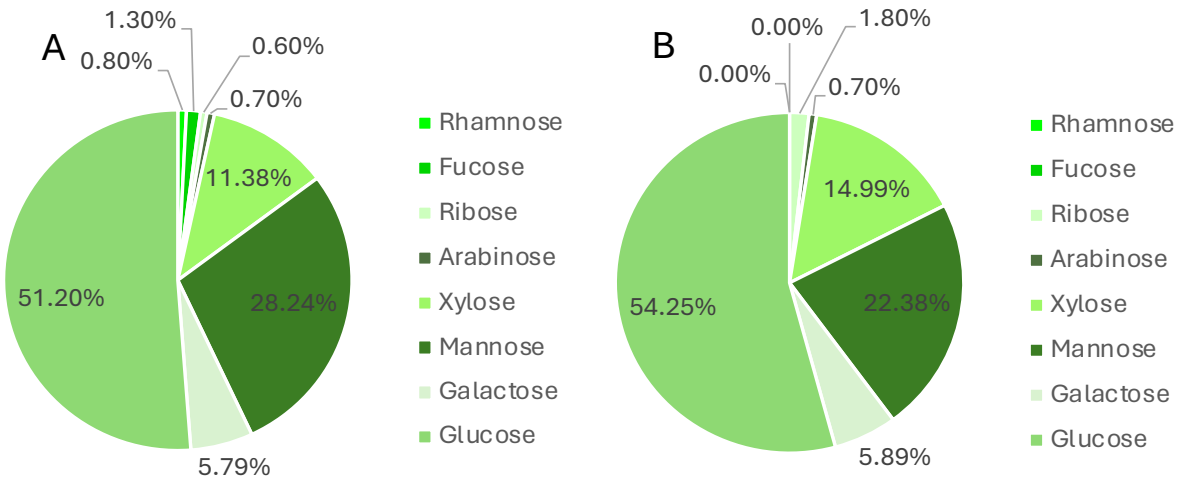

Figure 2-8: Monosaccharide compositions of bulk ice in A) the North-western Weddell Sea and B) Western Weddell Sea. Adapted from Underwood et al. (2010).

The EPS present in sea ice is generally found in either particulate or dissolved form (Underwood et al., 2010; Krembs, Eicken & Deming, 2011). The minority of EPS in natural sea ice is particulate EPS, with particulate EPS accounting for an average of 28% of the total EPS (Table 2-1) (Krembs, Eicken & Deming, 2011). In comparison, artificially grown sea ice with Melosira EPS is dominated by dissolved EPS, with particulate EPS levels as low as 7% of total EPS (Krembs, Eicken & Deming, 2011). The average total EPS concentration at each ice depth reported by Krembs, Eicken & Deming (2011) is 12 and 62 mg·Xanthan gum equivalent/L for natural sea ice (Arctic) and artificial sea ice using Melosira EPS, respectively. This indicates that artificial sea ice in this study contains significantly more EPS compared to normal sea ice.

Table 2-1: Vertical distribution of EPS in the bottom 10 cm of natural sea ice and artificial sea ice using Melosira EPS (Krembs, Eicken & Deming, 2011).

Ice Depth (cm)	Particulate EPS	Dissolved EPS
Natural Sea Ice Bottom 10cm		
0.0-2.5	2.65	6.84
2.5-5.0	2.98	9.57
5.0-7.5	2.43	8.82
7.5-10.0	4.91	10.55
Average	3.34	8.95
Artificial Sea Ice Bottom 10cm		
0.0-2.5	4.19	48.2
2.5-5.0	4.74	49.1
5.0-7.5	2.87	56.9
7.5-10.0	5.29	67.2
Average	4.3	55.4

** EPS concentrations are reported in mg·Xanthan gum equivalent/L.

Krembs et al. (2002) indicated EPS concentrations of 1.00 to 7.71 mg·Xanthan gum equivalent/L during March to May (spring) in Arctic sea ice. In comparison a study by Dumont et al. (2009) investigated transparent exopolymeric particles (TEP) in the Antarctic at various ice depths (0-90cm). The investigation was carried out from September to November (spring) in the Australian Sector of the Southern Ocean and during the period of November to January (spring/summer) in Western Weddel. The maximum and minimum concentrations of TEP in vertical profiles were 0.003 and 3.07 mg·Xanthan gum equivalent/L, respectively. Maximum concentrations of EPS in vertical profiles generally were found at the bottom of ice by the ice ocean interface (Krembs et al., 2002; Dumont et al., 2009).

2.4.2. EPS Impact on Ice Structures and Textures

As discussed in Section 2.1.2, sea ice algae are sensitive to change in factors such as temperature, salinity, nutrients and irradiance. Sea ice provides an extreme environment

where these factors change and elicit a response in the form of EPS to help algae adapt to this environment. Although the factors behind EPS secretion in the sea ice environment are well understood, there has been limited research on the impact of EPS on sea ice itself. As discussed in Section 2.4.1, extracellular polymeric substances consist primarily of carbohydrates and proteins. There is limited research on the effect of polysaccharides and proteins on sea ice texture and structure.

Krembs, Eicken & Deming (2011) investigated the impact of EPS on sea ice textures and microstructure. Samples without EPS exhibited coarser grain structure with increased ellipsoidal brine inclusions and a higher occurrence of lamellar crystal features and inclusions as shown by A, C and E in Figure 2-9 (Krembs, Eicken & Deming, 2011). In contrast, B, D, and F in Figure 2-9, show ice grown with EPS, which displays predominantly intergranular brine inclusions marked by irregular convoluted shapes and a disordered arrangement. Image analysis of C and D in Figure 2-9 indicated an increase in up to 15% number density of brine inclusions in samples containing EPS. Similarly to Krembs, Eicken & Deming (2011), Matlakala (2022) investigated the EPS impact on ice textures and structure. Notable differences in the investigations were the types of EPS and methods used to analyse sea ice textures and structures. Krembs, Eicken & Deming (2011) used Melosira EPS, while Matlakala (2022) made use of xanthum gum, which is considered the reference standard of EPS (Passow & Alldredge, 1995). Krembs, Eicken & Deming (2011) made use of microscopy to visually analyse ice structures and textures while Matlakala (2022) used X-ray computed tomography and thin sections of ice placed between polarised sheets.

As shown in Figure 2-10, the sample without EPS had three distinct zones of granular, transitional and columnar textures. The granular and columnar textures were clearly distinguishable with well-defined crystals (Matlakala, 2022). In contrast, the sample with EPS as illustrated in Figure 2-10 had no transitional layer. The granular textured zone had small rounded and oval shaped crystals while, the columnar textured zone crystals were not distinguishable from each other with blotchy and blurred crystals (Matlakala, 2022).

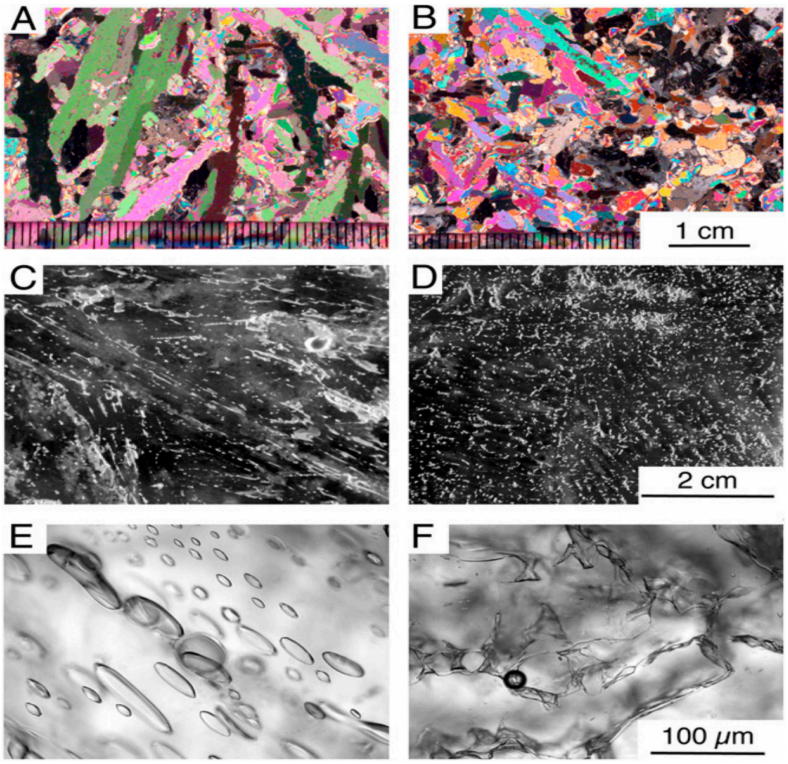

Figure 2-9: Microscope images of artificial ice grown at -10 °C with EPS (right) and without EPS (left) with A and B show ice texture at low magnification under polarised light, C and D with contrast staining, and E and F showing pore structure at high magnification (Krembs, Eicken & Deming, 2011).

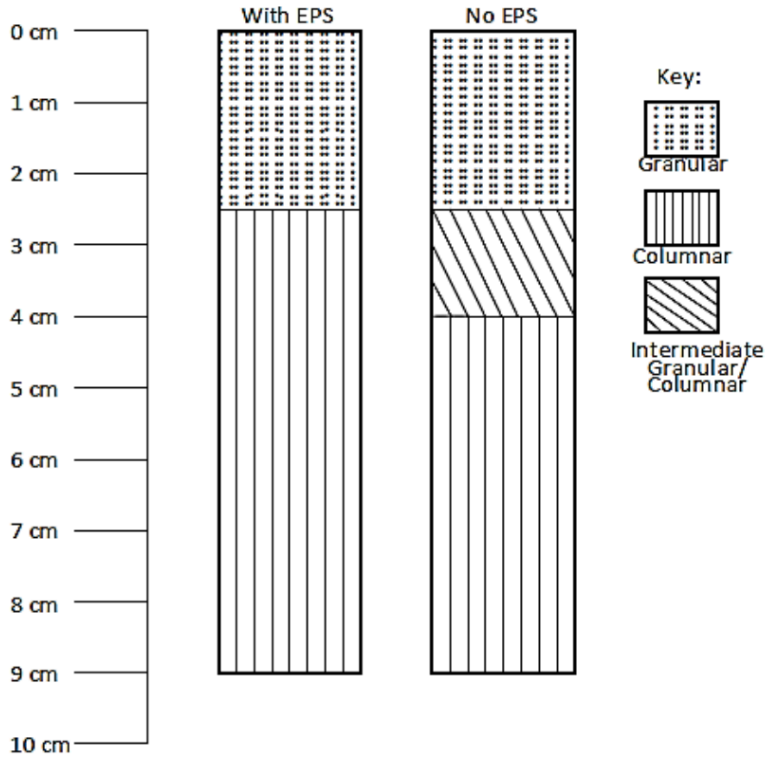

Figure 2-10: Stratigraphy diagrams for ice grown from solutions of starting artificial ocean salinity of 30 psu at -10°C with and without EPS (Matlakala, 2022).

The EPS sample as shown in Figure 2-11 had larger, more interconnected, and vertically elongated brine inclusions (Matlakala, 2022). Samples containing EPS had increases in bulk salinities from 12% to 35% relative to controls without EPS and hence a higher salt retention (Krembs, Eicken & Deming, 2011). Similarly, Matlakala (2022) reported higher bulk salinities and overall brine retention for samples containing EPS. Krembs, Eicken & Deming (2011) attributed the higher bulk salinity in EPS samples to lower ice permeability due to pore clogging by EPS. In the study by (Krembs, Eicken & Deming, 2011), Melosira EPS reduced ice growth rates more than that of xanthan gum, which is due to the inclusion of ice binding proteins (IBP) in Melosira EPS.

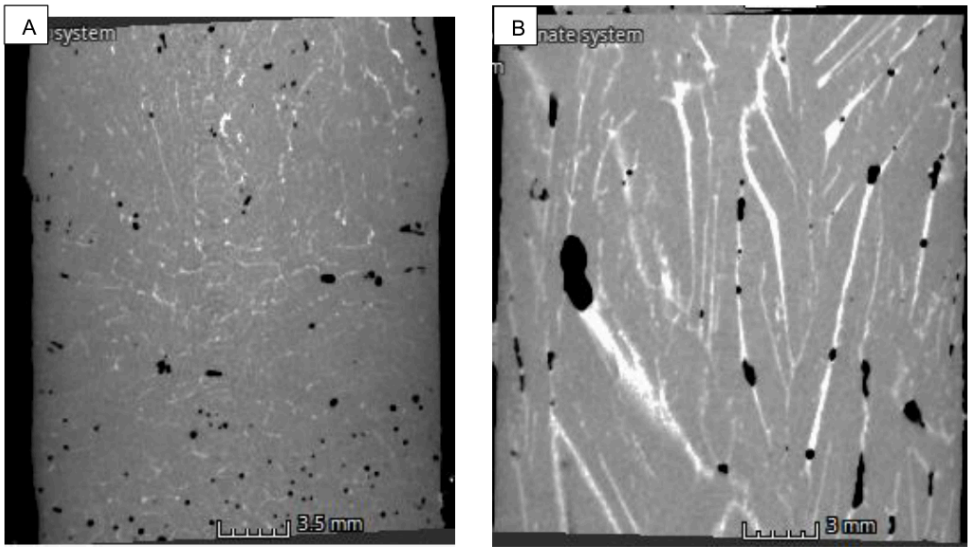

Figure 2-11: Micro-CT scan visuals for the top part of ice grown at -10°C from solutions of starting artificial ocean salinity of 30 psu (A) without EPS, (B) with EPS (Matlakala, 2022).

2.5. Artificial Sea Ice Experiments

As discussed in Section 1.2, limiting factors with *in situ* research has favoured a shift towards *ex situ* research in land-based laboratories. The shift to land-based laboratories favours artificial sea ice experiments to study sea ice properties and characteristics. Artificial sea ice experiments are important as specific parameters can be manipulated in controlled environment (Weeks, 1962). To determine sea ice properties and characteristics, ice growth must mimic that of natural sea ice. As mentioned in Section 2.2.1, sea ice formation process is driven by convective cooling of sea water by the atmosphere. Thus, atmospheric freezing of

saline solutions is ideal to artificially simulate the natural sea ice. Weeks (1962) first designed a tank made of steel to artificially grow sea ice (Figure 2-12).

Natural ice grows in a top down manner and therefore the insulation is empirical to ensure ice formation does not occur from tank walls as shown in Figure 2-12 (Weeks, 1962; Perovich & Grenfell, 1981; Marks, Lamare & King, 2017; Hall et al., 2023). The experimental set-up consists of pumps, fans and pressure relief system. Standard artificial ice experiments induce atmospheric freezing in tanks by controlling the ambient air temperature in cold rooms (Weeks, 1962; Perovich & Grenfell, 1981; Marks, Lamare & King, 2017; Hall et al., 2023). In these refrigerated rooms temperature stratification can occur and therefore fans are used to circulate the cold air across the ice surface (Weeks, 1962; Perovich & Grenfell, 1981; Marks, Lamare & King, 2017; Hall et al., 2023). Similarly, tanks require pumps to induce agitation of the underlying saline solution as temperature and salinity stratification may occur (Perovich & Grenfell, 1981; Hall et al., 2023). Hall et al. (2023) notes some of these refrigerated rooms having warming periods to remove ice from cooling units, which can result in fluctuating temperature.

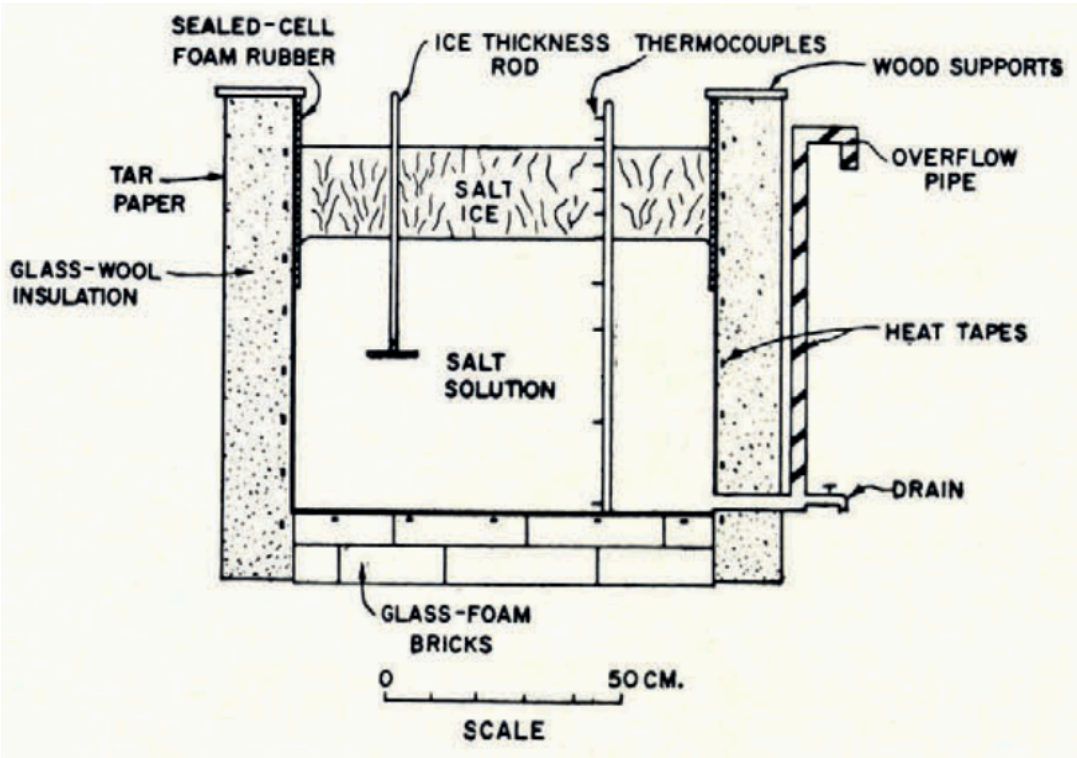

Figure 2-12: Schematic diagram of a freezing tank experimental set up with includes axillary equipment (Weeks, 1962).

Depending on the requirements of the experiment, inducing ice growth using the atmosphere is not always a viable option and therefore alternative measures to induce ice growth must be considered. One method to accomplish ice growth from the top of a tank is by employing a cold plate or lid positioned at the top of the tank to initiate ice growth. The cold plate (cooling plate) was originally designed to be used for heat dissipation in refrigeration loops and has since been integrated into various industries for thermal management purposes (Sparrow, Chevalier & Abraham, 2006). Cooling plates have been adapted for saline solutions growing ice in a top-down manner resembling sea ice growth (Cox & Weeks, 1975; Notz, Wettlaufer & Worster, 2005; Schulson, Renshaw & Snyder, 2012).

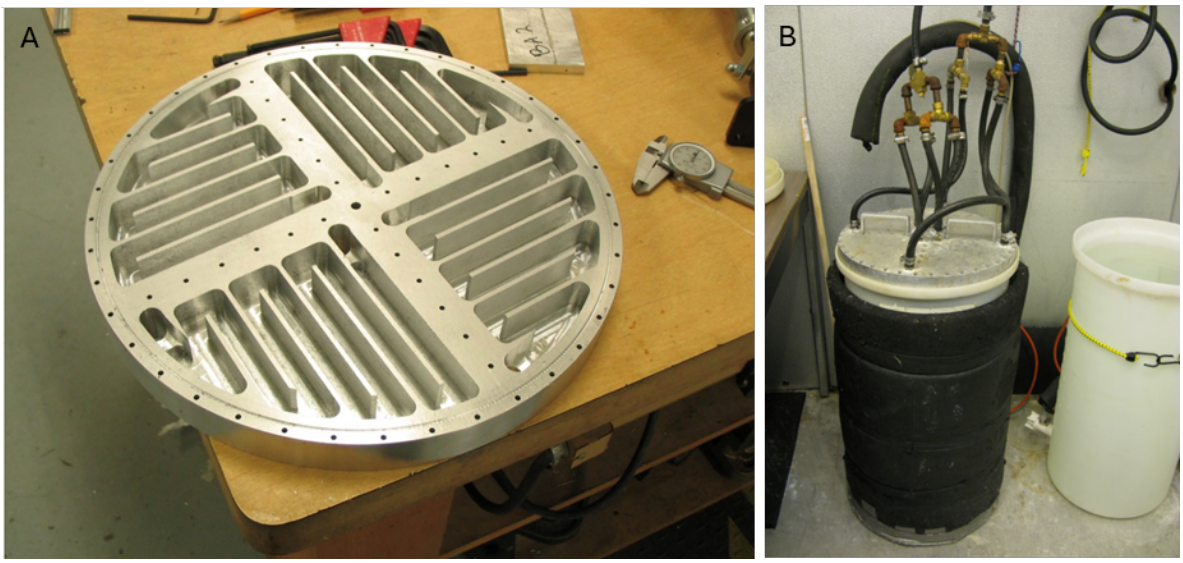

Figure 2-13: (A) Cold plate internals and (B) cold plate set up used for direct cooling of saline solution (Schulson, Renshaw & Snyder, 2012).

The cold plate, a metallic disk with internal channels machined into it, is positioned on top of the tank, making direct contact with the saline solution, as shown in Figure 2-13 (Schulson, Renshaw & Snyder, 2012). A chiller system pumps coolant through a cold plate facilitating heat transfer from the coolant to a saltwater solution, thus lowering the temperature of the saltwater solution. As the temperature drops below freezing, ice begins to form, growing downwards from the plate.

Alternatively, ice formation can be induced by introducing a cold finger into the solution to serve as a nucleation point. A cold finger is a tool designed to generate a localised cold surface.

The cold finger experiment employs a metal probe, termed a "cold finger," submerged within a container filled with saltwater solution. Illustrated in Figure 2-14, the cold finger comprises an inner metal tube within an outer metal tube. Coolant from a chiller system is circulated through the inner tube of the cold finger, subsequently exiting through the outer metal tube (Kuiper et al., 2003). This coolant facilitates heat transfer, thereby reducing the temperature of the outer tube, which contacts the saltwater solution. Consequently, the temperature of the saltwater solution decreases. As the temperature of the saltwater solution drops below its freezing point, ice nucleation occurs on the surface of the cold finger, initiating the formation of ice, which then grows outward from the probe.

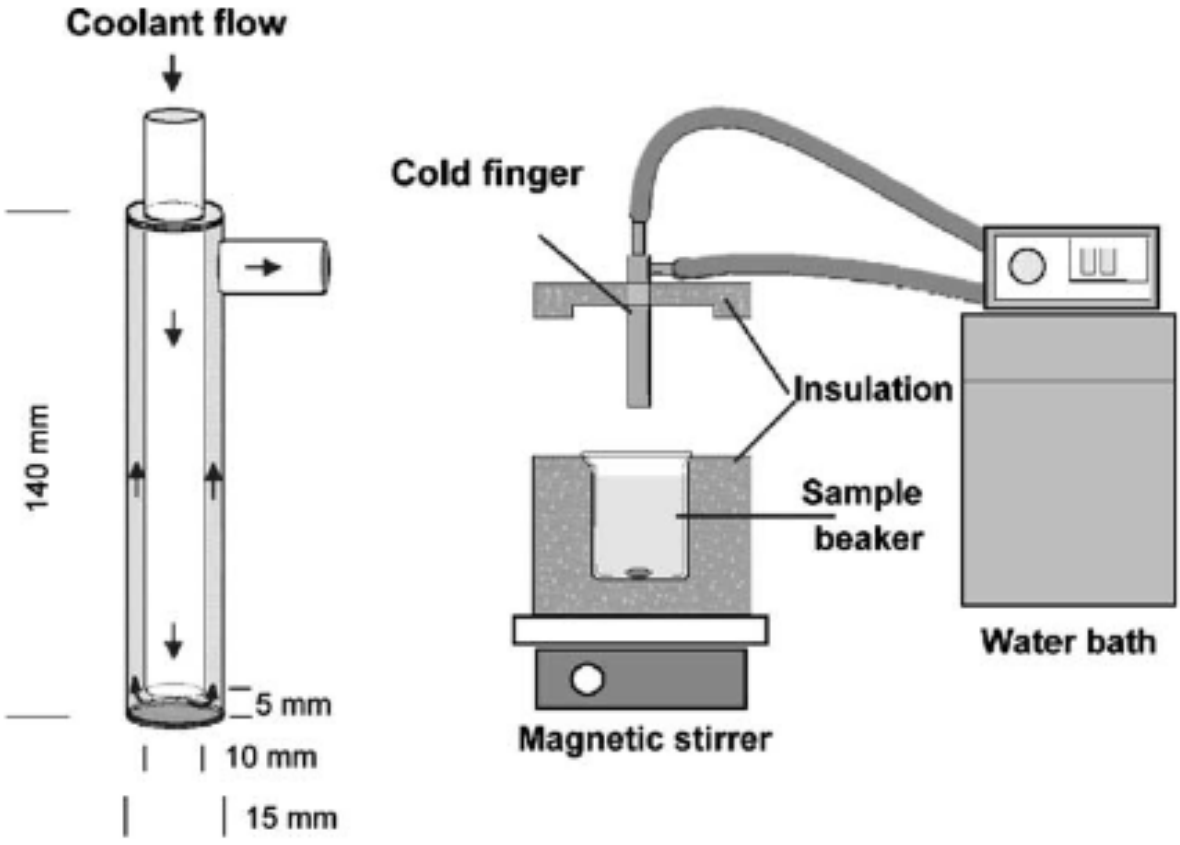

Figure 2-14: Schematic diagram of a cold finger (left) and experimental set up with water bath, magnetic stirrer and chiller (right) (Kuiper et al., 2003).

Originally, developed for freshwater research by Kuiper et al. (2003), the cold finger experiment was initially utilised to selectively adsorb and purify ice-binding proteins from complex mixtures. Building on this work, Ewert & Deming (2011) later adapted the cold finger

experiment for use with saline solutions, expanding its applicability to sea ice research. Ewert & Deming (2011) used the cold finger apparatus to investigate the retention of EPS produced by *Colwellia psychrerythraea* strain 34H (marine bacterium) in saline ice environments. The scope of the study did not include sea ice texture and structure, and the natural convective flows of sea ice, however it did record bulk ice salinities and temperature profiles (Ewert & Deming, 2011). While the study lacked methods to evaluate natural ice growth processes, it provided valuable insight into the directionality of ice growth and the potential influence of biological material, such as extracellular polysaccharides, on ice formation. The artificial saline ice was formed using the cold finger apparatus (Figure 2-14), producing a hemispherical ice shape as illustrated in Figure 2-15 (Ewert & Deming, 2011).

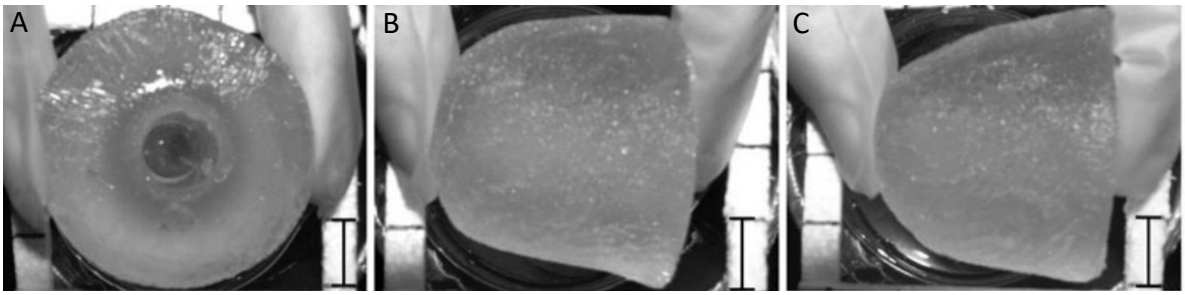

Figure 2-15: Photographs of ice formed using cold finger apparatus with (A) photographed from the top, with axis perpendicular to underlying surface; (B) the ice photographed from the side, with axis parallel to underlying surface and (C) the ice photographed from the side after a 90℃ rotation. Bars indicate 1.25cm. Adapted from (Ewert & Deming, 2011).

2.6. Rationale of Study

Extensive knowledge of sea ice algae particularly in the Eastern Marginal Ice Zone of the Southern Ocean, remains limited. Sea ice algae play a pivotal role in the aquatic food chain as primary producers and are integral to the carbon cycle (Forgereau, Lange & Campbell, 2023). Their primary habitat is within sea ice, where key environmental factors dictate their survival and development. Numerous studies have highlighted the physiological responses of algae to changes in environmental factors including temperature, salinity, irradiance and nutrients (Ackley & Sullivan, 1994; Stoecker et al., 1997; Montagnes & Franklin, 2001; Morel, Milligan & Saito, 2003; Mangoni et al., 2009; Sunda, 2012; Rajanahally et al., 2014; Hancke et al., 2018;

Forgereau et al., 2023; Swadling et al., 2023). Additionally, studies have examined how these parameters effect and are affected by sea ice formation. Although there is extensive literature on the distribution of algae within sea ice, there is a notable gap in knowledge on the interactions of sea ice and algae under varying environmental conditions. Therefore, as environmental conditions change due to global warming it is empirical to study the effects of ocean warming, varying irradiance levels and atmospheric temperatures on sea ice formation and therefore effect on sea ice algae.

Artificial sea ice experiments are important tool to supplement *in situ* research into the dynamic relationship between sea ice and sea ice algae. Artificial experiments allow for more controlled experimentation in which key environmental conditions can be evaluated in isolation. However, current studies performing artificial sea ice experiments focus on sea ice growth dynamics. To address this, artificial sea ice growth techniques need to be evaluated and adjusted to facilitate the inclusion of algae in experimentation. This includes considerations such as light permeability into the system and material of constructions used in experimentation. The materials used in artificial algae experiments are largely dictated by trace metal nutrients sources for sea ice algae and the durability within saline environments. This work in this study will be to develop a system in which artificial sea ice can be grown in saline solutions containing algae. The developed system will be used to assess the interactions between sea ice algae under varying environmental conditions.

3. Aims, Objectives and Key Questions

This project aims to investigate the dynamic relationship between sea ice and sea ice algae, focusing on changes in environmental conditions such as irradiance, ocean temperature and atmospheric temperature.

The objectives that emanate from this are:

- Develop a system (equipment and methodology) that allows the dynamic relationship between sea ice and sea ice algae to be investigated under various irradiances, oceanic and atmospheric temperatures.
- Investigate the dynamic relationship between sea ice and sea ice algae under various irradiances, oceanic and atmospheric temperatures using the system.

The key questions to be addressed in this project include:

1. What specialised equipment can be designed to facilitate experiments involving small volumes of sea ice algae under sub-zero conditions?
2. What sensor/model can be developed to aid in prediction of sea ice growth dynamics within an acceptable margin of error (0-10%)?
3. Are there existing experimental and sampling methodologies available to complement the design of the proposed equipment to facilitate the investigation of the dynamic relationship?
4. How do changing irradiance conditions affect sea ice algae communities during acclimatisation and ice formation?
5. How do changes in oceanic temperatures affect sea ice algae communities during acclimatisation and ice formation?
6. How do changes in atmospheric temperature effect sea ice algae communities?

4. Design and Optimisation of Cold Finger

Transporting large volumes of algae from the field are preferable to small quantities, as larger volumes provide a more representative account of variability in algal species and reduces volume sampling bias, which aids in the reliability of results. However, logistical challenges in obtaining sea ice algae from the Antarctic polar region limit transportation to small volumes (3-litres). A possible route for increasing algal density and volume is through culturing (Vaulot et al., 2023). However, this method is likely to change algae communities and requires an extended period to achieve.

The environmental chamber (EC) has an internal volume of 245 litres. The internal working volume of the EC is 94 litres due to the inclusion of a chiller, PAR sensors, a LED light bar and insulation (Figure 4-1). The internal working volume has a length of 730mm, a width of 330mm and a height of 390mm. The EC provides an environment in which temperature and irradiance can be controlled which is important for evaluating different environmental conditions on sea ice algae growth and uptake dynamics. This EC is designed to house four 1-liter aquaria, with three allocated for experimental purposes and one serving as the control (Figure 4-1).

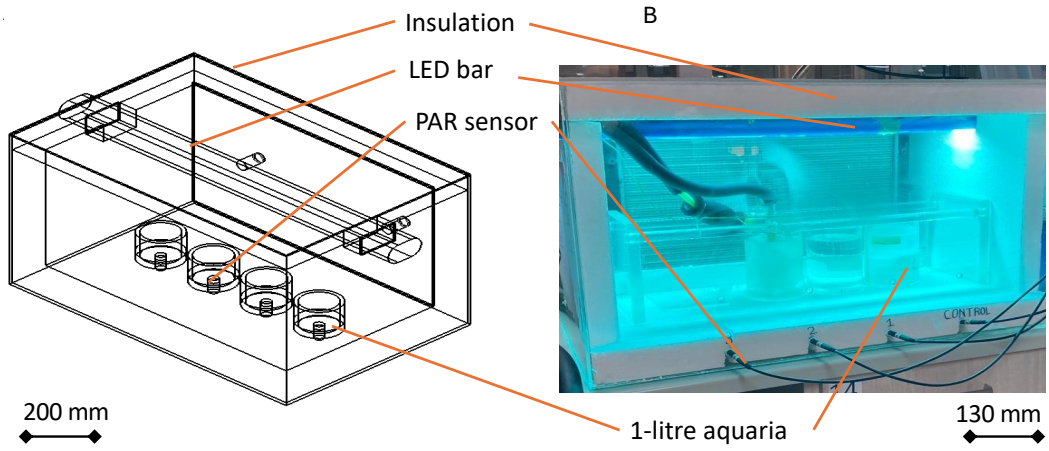

Figure 4-1: Schematic diagram and annotated image of environmental chamber with four 1L aquaria, illustrating insulation, 1-litre aquaria, light source and light measurement devices.

The environmental chamber's temperature is maintained by a 600W chiller, which operates within a range of -30.0°C to 40.0°C. The chiller is connected to a cooling plate attached to one of the side walls. The. temperature variation across the EC is +1°C between the cooling plate

and the opposing parallel wall (Kumadiro, 2023). Temperature readings in the chamber are captured using a temperature measurement device equipped with 32.0 sensors, with each sensor systematically read every 5 seconds. The chiller's temperature setting is manually adjusted based on these temperature readings. Once the desired temperature is reached, the chillers control systems maintain the temperature at the set point.

In contrast, the irradiance levels in the chamber are regulated by a 200W LED light bar with spectrum range of 450-650 nm and an operational range specified from 0.00 to 3500 µmol.photons.m^{-2}.s^{-1} (Kumadiro, 2023). This is well-suited for photosynthesis in algae that utilise wavelengths between 400 and 700 nm (Katam et al., 2022). The output of the LED light bar is assessed using PAR (Photosynthetically Active Radiation) sensors that can measure up to 4000 µmol.photons.m^{-2}.s^{-1}. The PAR sensors are situated within the bottom insulation of the EC, with the part of the sensors that detects light level with the top of the polystyrene insulation. The irradiance variation across the EC is considered negligible (Kumadiro, 2023). Depending on the setup, the sensors are either directly exposed to the light or the light must pass through the clear Perspex 1-litre aquaria containing the saline solution. Adjustment of the LED bar's light intensity is manually performed through the light bar control panel, guided by PAR readings.

4.1. Design Considerations

Previously 3 litre, 30 litre and 300 litre tanks with the same aspect ratio were used for artificial experimentation (Hall, 2019; Guni, 2022; Matlakala, 2022). However, changes in volume effect the thermodynamics and growth dynamics. Thus, reducing the reactor volume to 1-liter affects growth dynamics, leading to faster ice growth with higher normalised bulk salinities. The focus of this study is on the uptake dynamics of sea ice algae into sea ice and thus understanding the ice growth development is essential to understanding these uptake dynamics. It is also crucial to consider the duration of experiments and the ability of algae to remain distributed in the aquaria. Sea ice algae cells are denser than seawater and, due to their lack of locomotive capabilities, tend to sink through the water column rather than remain suspended (Miklasz & Denny, 2010). Suspension of the sea ice algae in the aquaria usually

requires methods such as shake tables or air bubbling. However, in the absence of such suspension methods during the experiment, the sea ice algae are expected to settle to the bottom of the aquaria.

In the context of ice growth, it is crucial to consider the relationship between thickness and heat transfer. As ice accumulates thickness, its insulative properties reduce the rate of heat exchange with the surrounding water (Maksimov & Amer, 2017). The cold plate grows ice top-down, causing growth to slow as ice thickness increases due to reduced heat transfer. On the other hand, the cold finger, positioned vertically in the tank, fosters simultaneous ice growth at all depths. This results in less ice thickness relative to the cold source, enhanced heat transfer, and faster ice growth. This difference in growth dynamics means that the cold finger is more likely to incorporate a larger volume of sea ice algae into the developing ice structure before they settle at the bottom of the 1-litre aquaria. Additionally, the cold plate is likely to impede light exposure during experimentation and therefore hindering the investigation of varying light conditions.

4.1.1. Materials of Construction

The important considerations for the cold finger material of construction include thermal properties, chemical compatibility, algae compatibility, and cost. Various materials are available for selection, broadly categorised as composites, ceramics, polymers, and metals (Rösler, Harders & Bäker, 2007). The two primary considerations for thermal properties include their suitability across a broad spectrum of temperatures and their thermal conductivity. The material of construction should withstand temperature ranges from -20°C to room temperature and the ability to withstand simultaneous exposure to different temperature profiles. For optimal heat transfer from the cold finger to the saline solution, it's important to minimise resistance, hence favouring higher thermal conductivities. Metals are ideal for material of construction due their high thermal conductivities, ductility, and high strength (Rösler, Harders & Bäker, 2007). These characteristics render metals particularly efficient for heat transfer processes while ensuring structural integrity across varying temperature environments.

The selection of a specific metal was determined based on its chemical compatibility and compatibility with algae. Algae compatibility, the most important design consideration, considers the sensitivity of the sea ice algae to the metal. As outlined in Section 2.1.2, sea ice algae exhibit sensitivity to environmental changes, specifically in nutrients. The material of construction must be considered for algae reactivity as outlined by the trace metals nutrients sources detailed in Section 2.1.2. In addition to algae compatibility, metals must also be evaluated for their chemical compatibility, particularly with corrosive substances such as salt water and ethylene glycol, which require construction materials capable of withstanding their corrosive properties. Several metals were considered for use, primarily chosen for their availability. Table 4-1 presents a summary of metals considered for the cold finger experiments based on algae compatibility, chemical compatibility, and cost. Each of these chosen metals demonstrated adequate resistance to ethylene glycol, with the exception of gold and titanium, for which no data was available (Mettler Toledo, n.d.; Graco, 2013). Carbon steel and cast iron despite their relatively low cost have high corrosion in saline environments and the potential to impede the algae uptake dynamics, which makes them poor choices. Gold and titanium are ideal for preventing corrosion in saline environments and their negligible reactivity with sea ice algae (Morel, Milligan & Saito, 2003). However, their downside lies in their considerable costs and the scarcity of data concerning their resistance to corrosion from exposure to ethylene glycol.

Stainless steel 316 and aluminium offer cost-effective alternatives to gold and titanium. Aluminium exhibits relatively high thermal conductivity, along with excellent compatibility with ethylene glycol, rendering it ideal for heat transfer. Similarly, stainless steel 316 offers good thermal conductivity and corrosion resistance against ethylene glycol, albeit to a lesser degree. However, stainless steel in comparison to aluminium is more favourable in resisting corrosion in saline environments. While stainless steel provides better corrosive resistance in a saline environment, comparatively gold and titanium provide better resistance. A further drawback of stainless steel 316 and aluminium is their reactivity with sea ice algae as highlighted in Table 4-1.

Table 4-1: Key Design considerations for material of construction of the cold finger in saline and algal environment.

Metal	Sea Water Resistance	Algae Compatibility	Relative Cost
Aluminium	Fair (Mettler Toledo, n.d.). Not recommended (Graco, 2013). Aluminium oxides in the presence of air, creating a film preventing corrosion in salt water(North & MacLeod, 1987). However, the high concentration of chloride irons break down the oxidative film.	No. Aluminium rarely found in pure form. Aluminium alloys generally found with zinc, silicon, manganese, and iron (Maciej Serda et al., 2013). All of which are reactive with algae.	Medium-Low
Carbon Steel	Not recommended (Mettler Toledo, n.d.). Not recommend (Graco, 2013). Highly susceptible to saltwater corrosion.	No. Carbon steel is made of carbon, iron, manganese and phosphorous which are reactive with sea ice algae (AZO Materials, 2012)	Low
Cast iron	Not recommended (Graco, 2013). Highly susceptible to saltwater corrosion.	No. Cast iron comprised of the following elements which are reactive with algae: iron, carbon, silicon, manganese, and phosphorus (Genculu, n.d.).	Medium
316 - Stainless steel	Fair (Mettler Toledo, n.d.). Fair to poor (Graco, 2013). Stainless steel 316 forms protective oxidative layer, but the high concentrations of chloride ions result in corrosion (Malik et al., 1999).	No. Stainless steel 316 is comprised of the following elements which are reactive with algae: iron, carbon, nitrogen, silicon, manganese, and phosphorus (San Marchi et al., 2008)	Medium-High
Gold	Excellent. Resistant to sea water in pure form, alloyed metals may be subjected to corrosion (North & MacLeod, 1987).	Yes. Not a primary nutrient source.	Very High
Titanium	Excellent (Mettler Toledo, n.d.). Titanium forms a stable self-repairing oxidative layer in the presence of sea water, rendering it corrosion resistance (Gadiyar & Shibad, 1980).	Yes. Not a primary nutrient source.	High

To reduce the high costs of gold and titanium and the lack of data regarding their interactions with ethylene glycols, the option of metal plating was explored. Stainless steel 316 was selected for plating, primarily because it was readily accessible at the chemical engineering mechanical workshop. Titanium plating was initially preferred due to its relatively lower cost and higher resistance to corrosion in saline solutions compared to gold. However, due to the difficulties with machineability and availability of titanium, gold plating emerged as a viable alternative due to its availability (Gadiyar & Shibad, 1980). By gold plating the stainless steel 316 cold finger, the design incorporates good thermal conductivity, corrosion resistance to both ethylene glycol and saltwater, while also addressing the algae considerations discussed previously.

4.1.2. Shape and Size

The main design considerations for the cold finger included the size, shape and circulation of the coolant within the cold finger. These factors play a crucial role, as they directly influence the dynamics and extent of ice growth. The cold finger operates by allowing a liquid coolant to enter through its internal layer and exit through the external layer (Figure 2-14).

The equipment design is typically guided by two primary factors: pipe-flow dynamics and heat transfer efficiency. Circular pipes are commonly employed for liquid fluid flow due to their ability to withstand significant pressure differentials between their interior and exterior environments. Non-circular pipes are commonly utilised in heating and cooling systems due to a greater surface area for heat transfer to occur (Cengel & Cimbala, 2014). Nagayach & Agrawal (2012) indicated that non-circular tubes exhibit better heat transfer capabilities for tubes with equivalent cross-sectional areas (Cengel & Cimbala, 2014). This advantage stems from their higher surface-to-volume ratio, providing a larger surface area per unit volume of coolant. However, the use of non-circular shapes results in uneven heat distribution, this would lead to non-uniform ice growth within the context of artificial sea ice growth. In contrast, circular tubes ensure symmetrical heat distribution, facilitating uniform ice growth (Nagayach & Agrawal, 2012). In the context of cold finger experiments, uniform ice growth offers benefits such as consistent sampling, better control over ice growth, and simplification of thermodynamic model development. While heat transfer efficiency is prioritised over pipe-

flow dynamics, as the focus is not on the fluid dynamics of the circulating coolant, uniform ice growth is a more significant factor to consider. Consequently, a circular cold finger design was selected for the inner and outer shells.

The dimensions of the 1-liter aquarium and circulation of the coolant were factors considered in sizing of the cold finger. The aquarium measured 110mm in external diameter, 100mm in internal diameter and 150mm in height as shown in Figure 4-2, providing the framework within which the cold finger had to operate. The considerations for the length of the cold finger included anticipated bottom ice growth, exit nozzle and support framework. As shown in Figure 4-2, the cold finger length was determined to be 165mm. This allowed for a 30mm between the bottom of the cold finger and the bottom of the vessel for anticipated ice growth. This also facilitated the 10mm exit nozzle and support framework, that kept the cold finger located in the centre of the tank.

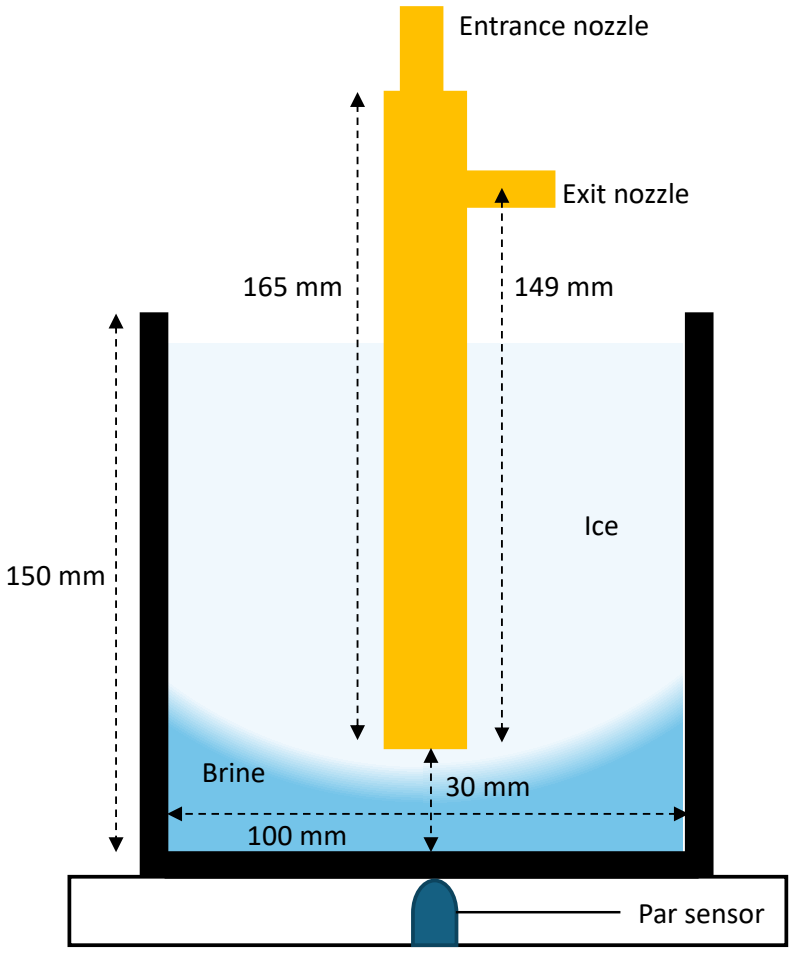

Figure 4-2: Schematic diagram of cold finger in 1-litre aquaria with basic dimensions.

The inner and outer shells of the cold finger had to be sized adequately to facilitate the flow of coolant. To address requirements, a standard 10.0 mm pipe with a thickness of 0.94 mm was utilised for the internal diameter, while a 16.0 mm pipe with a wall thickness of 1.50 mm was chosen for the outer casing. By keeping the pipe thickness to a minimum, enhanced heat transfer from the coolant to the saline solution was ensured. Refer to Figure A-1, Figure A-2 and Figure A-3 in Appendix A for engineering drawings with all the dimensions of the cold finger and the scaffolding support frame work.

4.2. Growth Dynamics

Understanding the uptake dynamics of sea ice algae involves studying the radial growth of ice from the cold finger within the 1-litre aquaria. It is important to run experiments undisturbed and unimpeded to observe dynamics more accurately. The major impedance is wall effects and therefore to mitigate these effects ice was grown up to 65% of the vessel volume (80% radially). To determine the time required for ice growth to reach this optimal extent, a rudimentary model was developed to predict ice growth over time.

4.2.1. Development of a Thermodynamic Model

A key assumption in developing this model was that the rate of ice growth is equal to the rate of heat removal through the ice. The ice growth can be modelled employing the principles of conduction as no convection occurred due to the cold finger surface being in contact with the solution at its freezing point. Therefore, the model is unable to accurately predict ice growth for solutions above their freezing point. For the detailed equations and step-by-step description of the development of the thermodynamic model, refer to Appendix B.1. This rudimentary model for predicting ice growth is a function of time is shown in Equation 4-1. Refer to Appendix B.2 for a code based on Equation 4-1 that determines radial growth as a function of time.

Equation 4-1:

$$\frac{dr}{dt} = \frac{k(T0-T1)}{\rho \Delta H_{fusion}(r-R0)\, ln\left(\frac{R0}{r}\right)}$$

4.2.2. Thermodynamic Model Application:

As mentioned previously, ice is required to grow to 80% of the vessel radius to mitigate wall effects. However, the time it takes to achieve this 80% radial growth varies with different induced cold finger temperatures. Given that the internal diameter of the 1-litre aquarium is 100mm, 80% of the aquaria radius is 40mm. Adjusting for the 8mm radius of the cold finger, the necessary ice growth radially is 32mm. The code provided in Appendix B.1 was utilised to simulate the process at different cold finger temperatures (-5°C, -10°C, -15°C). The code plots Equation 4-1 graphically as shown by Figure 4-3, illustrating ice growth as a function of time.

The time for ice growth to reach the desired 80% can be extrapolated from Figure 4-3, with each experiment duration to be 15 hours and 4 minutes, 5 hours 53 minutes and 3 hours 39 minutes for the respective cold finger temperatures of -5°C, -10°C and -15°C. Table 4-2 contains results of experimental ice growth measurements for evaluation of thermodynamic model performance. For each experiment, ice was grown in pure saltwater solution of 35 PSU salinity and the environmental temperature was set to oscillate around -1.8°C.

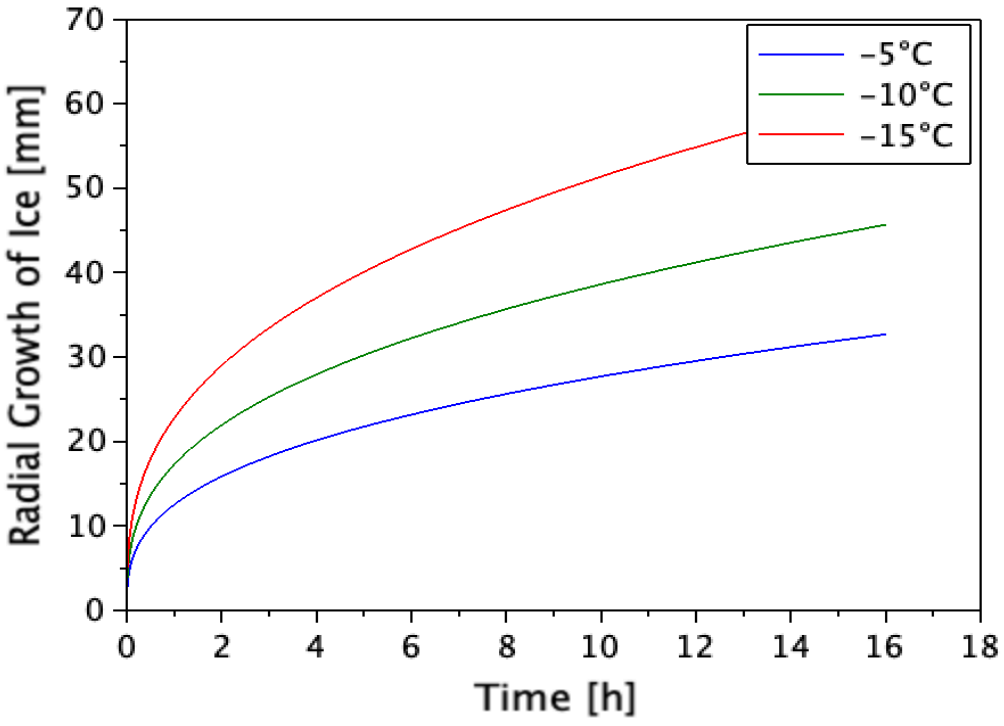

Figure 4-3: Plot of radial ice growth with time at a cold finger operating temperature of -5°C, -10°C and -15°C.

Table 4-2: Overall ice growth and performance of thermodynamic model.

Temperature (°C)	Growth Time	Theoretical Growth (Model) (mm)	Average Experimental Ice Growth (mm)	Model Performance (%)
-5	15h 4min	32	30.7	-4.3
-10	5h 53min	32	33.7	5.0
-15	3h 39min	32	31.0	-3.2

Table 4-2 indicates the thermodynamic model predicts ice growth with an acceptable accuracy with an error of $\pm$ 5.0 % for a base solution of 35 PSU and -1.8°C. The model overshoots ice growth for cold finger temperatures of -5°C and -15°C, but undershoots ice growth for -10°C. This model showed an acceptable accuracy in predicting ice growth, however this model does not account for the potential influence of sea ice algae on ice growth. The inclusion of sea ice algae in the base solution results in the inclusion of EPS as well, with increases in EPS concentration during the ice formation (Kim et al., 2023). As discussed in Section 2.4.2, the sea ice algae secrete EPS as a survival mechanism with previous studies finding altering effects of EPS on ice formation dynamics (Costa, Raaijmakers & Kuramae, 2018).

4.3. Comparing Natural Sea Ice and Cold Finger Growth Dynamics

The cold finger is useful tool to create a nucleation point for which ice growth can be induced. However, the cold finger applicability in a sea ice context must be evaluated. Cold finger ice formation is in a radial direction whereas natural ice formation which occurs in a top-down manner. For this reason, textural and structural analysis was conducted to compare whether cold finger could simulate natural sea ice dynamics. Solutions containing differing EPS concentrations was used to simulate the inclusion of sea ice algae on ice growth dynamics.

4.3.1. Experimental Methodology for Growth Dynamics Evaluation

For each experiment, ice formation was induced for 3 hours by maintaining a cold finger temperature of -15°C in a solution with 35 PSU at room temperature. The EPS concentration was varied across experiments, with concentrations of 0, 1, 10, and 1000 mg/L. Each EPS concentration was tested in triplicates to ensure robust analysis. As discussed in Section 2.4.1,

the major constituent of EPS is polysaccharides (Kim et al., 2023). The two largest monosaccharides dominating sea ice are glucose and mannose (Kim et al., 2021). Xanthan gum consists of glucose, mannose and glucuronic acid and therefore xanthan gum was used as a synthetic EPS.

The cold finger was introduced into the centre of the 1-litre aquaria and grown for 3 hours. This growth time was chosen to mitigate wall effects on ice dynamics. After 3 hours, ice was removed from the cold finger and the diameter of ice growth was measured. The ice was sectioned as per Figure 4-4 for both cross polarisation (XP) and micro-computed tomography (μCT). The ice sample was sectioned vertically down the centre into two halves, one for analysis and the other as a backup sample.

XP is an imaging technique that involves light illuminating through two polarisers placed perpendicular to each other (Hanlon, 2018). Ice samples for XP were cut into 1mm thin sections using a thermal macrotome (Johnson, 2020). These samples were placed between the polarised sheets above the light box. Due to the variation in the direction of individual ice crystals, the light reflects differently enabling the identification of individual ice crystals. Photographs of samples were taken, noting the scale, label and orientation. The images were analysed using image J software for the measurement of 20 random ice crystals (Schneider, Rasband & Eliceiri, 2012). These measurements in conjunction with the shape of the crystals was used to determine the texture.

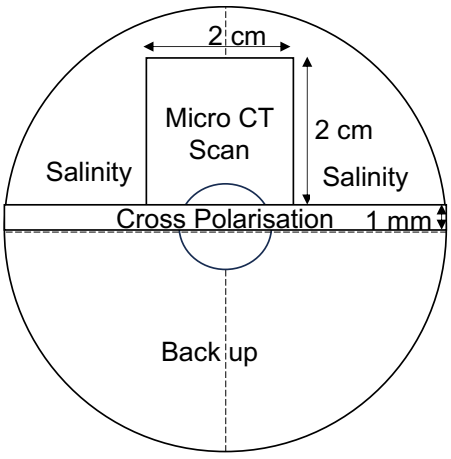

Figure 4-4: Schematic of ice sectioning for ice growth dynamic analysis, which includes samples for cross polarisation, Micro-CT scanning, salinity measurements and back up samples.

μCT scanning utilises X-rays and computer processing to generate 3D reconstructions of the internal structures of sea ice. Samples for μCT scanning were then cut using a thermal wire cutter. Samples for μCT analysis were cut into 2x2x5 cm cuboids and stored in -10°C conditions prior to and during scanning using a high-resolution Nikon XT H 225 Industrial Scanner at X-Sight X-ray Services. The μCT scans were processed using VGSTUDIO software to apply thresholds to the greyscale scans that distinguished the brine and air phases. The output of VGSTUDIO software includes properties values of each inclusion, 2D grey-scale images and 3D reconstructions of the ice, brine and air phases. The output of VGSTUDIO was analysed using a code outlined by Swait (2024). The remaining ice samples were melted, and salinity measurements were recorded, along with the underlying seawater solution that remained in the 1-litre aquaria.

4.3.2. Results of Growth Dynamics

Within the scope of this project, it is pivotal to evaluate the cold finger ability to simulate natural ice structures that allow for the natural flow of nutrients and microorganisms in the sea ice. It is important to understand how the incorporation of algae may influence the growth dynamics in this setup.

The inclusion of low concentrations of EPS (1 and 10 mg/l) in the saline solution had negligible effect on ice physical properties as shown in Table 4-3 (Refer to Appendix B.3 for all salinities and growth dimensions). There is no correlation between EPS and salinity at these low concentrations as an EPS concentration of 1mg/l has a marginally increased ice and underlying seawater salinity relative to the sample with no EPS. The 10 mg/l EPS sample had marginally lower ice and underlying seawater salinity.

Table 4-3: Summary of key finding on normalised growth dynamics at differing EPS concentrations.

EPS Concentrations	Normalised Underlying Salinity (PSU)	Normalised Ice Salinity (PSU)	Ice Growth (mm/h)
0 mg/l	1.24	0.41	23.0
1 mg/l	1.23	0.41	23.0
10 mg/l	1.23	0.41	22.0
1000 mg/l	1.04	0.88	24.7

**All salinities were normalised relative to the starting salinity of the experiment.

Similarly, ice growth rates at low concentrations had no distinct impact of EPS on ice growth. However, the experiments with high EPS concentrations (1000 mg/l) had higher ice growth rates, higher bulk ice salinities and hence decreased underlying seawater salinity. This indicates that very high EPS concentration may facilitate higher brine retention within the ice. The increased bulk ice salinities observed with the EPS concentrations of 1000 mg/l was supported by increased ice salinities in studies reviewed in Section 2.4.2 (Krembs, Eicken & Deming, 2011; Matlakala, 2022).

The most prominent difference between natural sea ice growth and cold finger ice growth is the dimensional plane of growth. Natural sea ice grows vertically, whereas cold finger ice grows radially within the horizontal plane. The effects on the orientation of crystal growth are presented in Figure 4-5. For further cross polarised images containing scale bars of sea ice grown using cold finger, refer to Table B-4 in Appendix B.3. As shown in Figure 4-5 A and Figure 4-6, the saltwater sample containing 0 mg/l of EPS exhibited randomly orientated crystal comprising granular and transitional textured ice. EPS concentrations of 1 and 10 mg/l exhibited granular, transitional and columnar textured ice. In contrast EPS concentration of 1000 mg/l was composed of columnar textured ice with no observed granular and transitional-textured ice. This observation contrasts with literature studies by Krembs, Eicken & Deming (2011), which observed randomly orientated crystal structure with samples containing Fresh Melosira EPS. However, this is supportive the study by Matlakala (2022) which observed EPS samples favouring columnar textured ice as shown in Figure 2-10 in Section 2.4.2. The extent of ice growth using the cold finger was significantly less than that of studies reviewed in literature, which may account for differences in the results (Krembs, Eicken & Deming, 2011; Matlakala, 2022).

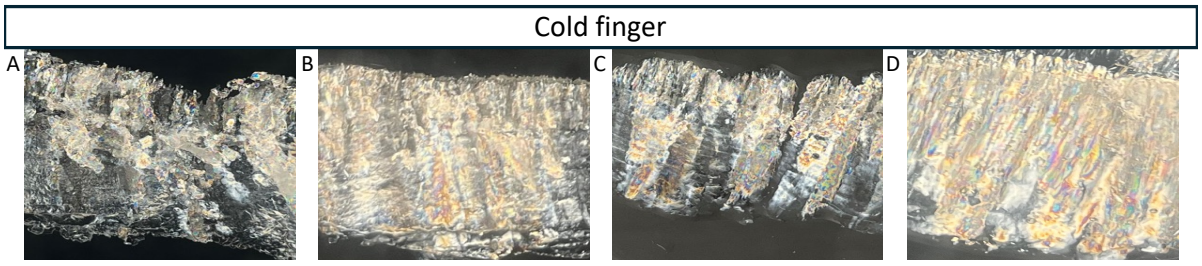

Figure 4-5: Cross polarised images of ice grown from the cold finger at differing EPS concentrations A) 0 mg/l, B) 1 mg/l, C) 10 mg/l, D) 100 mg/l and E) 1000 mg/l.

The general trend indicates increasing crystal size with increasing EPS concentrations (refer to Table B-2 in Appendix B.3 for average crystal sizes). The saltwater sample containing no EPS has a relatively larger average crystal size in the transitional zone compared to EPS concentrations of 1 and 10 mg/l which is likely due to the absence of columnar textured ice. This may have resulted in an extended transitional layer with more columnar shaped crystals. The average crystal sizes in the transitional zone increased as EPS concentration increased, which indicates the presence of more columnar shaped crystals. Thus, the presence of EPS favoured ordering of ice crystals in the radial plane and therefore the formation of columnar textured ice (Figure 4-6).

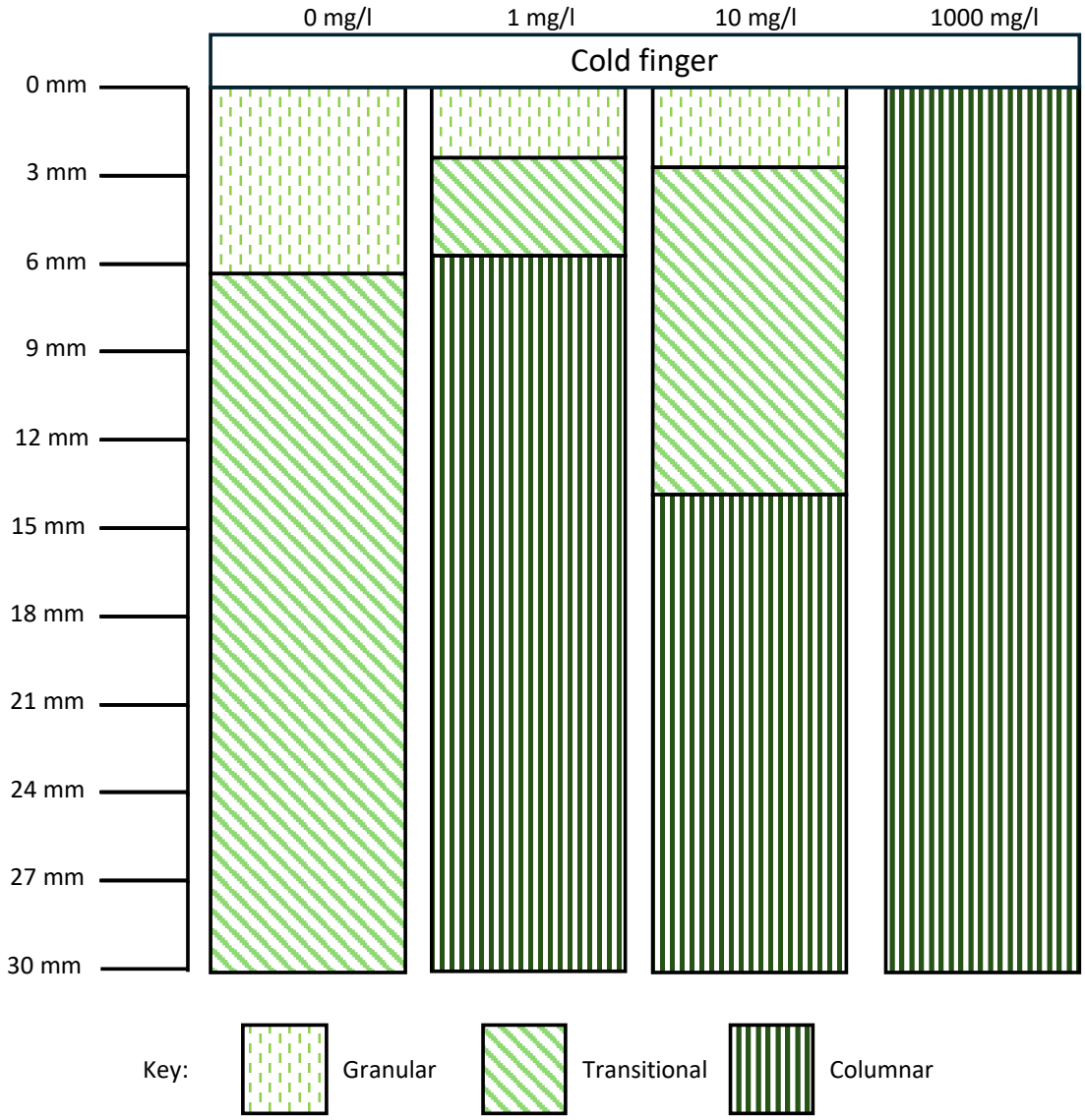

Figure 4-6: Stratigraphy diagram of ice grown from the cold finger at varying EPS concentrations (0, 1, 10, 1000 mg/l).

Brine inclusions in natural sea ice form vertically elongated channel-like structures within columnar-textured ice as discussed in Section 2.2 (Weeks & Ackley, 1982; Gow & Iii, 1991). Brine inclusions within this study would be expected to occur mainly horizontally due to the radial growth causing crystal orientation in the horizontal plane. However, as shown in Figure 4-7, brine inclusions are slanted downwards off the horizontal plane, suggesting that gravity influences the orientation of the brine inclusions (refer to Table B-5 in Appendix B.3 for 2D grey scale and 3D reconstructed images of all EPS concentrations).

Within ice samples containing EPS, there is an observed general trend of increased brine and air porosity with the EPS concentration of 1000 mg/l compared to no and lower EPS concentrations. In contrast, the number density of both brine and air inclusions observed in Figure 4-8 do not indicate any significant trend due to the presence of EPS. Krembs, Eicken & Deming (2011) observed increased brine inclusion number density. The increased porosity in conjunction with steady inclusion number density and the 2D grey scale images found in Table B-5 in Appendix B.3 suggests more elongated and interconnected brine channels in samples that contain higher concentrations of EPS. This supports observations found in both studies (Krembs, Eicken & Deming, 2011; Matlakala, 2022).

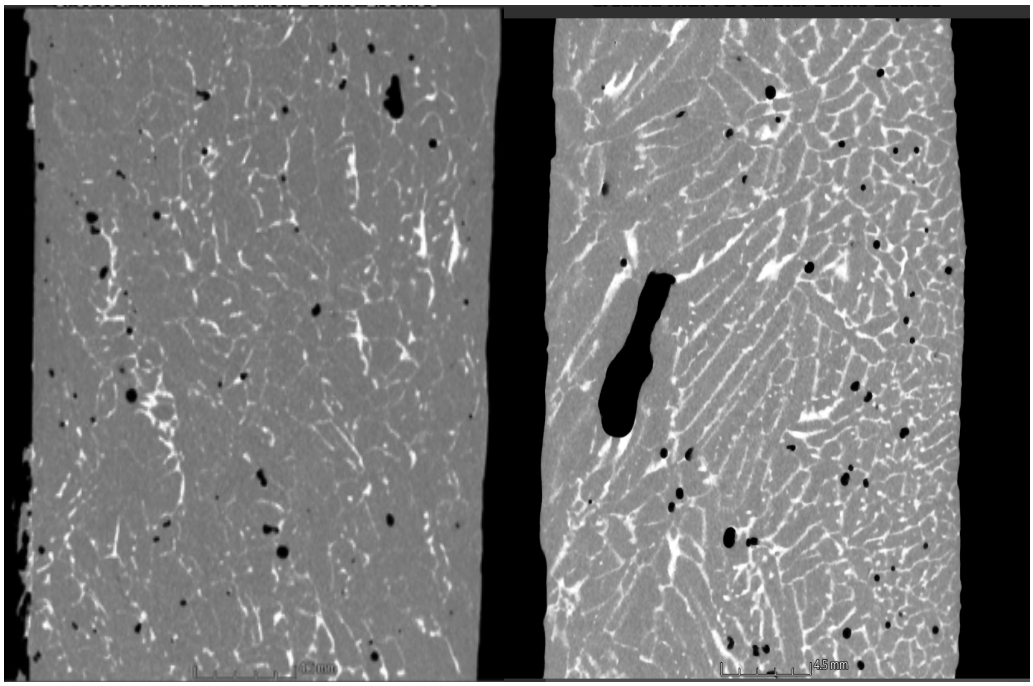

Figure 4-7: Grey scale image slice from CT scan at different EPS concentration of 0 mg/l (left) and 1000 mg/l (right).

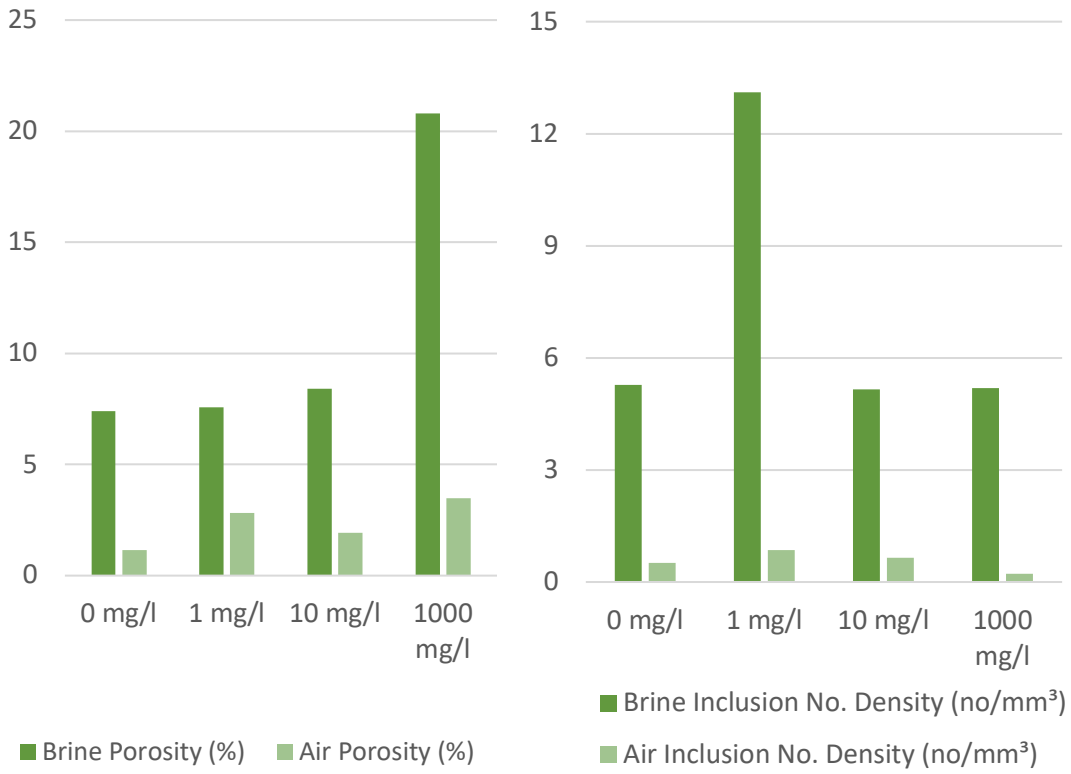

Figure 4-8: Summary of air and brine inclusion characteristics at differing EPS concentrations (0, 1, 10, 1000 mg/l) with (Left) illustrating ice porosity and (right) illustrating inclusion number density. The figure indicates EPS has no effect on inclusion characteristics.

4.3.3. Discussion Cold finger Growth Dynamics

The results of this study provide insight into the ability of the cold finger to simulate natural ice formation dynamics. By comparing the ice growth and physical properties of samples with varying EPS concentrations to natural sea ice, this study highlights similarities and differences in ice formation dynamics that sea ice algae may cause. This provides a better understanding of how the cold finger will perform during sea ice uptake dynamic experiments. The lower concentrations of EPS (1 and 10 mg/l) investigated in this study are representative of levels found in natural sea ice as discussed in Section 2.4.1 (Dumont et al., 2009; Underwood et al., 2010; Krembs, Eicken & Deming, 2011; Kim et al., 2021, 2023).

At low EPS concentrations, no significant changes were observed in growth rates and bulk salinities, suggesting that sea ice algae have minimal impact on physical properties of the ice. In extremely high EPS concentrations (1000 mg/l) EPS was found to increase bulk ice salinities

and growth rates. With increasing EPS concentrations, columnar textured ice was favoured. This suggests that the sea ice algae may influence the crystal structure by promoting more ordered crystal orientation. The increased brine and air porosity in EPS samples, particularly at high EPS concentration, suggest that sea ice algae may aid in the formation of larger more interconnected inclusions. This supports observations of higher bulk salinities at higher EPS concentrations (Krembs, Eicken & Deming, 2011; Matlakala, 2022).

The most prominent difference in dynamics between natural sea ice and cold finger ice growth is the direction of ice growth. The natural direction of sea ice is in the vertical plane influencing crystal orientation and inclusions (Petrich & Eicken, 2017). The radial ice growth induced by the cold finger appears to result in horizontal crystal orientation. However, inclusions were primarily slanted downward from the horizontal plane, suggesting that gravity may influence inclusion orientation in addition to the direction of ice growth. This indicates that ice growth induced using a cold finger could allow for natural convective flows of brine in the ice and hence facilitate natural nutrient and biological exchanges.

5. Design and Optimisation of Cold Finger Experiment Methodology

The design and optimisation of the cold finger as discussed in Section 4, provided a useful tool for ice growth and an understanding into the dynamics of ice growth associated with the cold finger. In the context of this study, achieving robust and reproducible results requires iterative modifications of the experimental and analytical methods. This section covers the development of a methodology that enables the investigation of uptake dynamics of sea ice algae into artificial sea ice.

The sea ice algae used in this study were sourced locally due to the limitations associated with collecting sea ice algae from the Marginal Ice Zone of Antarctic. Therefore, Antarctic sea ice algae strains that could be sourced locally was limited. Two pennate diatom species, *Cocconeis sp*. and *Pseudo-Nitzschia sp*., were locally sourced and classified at the genus level for this study. *Cocconeis sp.* are relatively small diatoms with an oval or elliptical shape, while *Psedo-nitzchia* are relatively large diatoms with an elongated, rectangular morphology (Figure 5-1). The size ranges of both diatoms in this investigation are illustrated in Figure 5-1, with Cocconeis sp. ranging from 5-13μm and *Pseudo-Nitzchia* ranging from 8-26μm. The smaller sized *Pseudo-Nitzchia sp.* as shown in Figure 5-1 are generally after cell division has occurred. The differences in cell shapes and sizes between the two species*, Cocconeis Sp*. and *Pseudo-Nitzchia sp.*, aid in investigating how the morphology the species impacts uptake dynamics.

Small quantities available of each diatom species required culturing to achieve the necessary concentrations and volumes for experimentation. Each species was cultured separately for 2 months using F2 medium and sterilised filtered seawater (Vaulot et al., 2023). The culturing environment included a temperature of 8°C, continuous aeration and periodic grow lights on 12-hour cycle. Once species populations were sufficiently dense, the two species were combined and cultured under the same conditions for additional 2 months. After the community stabilised, the environmental temperature was gradually reduced to 2°C to minimise temperature shock during the experiments. This served as the base culture from which the 1-litre aquaria would be filled for experimentation.

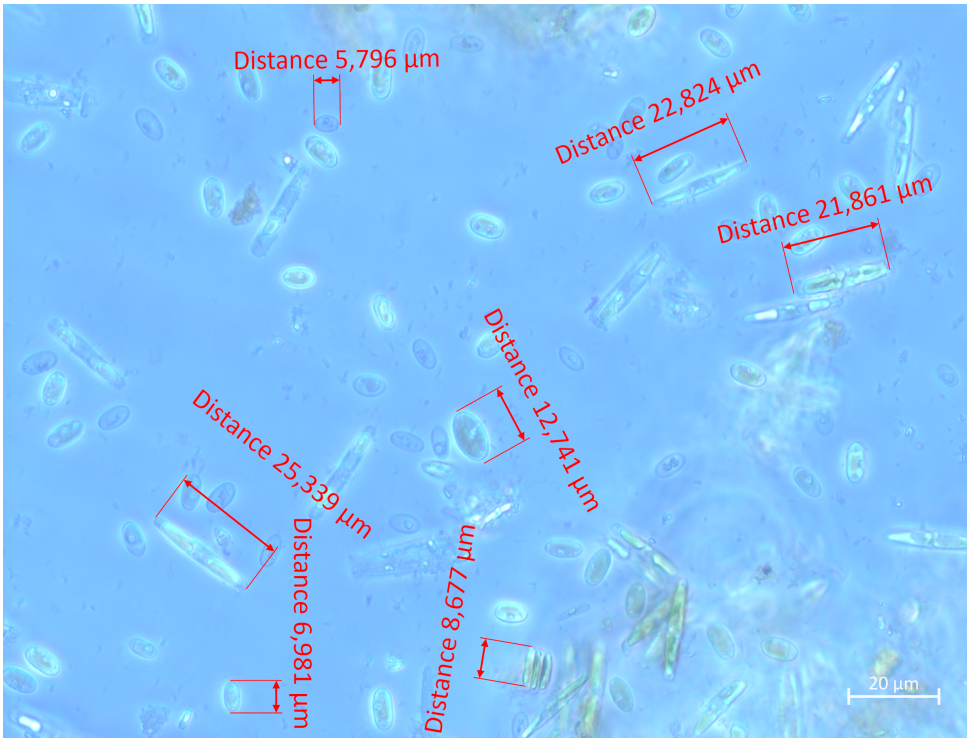

Figure 5-1: Microscope photograph illustrating size ranges of Cocconeis sp. and Pseudo-Nitzchia sp.

Cold Finger experiments were performed to create insights into sea ice algae uptake dynamics with changing environmental conditions due global warming. Three experiments were performed: the first experiment with an irradiance of 0 µmol.photons.m^{-2}.s^{-1} and an ocean temperature of -1.8°C, the second experiment with an irradiance of 30 µmol.photons.m^{-2}.s^{-1} and ocean temperature of -1.8°C and a third experiment with an irradiance of 30 µmol.photons.m^{-2}.s^{-1} and ocean temperature of 0°C. In each of these experiments ice growth was induced using the cold finger at -5°C, -10°C and -15°C.

As discussed in Section 4.1, the cold finger experiments are housed in the environmental chamber (Figure 4-1). The environmental chamber includes light bar and radiator to control the light and temperature conditions. Shown in Figure 4-1, CS310 Quantum PAR sensors are located beneath the 4 tanks, with the PAR sensors connected to the Campbell Scientific CR300 data logger. The data logger records the light readings on the PAR sensors periodically at set time intervals. The cold finger is supported in the centre of the 1-lire aquaria by an adjustable Perspex scaffolding (Figure 4-1).

The design and optimisation of the experimental methodology occurred over three iterations, namely the initial experiment, the first optimisation experiment and the fully optimised experiment. The designing and optimising of the experimental methodology was conducted and repeated under controlled conditions to ensure comparable results. The environmental chamber maintained consistent parameters, simulating typical winter conditions with no light and an ocean temperature of -1.8°C.

The basic experimental methodology outlined in Figure 5-2 was used in the three iterations of design and optimisation. The experimental methodology was broken down into 3 sub-methods. The first sub-method is experimental procedure which is highlighted by the red dotted line and contains the acclimatisation of the sea ice algae, ice formation and segmenting. The second sub-method is highlighted by the blue dotted line and is the processing of samples. The final sub-method is analysis and refinement of data from sub-method 2 and is highlighted by the green dotted line.

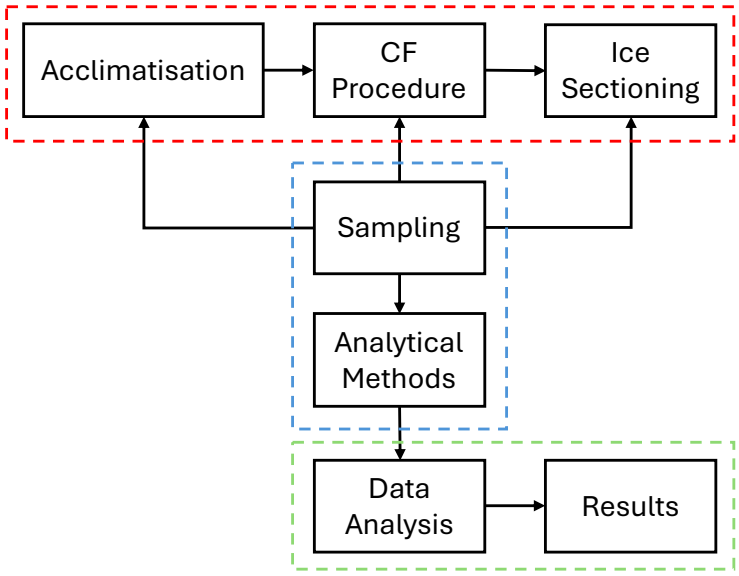

Figure 5-2: Flow chart of the basic experimental skeleton of the cold finger experiments.

5.1. Experimental Procedure

As discussed in Section 2.1.2, sea ice algae are sensitive to change in their immediate environment and specifically to temperature, salinity, irradiance and nutrients. Thus, the initiation of the experimental procedure begins with the acclimatisation of sea ice algae to the

new experimental conditions in the environmental chamber. As outlined in Section 4.1, each experiment requires 4 aquaria, 3 containing sea ice algae and 1 control (a pure saline solution). The sea ice algae stock was removed from the base culture and transferred into each 1-litre aquarium. The algae undergo a 10-day acclimatisation period to adjust to the new irradiance and temperature conditions prior to inducing ice conditions. Throughout the 10-day acclimatisation period, the algae were stirred daily to compensate for the lack of mobility of diatoms (Miklasz & Denny, 2010). Samples were taken periodically from each 1-litre aquaria during the 10-day acclimatisation to measure their concentrations.

After completion of the 10-day acclimatisation period, the cold finger procedure could begin. The cold finger procedure starts by setting the chiller controlling the cold finger temperature to a desired temperature. On reaching the desired temperature, the cold finger was subsequently placed and submerged in the centre of the first 1-litre aquaria. The experimental duration was in accordance with the time generated by the thermodynamic model in Section 4.2.2.

Additionally, ice diameters were not measured in the initial experiment, however in the first optimisation and fully optimised experiments, ice diameters were measured. The first optimisation experiment observed smaller diameters than the required 80% of the vessel diameter as shown in Table 5-1. This was attributed to bends in pipes hindering the supply of the low temperature ethylene glycol coolant to the cold finger. For the fully optimised experiment, ice was removed from the cold finger, once ice growth was in a 5% region of the desired 80% ice growth. This ensures that relatively the same amount of ice was collected for comparable uptake dynamics. The times generated by the thermodynamic model served as the minimum time required for ice growth to reach 80% of the vessel diameter. This became more applicable for future experiments where the ocean temperature was above the freezing point of sea water. The thermodynamic model was strictly designed using conductive heat transfer and does not incorporate the time required for convective heat transfer to lower the sea water to its freezing point. Additionally, this accounts for any faults by equipment that may affect experimental output.

Once the ice reached the approximate desired growth, it was removed from the cold finger. For the preservation of ice, the temperature on the chiller was set to above freezing point of saltwater to ease ice detachment from the cold finger without damaging the ice sample. Subsequently, the ice was sectioned and sampled as per Figure 5-3. The process was repeated for the other cold finger temperatures.

Table 5-1: Ice growth dimensions and times for optimisation experiments.

	Theoretical Growth (model)		Initial Experiment		First Optimisation Experiment		Fully Optimised Experiment	
	Time	Size (mm)	Time	Size (mm)	Time	Size (mm)	Time	Size (mm)
-5°C	15h 4 min	80.0	15h 4 min	-	15h 4 min	72.0	15h 5min	80.0
-10°C	5h 53min	80.0	5h 53min	-	5h 53min	80.0	6h 5min	81.4
-15°C	3h 39min	80.0	3h 39min	-	3h 39min	64.4	3h 45min	81.6

All ice segments were sectioned using a thermal wire cutter made of a Nickel and Chrome (NiChrome). The thermal wire cutter reduces melting of the sample to only the ice in contact with the wire. The ice samples removed from the cold finger were sectioned for the initial experiment as per Figure 5-3 A. The samples were originally segmented into two halves by cutting the ice vertically down the centre. The left side was further sectioned horizontally to create a horizontal profile with ice depth, consisting of four ice segments. The right side was reserved as a backup for potential further analysis. However, this method of ice segmentation was limited to horizontal profiles and, as a result, failed to account for the uptake profile in the radial direction of ice growth.

To address this limitation of initial ice segmentation, the experimental setup for both the first optimisation and fully optimised experiments transitioned to the ice segmentation approach shown in Figure 5-3 B. The ice samples removed from the cold finger were sectioned vertically down the centre. The left side was sectioned vertically to create a profile of sea ice algae at different radial measurements, while the right-hand side was sectioned horizontally to create a profile with ice depth (along length of cold finger). Both the vertical and horizontal profiles consist of 3 ice segments. The vertical profile does not mimic the radial ice growth exactly,

which was attributed to the difficulty of sectioning the ice in a radial manner. Hence the ice was segmented using straight lines.

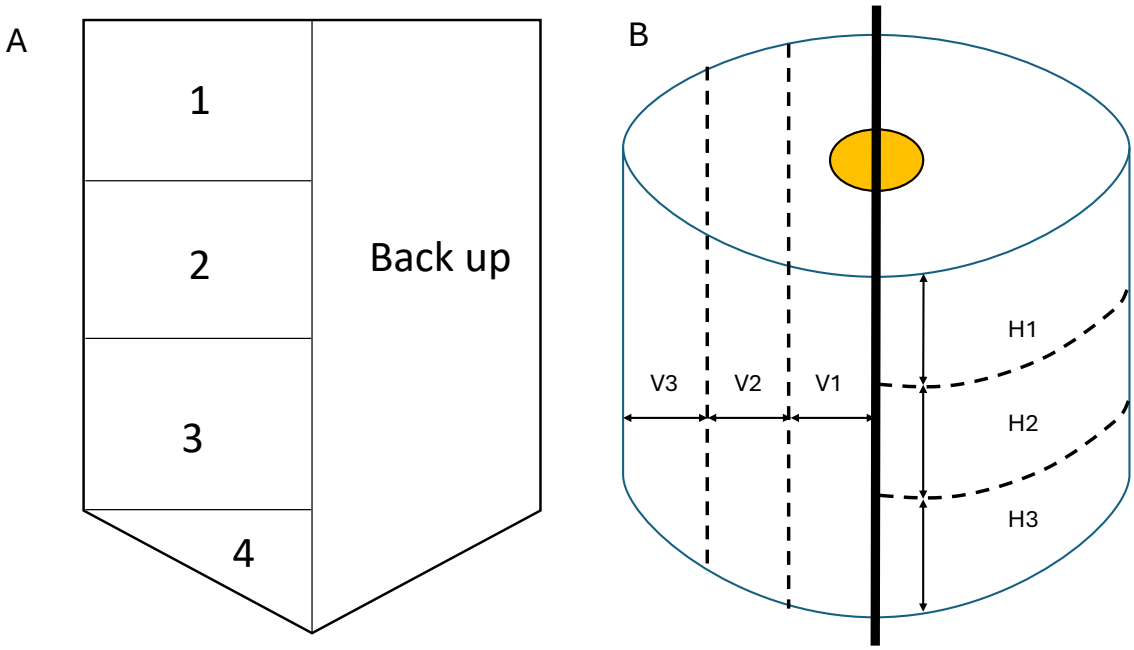

Figure 5-3: Schematic diagram of (A) initial and (B) optimised ice sectioning for cold finger experiments.

Sampling was required for analytical analysis, salinity and volume measurements. Salinity measurements were not included initially but were incorporated during the first optimisation and final optimised experiments. After evaluating the first optimisation experiments, it became evident that absolute cell counts necessary for quantifying overall uptake, could not be determined without volume measurements. Therefore, for the fully optimised experiment, volume measurements of ice sections were recorded. Measurements for both salinity and volume were taken at the beginning of the experiment, the underlying seawater salinity after ice removal, and from each ice profile as shown in Figure 5-3 B. Volumes measurements were taken before analytical samples collection.

During the initial experiment, 0.5ml samples for flow cytometry were collected on day 0, 2, 4, 6, 8, 10 and from each ice section as per Figure 5-3. However, the underlying seawater solution was not sampled, making it unclear whether sea ice algae cells were dying during ice formation or if diatoms were simply excluded from the ice. Flow cytometry samples were preserved with poloxamer (10%) and glutaraldehyde (25%). For the first optimisation and fully

optimised experiments, flow cytometry sample volumes were increased from 0.5 ml to 1 ml due to low cell concentrations in the ice, which resulted in extended flow cytometer run times and therefore increased usage of sample volume. 10 µL of poloxamer and 10 µL of glutaraldehyde per 1ml of sample were added to the cryovials containing samples. After adding the preservatives, the samples were incubated for 10 minutes at room temperature before being stored at -20°C until analysis. The sampling days during acclimatisation remained the same, while the sampling of ice changed to ice sections in Figure 5-3 B. Additionally, the underlying seawater solution was sampled.

Time constraints associated with microscopy resulted in few sampling days during acclimatisation and thus samples are collected on day 0, 5 and 10. Microscopy requires preservation with Lugols solution. 10µL of Lugols solution per 1ml of sample was added into the falcon tubes containing the sample. Samples were stored at room temperature in complete darkness until analysis. For both the first optimisation and fully optimised experiments, microscopy samples followed the same sampling locations as flow cytometry.

5.2. Analytical Methods

To fully analyse the uptake, the dynamics of sea ice algae into sea ice, population mapping of the algae communities must be quantified. Qualitative and quantitative analysis techniques for sea ice algae include molecular based methods, filtering, microscopy and flow cytometry (Karlson et al., 2010).

Filtering techniques are generally implemented as concentration steps of algae species with low cell densities and therefore implemented as a precursor to other counting methods (Anderson, 2010; Cembella & Rafuse, 2010; Dahl & Nautsvoll, 2010; Moncheva, 2010). Molecular-based techniques eliminate limitations of alternative algae analysis methods which depend on morphological identification (Karlson et al., 2010). However, molecular techniques require extensive data bases to identify algae species and therefore algae identification is limited to known species (Karlson et al., 2010).

Microscopy techniques are suitable and for identification and enumeration of sea ice algae species. Microscopy identifies algae species by their morphological structure or other defining characteristics (Karlson et al., 2010). Microscopy has three methods, namely the counting chamber methods, settlement bottle method and the Utermohl method (Edler & Elbrächter, 2010; LeGresley & McDermott, 2010; McDermott & Raine, 2010). The counting chamber methods are used as quantitative methods for high concentration sea ice algae cultures (LeGresley & McDermott, 2010). Both, the Utermöhl and settlement bottle methods are useful for quantifying and characterising algae communities (Edler & Elbrächter, 2010; McDermott & Raine, 2010). However, the Utermöhl method has a higher level of optical resolution, making it particularly useful for identifying new and previously known species in sea-ice biology (Edler & Elbrächter, 2010; McDermott & Raine, 2010).

In contrast to microscopy, flow cytometry is a rapid method of cell analysis. While flow cytometry is a rapid cell counter, cell sorting is based on fluorescent signals and size (Hyka et al., 2013). Flow cytometry is a more efficient method of analysis as it provides faster analyses and reduces human input and, hence human error.

5.2.1. Flow Cytometry

The availability of equipment and applicability of analysis technique guided the choice of analysis technique to map algae population. For the initial experiment flow cytometry was chosen for its ability to quickly analyse samples while requiring small sample volumes, with the expectation that it would provide cell counts for individual species. Flow cytometry samples were run using A5 Symphony flow cytometer at the Institute of Infectious Disease and Molecular Medicine at UCT. The flow cytometer records the fluorescents emitted by the diatoms cells as the cells run past a laser beam. This allows for analysis of cells based on size and fluorescent. Generally, chlorophyll a and other pigments contained in diatoms are detected in yellow-green wavelengths and hence diatom cultures were analysed using yellow-green wavelength on the A5 Symphony.

Thresholding on the A5 Symphony was important for excluding noise and smaller bacteria and therefore primarily including diatoms. The starting point for threshold parameters were based

on values for analysing bacteria and small diatoms. Thus, the thresholds parameters for the initial experiment were 512 for forward scatter (FSC) and 211 for side scatter (SSC). This ensured that data recorded outside of the threshold settings was excluded and therefore reduce the noise collected. The output data recorded on the A5 Symphony was exported and analysed using FlowJo™ v10.8 Software (BD Biosciences., 2023). In the Flowjo™ v10.8 Software, cells were plotted using FSC and yellow-green 670mm wavelength. Cells were manually separated (gated), with cells counts being exported to excel for concentration calculations.

In the initial experiment, it was observed that the two diatom species had merging fluorescent signals on the Flowjo™ v10.8 Software plots and therefore quantification of individual species was not possible. However, with the use of size beads run on the A5 Symphony, the flow cytometry results could be quantified based on size classes (refer to Figure C-1, Figure C-2 and Figure C-3 in Appendix C for results of the initial experiment and the first optimisation experiment). The results of the size classes indicated that thresholds parameters were set incorrectly and therefore excluded larger nano-eukaryotes. Thus, uptake dynamics were based primarily off bacteria and small diatoms and thus not representative of the entire population. To incorporate the larger diatoms in the flow cytometry analysis, the thresholds parameters were adjusted. Samples were taken from the base culture and run, adjusting thresholding parameters accordingly. Optimal thresholds were determined to be 100 for FSC and 200 for SSC, which were subsequently applied to both the first and final optimised experiments. Individual diatom cultures (separate from the base culture) were analysed to isolate individual diatom populations in the base culture. While some individual species were distinguishable, significant overlap between populations was observed (Figure 5-4). This was likely attributed to smaller sized *Pseudo-nitzchia sp.* after cell division. Consequently, flow cytometry was primarily utilised to map absolute diatom concentrations and monitor trends in uptake dynamics.

Portions of diatom fluorescent signals merged with bacteria and noise (Figure 5-5). This resulted in difficulty in manually separating the diatoms from the noise and bacteria. For this reason, the FlowSOM algorithm, a clustering and visualisation technique was used to separate out merging populations by using self-organising maps (Van Gassen et al., 2015).

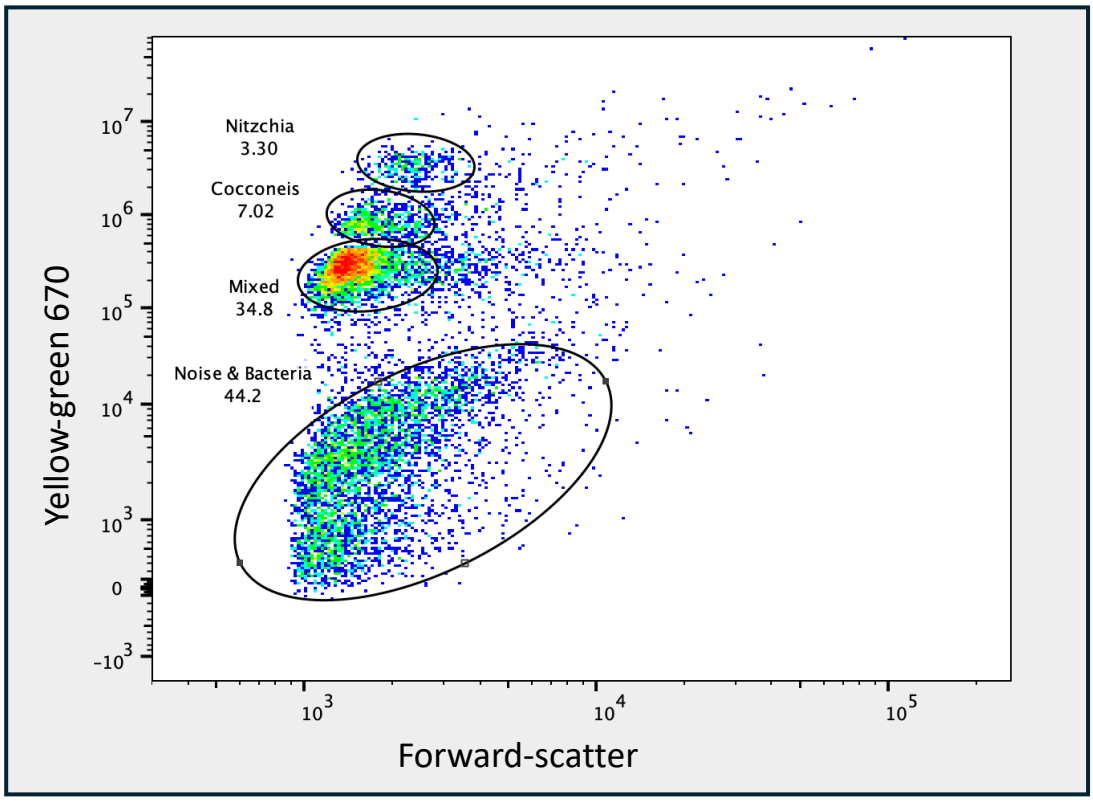

Figure 5-4: Flow cytometry plot for a sample during acclimatisation comparing scatter of data on yellow green wavelength and forward scatter.

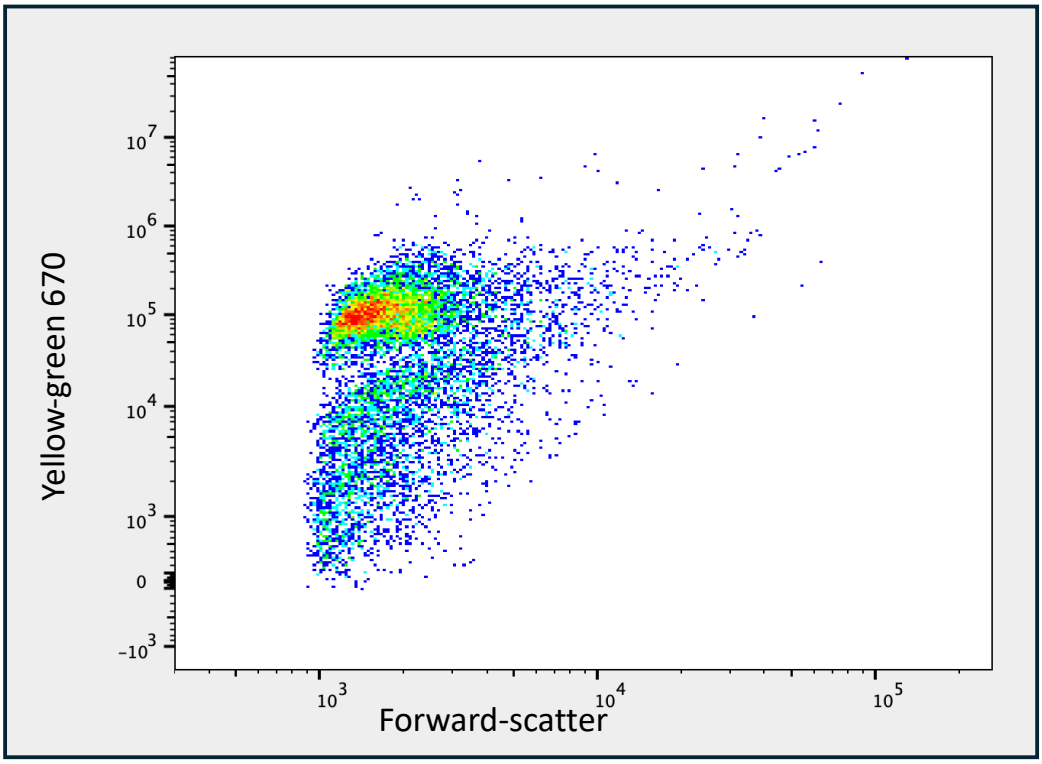

Figure 5-5: Flow cytometry plot of sample from ice comparing scatter of data on yellow green wavelength and forward scatter.

Two additional challenges with flow cytometry arose during sample processing. Initially, the sample run times were excessively long due to blockages in the A5 Symphony flow cytometer and the low cell concentrations in ice samples. To address these issues, samples for both the first and fully optimised experiments were sonicated for 10 minutes to break up cell agglomerates due to cell clustering. The sonicated samples were then pipetted through 35µm filters to remove any large clusters and biofilm that could potentially block the flow cytometer. For the first optimisation experiment, the flow rate of the A5 Symphony was increased from low to medium, ensuring that the event abortion rate remained below 5%. While this adjustment improved the speed of sample analysis, run times were still lengthy. Consequently, for the fully optimised experiment, the flow rate was further increased to high, significantly reducing run times and hence operating costs.

5.2.2. Microscopy

The inability of flow cytometry to quantify individual species necessitated the inclusion of an additional analysis technique to count diatom species individually. The Utermöhl counting method using microscopy was employed for this purpose. Samples were allowed to settle for 24 hours before analysis to ensure all cells had settled at the bottom of the slides. Microscopy slides were then examined using a Zeiss Axio Observer Inverted Microscope. To prevent bias, 15 randomly selected fields of view were counted at 630x magnification, with images of each field captured and saved for reference (can produce on request). This procedure was followed for both the first optimisation and fully optimised experiments.

During the first optimisation experiment, the cell density in the underlying seawater solution samples was exceptionally high, leading to significant cell clustering (Figure 5-6). Ice formation reduces the volume of the underlying seawater solution, causing high cell agglomerates and detritus accumulation likely due to the bottle effects (Fogg & Calvario-Martinez, 1989). As a result, cell counts were estimated rather than precisely measured. To address this, the fully optimised experiment included dilution of the sample using filtered sea water to reduce clustering and allow for more accurate cell counting (Figure 5-6).

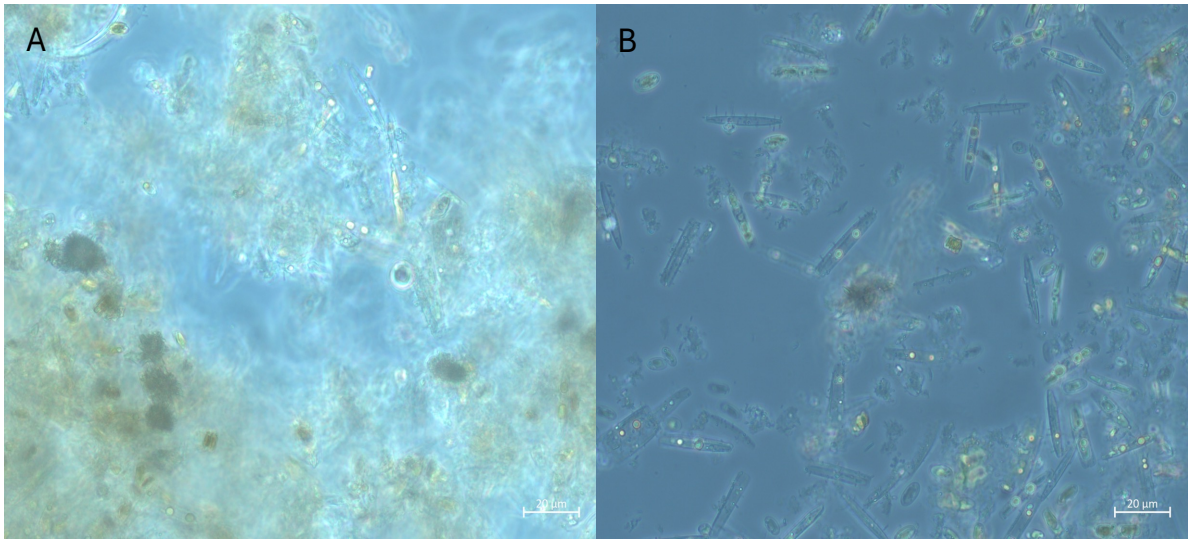

Figure 5-6: Microscopy images illustrating cell density A) before dilution and B) after dilution.

6. Impacts of Changing Environmental Conditions on Sea Ice Algae

This section presents the results and discussion of the investigation into the responses of sea ice algae to changing environmental conditions during acclimatisation and ice formation. The studies focuses on key factors, including variations in light intensity, ocean temperature, and atmospheric temperature. The impact of these factors was analysed to determine their influence on the sea ice algae growth and uptake dynamics into ice. Ice growth was induced using a cold finger apparatus which was designed and optimised in Section 4. The methodology in Section 5 was employed to study the uptake dynamics of sea ice algae into artificial ice grown using the cold finger designed in Section 4. The experiments yielded cell concentration data from two analysis techniques: flow cytometry and microscopy. Flow cytometry enabled more frequent sampling and provided total cell concentration of the sea ice algae community, while microscopy facilitated species-specific analysis of sea ice algae communities within samples.

Each experiment involved tanks with varying initial cell concentrations. To ensure meaningful comparisons between datasets, the data was normalised. Normalisation scales the data to a relative baseline, making it more comparable and easier to interpret. For acclimatisation, cell concentrations were normalised to the starting concentrations recorded on day 0. During the cold finger procedure, cell concentrations were normalised to the concentrations measured on day 10, which marked the start of the procedure and represented the sea ice algae concentrations at that time.

6.1. Comparison of Flow Cytometry and Microscopy

For more robust assessment of results, it is important to determine the comparability of trends in normalised cell concentrations reported using microscopy and flow cytometry. Statistical analyses were conducted to evaluate the degree of agreement between these two datasets. Flow cytometry and microscopy datasets for both acclimatisation and cold finger procedure were compared graphically and using parametric statistical tests to evaluate the significance of differences in variability and mean of normalised cell concentrations.

Initially, F-tests were conducted to compare the variances of the two datasets. The F-test aids in determining whether the variability in normalised cell concentrations measured by the two methods was statistically different. The results of parametric statistical test can be found in Table E-1 to Table E-4 in Appendix E.

Table 6-1: Summary of p-values from both F-tests and t-test comparing flow cytometry and microscopy normalised cell concentrations.

	P-value	
	Acclimatisation	Cold Finger Procedure
F-test	0	5.38-09
T-test	5.26E-13	1.86E-07

The results of the F-test indicated unequal variances. This suggests that the two methods exhibit differing levels of variability, which led to the application of a t-test for unequal variances to evaluate differences in mean cell concentrations for both acclimatisation and CF procedure. For comparison, t-tests were performed using data from acclimatisation on Day 0 and Day 10, as these were the only common data points available. The p-values in Table 6-1 indicate differences in mean cell concentrations are highly statistically significant at 5% significant level for both acclimatisation and CF procedure. This was evident in the experiment conducted with no light and an ocean temperature of -1.8°C as shown in Figure 6-6-1 and Figure 6-2.

During acclimatisation, flow cytometry samples exhibited higher cell concentrations on different sampling days, whereas CF procedure, microscopy showed higher cell concentrations at various sampling positions. Similar trends were observed for experiments conducted at different light and ocean temperature conditions as shown in Figure D-4 to Figure D-19 in Appendix D.4, which are consistent with the p values in Table 6-1. The overestimation of cell counts in flow cytometry may be attributed to the inclusion of noise caused by electronic interferences in the flow cytometer. On the other hand, microscopy tends to underestimate cell counts due to visual limitations and the potential for overlapping or superimposing cells, making it difficult to distinguish individual cells accurately.

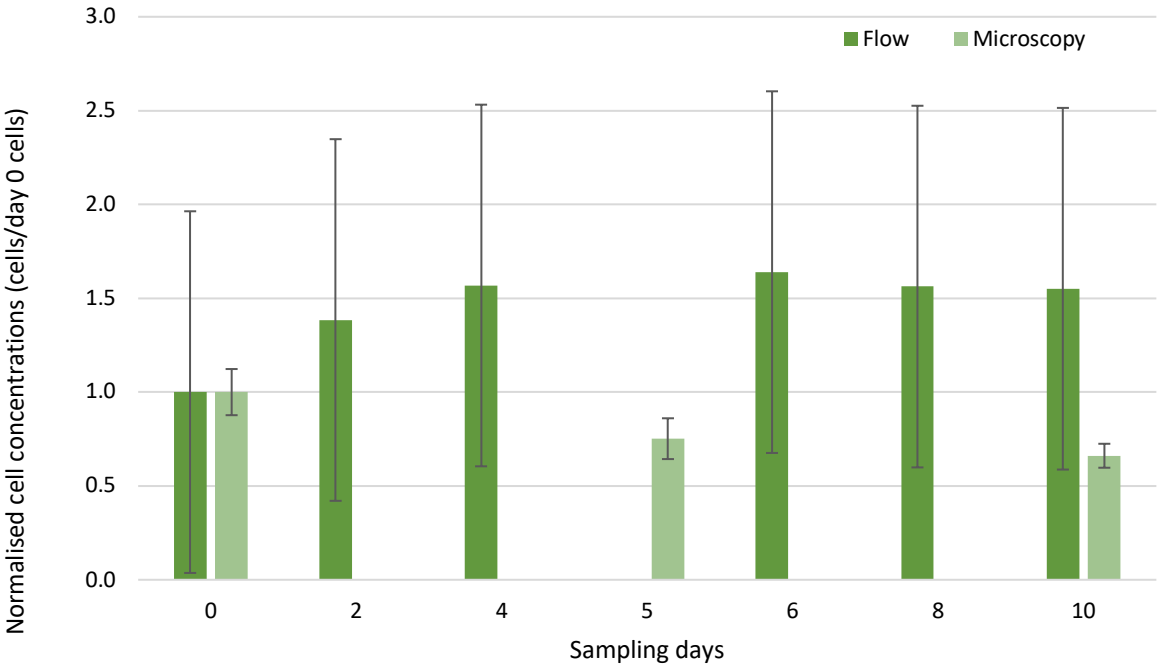

Figure 6-6-1: Normalised cell concentrations in the -10℃ tank comparing flow cytometry and microscopy during acclimatisation with no light and ocean temperature of -1.8℃.

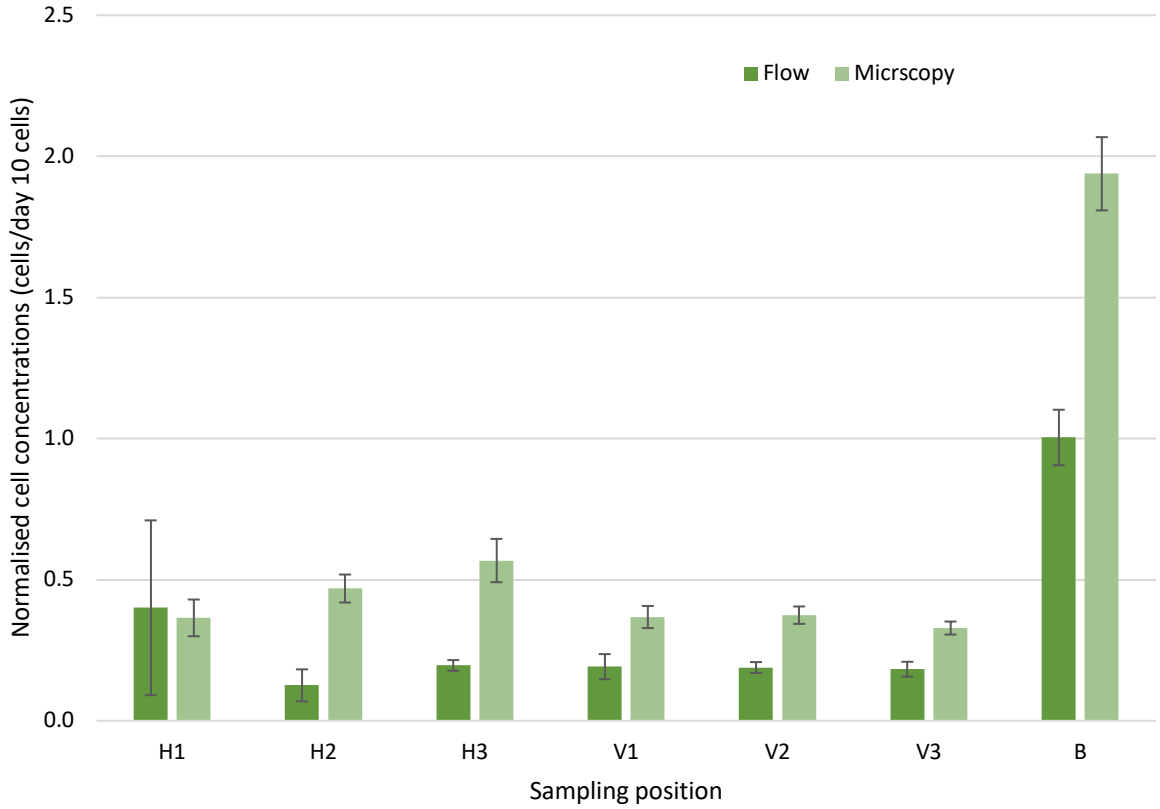

Figure 6-2: Normalised cell concentrations for atmospheric temperature of -10℃ comparing flow cytometry and microscopy uptake dynamics with no light and ocean temperature of -1.8℃.

The results of the statistical analysis indicate significant differences in variability and mean normalised cell concentrations between both analysis methods. These differences suggest that the two techniques are not directly comparable and should be analysed independently while considering their strengths and limitations. The discrepancy amongst analytical methods suggest one method may be more suitable for this investigation.

Microscopy is a well-established method for counting cells, with downsides in slow processing time and potential human bias. Flow cytometry provides high processing ability and elimination of human bias. While flow cytometry is commonly used to analyse algae cells, its application to sea ice algae is less common, as these organisms tend to form aggregates and biofilms, which complicate flow-based counting and analysis (Arrigo, Mock & Lizotte, 2010; Cheah & Chan, 2022) . According to Peperzak et al. (2020), flow cytometry accurately counts cells between 2–10 µm and remains reasonably accurate for the lower range of 10-50 µm, but accuracy decreases for cells above 50 µm and at high cell concentrations within the 10-50 µm range. Microscopy was found to be more accurate for higher cell concentrations and larger cells above 50 µm (Peperzak et al., 2020). Based on cell aggregates, biofilm, larger size cells and high cell concentrations, it is likely that flow cytometry struggled to accurately count the larger Pseudo-nitzschia sp. populations. In this project, both analysis techniques revealed general trends; however, microscopy provided more reliable and consistent data.

6.2. Comparing The Effect of Different Environmental Conditions on Sea Ice Algae Growth

The datasets of both microscopy and flow cytometry were analysed using graphical analysis and parametric statistical tests to evaluate the significance of differences in mean of normalised cell concentrations under various environmental conditions. Single-factor ANOVA tests were conducted to evaluate the influence of different environmental conditions on sea ice algae growth and uptake dynamics. The single factor ANOVA evaluates how ocean temperatures and light conditions influence growth patterns during acclimatisation, and their effect on algae uptake into the ice at different atmospheric temperatures. All ANOVA tests were conducted at a 5% significance level with results found in Appendix E.

6.2.1. Acclimatisation

Single-factor ANOVA tests were additionally used to determine whether changes in normalised cell concentrations occurred during acclimatisation. The flow cytometry results illustrated in Figure 6-3, indicated changes in normalised cell concentrations. This was consistent with the p-values in Table 6-2, which indicated statistical significance in differences in normalised cell concentrations across differing sampling days for each experiment. Graphically in Figure 6-3, experiments with no light and light at an ocean temperature of -1.8°C experienced increases in normalised cell concentrations from the initial starting cell concentration. In comparison the experiment conducted with light at an ocean temperature of 0°C, exhibited decreases in normalised cell concentrations.

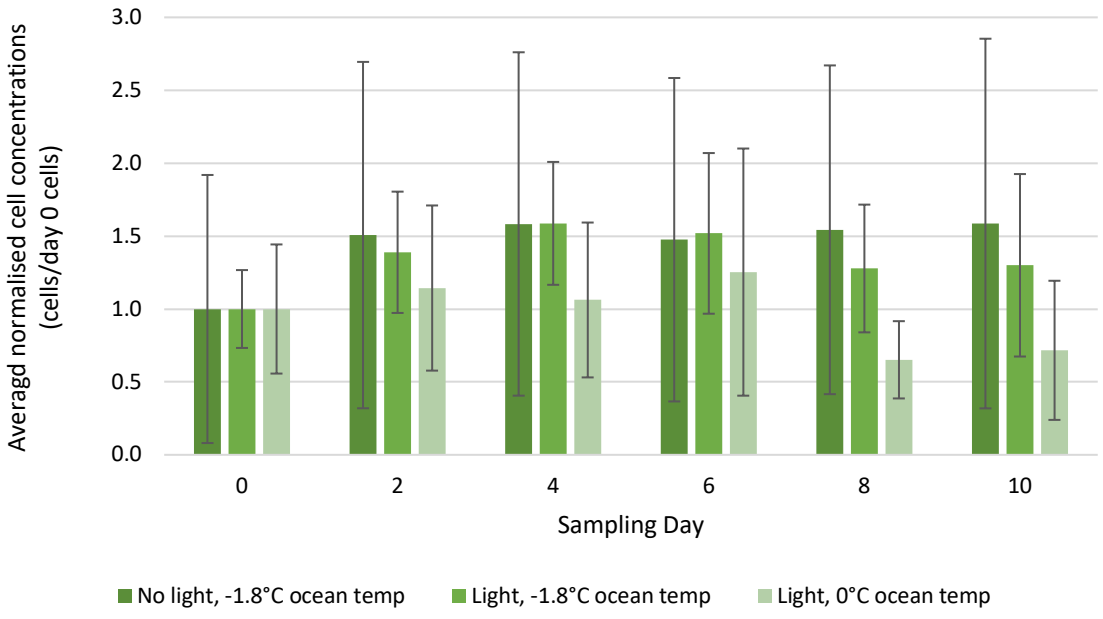

Figure 6-3: Averaged normalised cell concentrations comparing different light conditions and ocean temperatures during acclimatisation for flow cytometry.

Single-factor ANOVA tests were conducted for both the *Cocconeis sp.* and *Pseudo-nitzchia sp*. to evaluate whether each species responded differently to the varying environmental conditions. In the experiment conducted under no light and an ocean temperature of -1.8°C, both species exhibited similar trends, with cell concentrations gradually decreasing over the 10-day acclimatisation period (Figure 6-4). The p-values in Table 6-2, indicated the changes in

Cocconies sp. and *Psudeo-nitzchia sp*. cell concentrations were statistically significant. In the experiment conducted with light and an ocean temperature of 0°C, the changes in cell concentrations were also statistically significant, as shown by the p-values in Table 6-2. Figure 6-4 illustrates an initial increase in cell concentrations followed by a decrease, with *Pseudo-nitzschia sp.* experiencing a more pronounced decline in cell concentrations compared to *Cocconeis sp.* Conversely, in the experiment conducted with light and an ocean temperature of -1.8°C, *Pseudo-Nitzschia sp.* exhibited negligible changes in cell concentrations, while *Cocconeis sp.* showed a decrease in concentration by day 10. The p-values in Table 6-2 suggest that these changes were not statistically significant.

Table 6-2: Summary of p-values from single-factor ANOVA tests comparing normalised cell concentrations across sampling days for different light and ocean temperatures during acclimatisation.

Conditions	P-value		
	Flow	Microscopy: *Cocconeis sp.*	Microscopy: *Pseudo-Nitzchia sp.*
No light, -1.8°C ocean temp	0.00221	5.63E-07	0.000249
Light, -1.8°C ocean temp	0.0327	0.0697	0.994
Light, 0°C ocean temp	0.00330	1.18E-05	8.04E-09

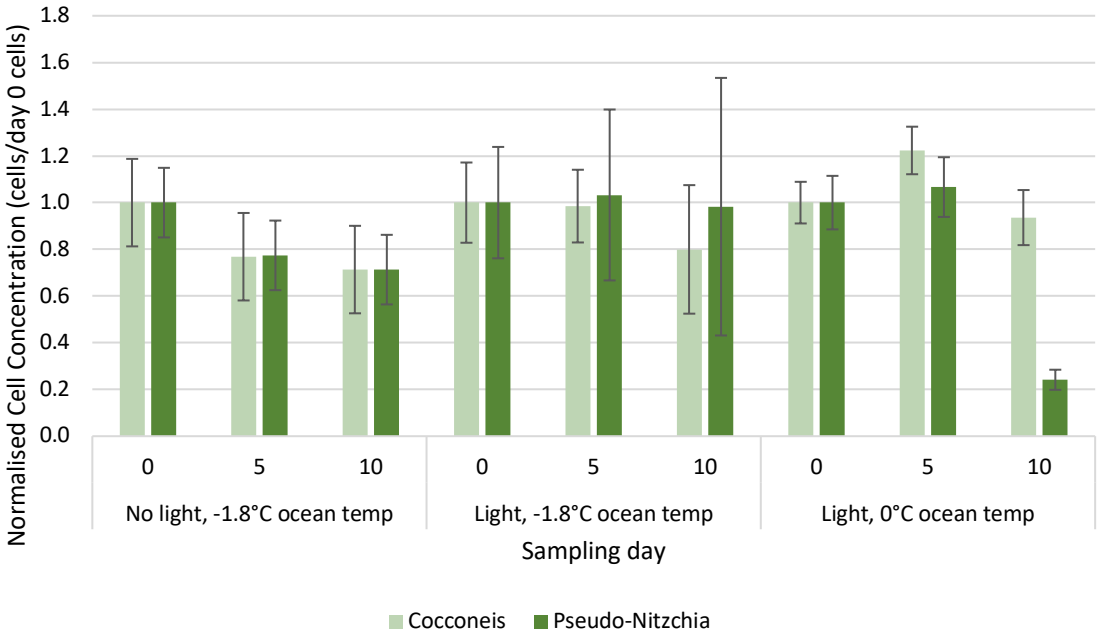

Figure 6-4: Normalised cell concentrations comparing different light conditions and ocean temperatures during acclimatisation for microscopy.

6.2.1.1. Effect of Irradiance on Sea Algae Growth

The effect of light conditions on sea ice algae growth was assessed by comparing the experiments with the same ocean temperature of -1.8°C at different light conditions of 0 µmol.m^{-2}.s^{-1} (no light) and 30 µmol.photon.m^{-2}.s^{-1}, respectively. The selection of 30 µmol.photon.m^{-2}.s^{-1} light condition is justified by its alignment with the optimal growth range for sea ice algae, which is between 26-400 µmol.photon.m^{-2}.s^{-1} (Maltsev et al., 2021). The lower end of this optimal growth range was chose to ensure it was just above the photo-inhibition threshold of 20-25 µmol.photon.m^{-2}.s^{-1}, ensuring that the algae were not shocked or stressed by sudden exposure to high light levels(Mangoni et al., 2009; Rajanahally et al., 2014). Additionally, this intensity is above the compensation irradiance range of 2-9 µmol.photon.m^{-2}.s^{-1}, ensuring photosynthesis could occur (Hancke et al., 2018).

Three par sensors recorded the light measurements per second for the duration of acclimatisation and the cold finger procedure (refer to Figure D-1, Figure D-2 and Figure D-3 Appendix D.1 for daily averaged par sensor data). The par sensor data indicated for the experiments conducted with light an average light reading of approximately 30 µmol.m^{-2}.s^{-1}. The experiment conducted with no light experienced par sensors reading of approximately 0.025 µmol.m^{-2}.s^{-1} on average.

Table 6-3: Summary of p-values from single-factor ANOVA tests comparing normalised cell concentrations for different light conditions during acclimatisation.

Conditions	P-value
Flow	2.30E-06
Microscopy: *Cocconeis sp.*	0.0621
Microscopy: *Pseudo-Nitzchia sp.*	0.0922

The flow cytometry data in Table 6-3 shows that under no light and light conditions, the sea ice algae population initially increases during the first four days of acclimatisation. In the light conditions, cell concentrations stabilise by day 6, decrease on day 8, and then stabilise again through day 10. Under no-light conditions, cell concentrations remained stable from day 6 through day 10. The changes in cell concentrations between light conditions yielded p-values below the 5% significance threshold as shown in Table 6-3, indicating that these changes were

statistically significant. Flow cytometry data shows higher growth under no-light conditions, which differ from findings in the literature observing increased cell growth with increased light (Rajanahally et al., 2014). The no light experiment had irradiance levels below the compensation irradiance required for growth (Hancke et al., 2018). Hancke et al. (2018) reported that, in extreme cases, initial growth could occur at levels as low as 0.170 $\mu mol \cdot m^{-2} \cdot s^{-1}$, which remains higher than the 0.0250 $\mu mol \cdot m^{-2} \cdot s^{-1}$ maintained throughout this experiment.

The microscopy data in Figure 6-4 visually suggests higher cell concentrations under light conditions compared to no-light conditions, which decreases across the acclimatisation period. Figure 6-4 for the light conditions illustrate a decline of *Cocconeis sp.* on day 10 while *Pseudo-nitzchia sp*. remains stable across the acclimatisation period. However, due to the substantial variation among replicate samples, particularly under light conditions on days 5 and 10, these apparent differences may not be statistically meaningful. This is supported by the p-values in Table 6-3, which indicate no significant differences in cell concentrations of both species between the light and no-light experiments. The observation of decreasing cell concentrations for both species under the no light conditions is expected as the light was below the compensation irradiance needed for growth (Hancke et al., 2018).

The data indicates that light conditions significantly influence sea ice algae growth. For the no-light condition, observed trends align with those reported in the literature and are supported by microscopy results. However, in the light experiment, both flow cytometry and microscopy showed a decline in cell concentrations toward the end of the acclimatisation period. This decrease is likely due to photo-inhibition caused by irradiance levels of 30 $\mu mol \cdot m^{-2} \cdot s^{-1}$, which exceed the photo-inhibition thresholds reported in the literature (Mangoni et al., 2009; Hancke et al., 2018).

6.2.1.2. Effect on Ocean Warming on Sea Ice Algae Growth

The effect of ocean temperature on sea ice algae growth was assessed by comparing the experiments with the same light conditions of 30 $\mu mol.m^{-2}.s^{-1}$ at differing ocean temperatures of -1.8°C and 0°C, respectively.

The flow cytometry data in Figure 6-3 shows that under varying ocean temperatures, cell concentrations for both conditions increased during the first four days of acclimatisation, stabilised by day 6, decreased on day 8, and then stabilised again through day 10. The initial increase in cell concentrations for the experiment at -1.8°C was relatively larger. The p-values in Table 4 suggest that differences in cell concentrations across different ocean temperatures were statistically significant and therefore supportive of the trends found in Figure 6-3. The decreased cell concentrations for the warmer temperature contradicts the general trend in literature which suggest sea ice algae growth shares a linear relationship with temperature (Montagnes & Franklin, 2001; Anderson, 2019).

Table 6-4: Summary of p-values from single-factor ANOVA tests comparing normalised cell concentrations for different ocean temperatures during acclimatisation.

Conditions	P-value
Flow	5.39E-06
Microscopy: *Cocconeis sp.*	0.00905
Microscopy: *Pseudo-Nitzchia sp*	0.0381

Similarly, the microscopy data showed that Figure 6-4 shows an increase in cell concentrations for both species by day 5, followed by a decline by day 10. *Cocconeis sp*. exhibited a relatively larger increase in cell concentration by day 5, whereas *Pseudo-nitzschia sp*. showed a drastic decrease in population by day 10. Despite the larger variation in replicate samples for -1.8°C, the graphical change in cell concentration was still distinct enough to suggest meaningful trends. The p-values in Table 6-4 indicate that the changes in cell concentrations were statistically significant. The initial increases in cell concentrations of both species with increased ocean temperature followed trends of increasing specific growth rates of diatoms with temperature (Montagnes & Franklin, 2001). Additionally, Montagnes & Franklin (2001) discussed general observations of decreasing cell size with increasing temperature. This trend was observed in the experiments with increased *Cocconeis sp.* cell concentrations (with an average smaller cell size) at the warmer ocean temperature.

The data highlights the impact of ocean warming on sea ice algae growth, with both flow cytometry and microscopy showing significant changes in cell concentrations. In accordance with Swadling et al. (2023), warmer temperature increases sea ice algae's metabolic activity,

which likely leads to higher nutrient uptake. Since nutrients were provided at the start of each experiment and were not replenished, the decline in cell concentrations under warmer temperatures, as observed in both microscopy and flow cytometry, may be attributed to nutrient depletion.

6.2.2. Investigation of Algae Uptake Dynamics into Sea Ice Using the Cold Finger

6.2.2.1. Effect of Atmospheric Temperature on Sea Ice Algae Uptake Dynamics

The effect of atmospheric temperature on sea ice algae growth was assessed by comparing the three cold finger temperatures of -5°C, -10°C and -15°C used in each experiment at different light and ocean temperatures. The overall uptake was calculated based on absolute cell concentrations. This was achieved by multiplying the total sample volume by the cell concentration for each analysis technique. Refer to Table D-1 to Table D-8 in Appendix D.2 and D.3 for ice growth diameters, growth times, ice volumes and salinities.

Single-factor ANOVA tests were conducted to assess the effect of atmospheric temperature on uptake dynamics across various environmental conditions. The results of these ANOVA tests are presented in Table 6-5. The p-values for both flow cytometry and microscopy analyses of the two species showed that differences in cell concentrations at varying cold finger freezing temperatures were not statistically significant. This suggests that atmospheric temperature does not have a significant impact on the uptake dynamics of sea ice algae.

Table 6-5: Summary of p-values from single-factor ANOVA tests comparing normalised cell concentrations for differing atmospheric temperature with various light and ocean temperatures.

Conditions	P-value		
	Flow	Microscopy: *Cocconeis sp.*	Microscopy: *Pseudo-nitzchia sp.*
No light, -1.8°C ocean temp	0.419	0.975	0.596
Light, -1.8°C ocean temp	0.678	0.373	0.668
Light, 0°C ocean temp	0.719	0.103	0.454

As shown in Table 6-6, the highest normalised percentage uptake for flow cytometry data, averaged across all experiments, occurred at -10°C, followed by -15°C, with the lowest uptake

observed at -5°C. Most of the sea ice algae were found in the underlying seawater solution (refer to Figure D-23 in Appendix D.4 for graph displaying normalised concentrations in the underlying seawater solution).

Table 6-6: Summary showing the relationship between atmospheric temperature and average normalised percentage uptake with flow cytometry data

Temperature (°C)	Uptake (%)	Uptake variance (%)
-5	1.74	0.177
-10	9.17	1.56
-15	5.75	2.94

Similarly, microscopy data shows that the highest normalised percentage uptake averaged across all experiments, occurred at -10°C, followed by -15°C, with the lowest uptake at -5°C (Table 6-7). The overall trend across all experiments indicates a higher uptake of *Cocconeis sp.* compared to *Cocconeis sp., Pseudo-Nitzschia sp*. showed significantly lower uptake at -5°C (Figure 6-6). The majority of both species were found in the underlying seawater solution (refer to Figure D-20 in Appendix D.4 for graph displaying normalized concentrations in the underlying seawater solution). The normalised concentrations of *Pseudo-Nitzschia sp*. in the brine solution were higher than those of *Cocconeis sp*., which suggests that a larger proportion of *Cocconeis sp*. was incorporated into the ice. Similar trends were observed in Figure D-21 and Figure D-22 in Appendix D.4 for experiments conducted at different light and ocean temperatures.

Table 6-7: Summary showing the relationship between atmospheric temperature and average normalised percentage uptake with microscopy data.

Temperature (°C)	Species	Uptake (%)	Uptake variance (%)
-5	*Cocconeis sp.*	13.5	2.66
	Pseudo-nitzchia sp.	4.76	1.25
-10	*Cocconeis sp.*	19.6	3.12
	Pseudo-nitzchia sp.	13.4	4.51
-15	*Cocconeis sp.*	15.4	1.72
	Pseudo-nitzchia sp..	10.8	1.47

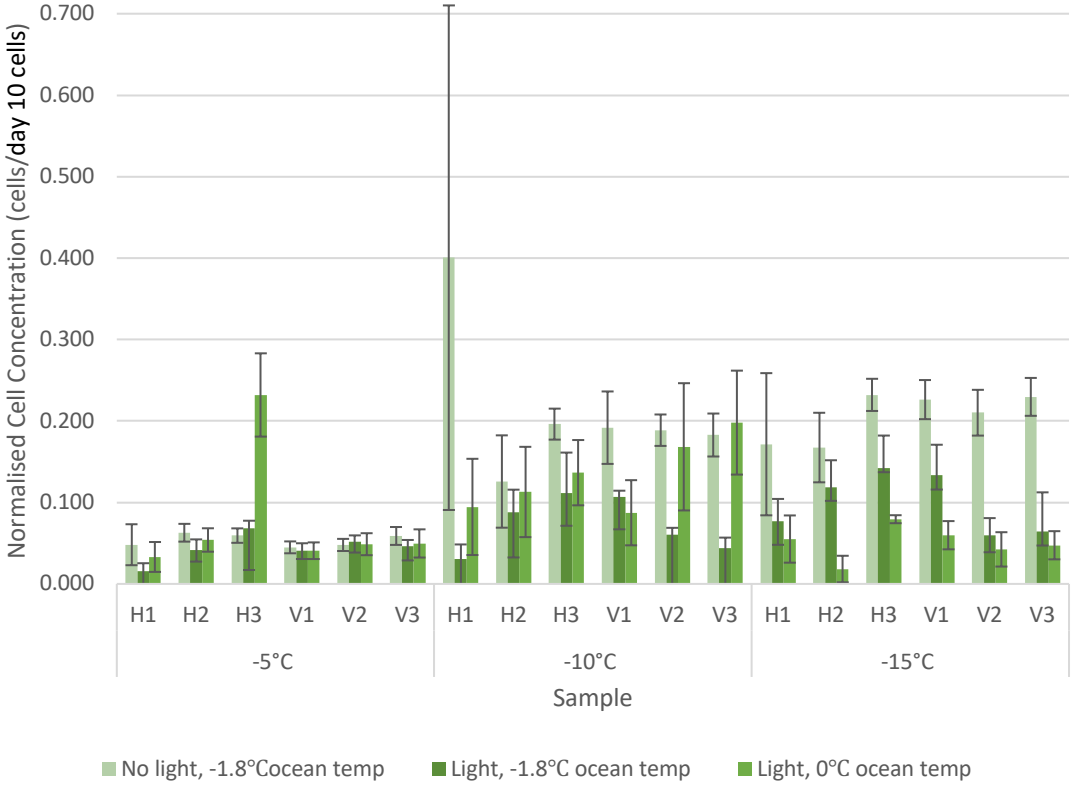

Figure 6-5: Normalised cell concentrations comparing atmospheric temperatures for different light conditions and ocean temperatures during uptake dynamics for flow cytometry.

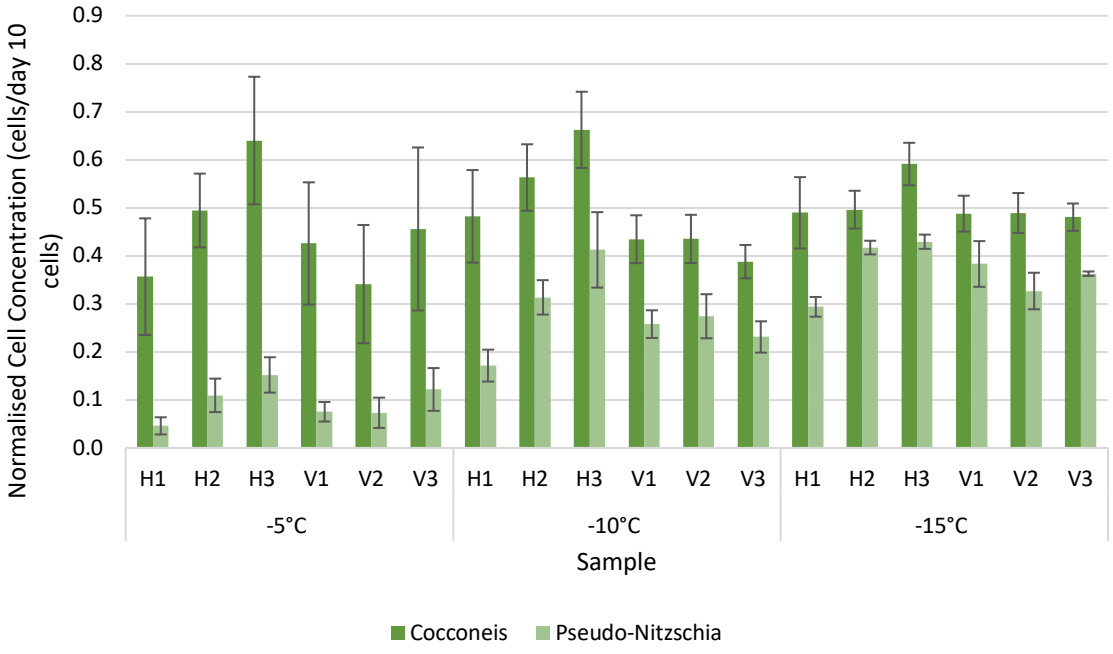

Figure 6-6: Normalised cell concentrations comparing atmospheric temperatures with no light conditions and ocean temperature of -1.8℃ during uptake dynamics for microscopy.

Matlakala (2022) found higher atmospheric temperatures led to the formation of more porous ice due to the slower growth dynamics. This results in less brine entrapment in ice grown at warmer atmospheric temperatures. This pattern is evident across all experiments, with ice grown at -15°C showing the highest bulk salinity, followed closely by -10°C, while both displayed noticeably higher salinity compared to the -5°C condition (refer to in Table D-6, Table D-7 and Table D-8 in Appendix D.3 for detailed salinity measurements). Under abiotic conditions, nutrients are dissolved solutes that behave similarly to salts (Vancoppenolle et al., 2010). Consequently, higher salinity correlates with higher nutrient concentrations, which can enhance algae growth. Since sea ice algae live within the brine inclusions of the sea ice matrix, ice with higher brine retention would likely contain more algae.

Additionally, diatoms are non-motile and tend to sink due to lack of circulation (Miklasz & Denny, 2010). For this reason, it was expected that ice grown at -15°C would have the highest uptake of sea ice algae due to faster ice growth rates, which would facilitate greater brine retention and higher nutrient availability, allowing more algae to be incorporated. However, at -15°C, brine channels are likely more isolated and closed, which may limit algae uptake into the ice. At -5°C, it is postulated that the slow growth dynamics reduce the amount of algae incorporated into the ice, as settling rate for some algae may exceed the rate of ice formation. The salinity profiles show that ice grown at -10°C maintained high salinities, and therefore likely higher nutrient concentrations, similar to -15°C (refer to in Table D-6, Table D-7 and Table D-8 in Appendix D.3 for detailed salinity measurements). However, ice grown at -10°C would likely have facilitated more porous ice, leading to more interconnected brine channels, enhancing nutrient availability, which likely contributed to the highest observed algae uptake in the -10°C ice.

Despite the single-factor ANOVA tests indicating that atmospheric temperature did not significantly impact the uptake dynamics of sea ice algae, uptake trends varied. The highest uptake values were observed at -10°C, followed by -15°C, with the lowest values at -5°C Species-specific differences were evident, with *Cocconeis sp.* showing greater incorporation into the ice compared to *Pseudo-nitzchia sp*., which was more abundant in the underlying seawater solution. This is likely due to the larger size of *Pseudo-nitzchia sp.*, which may have resulted in exclusion from the sea ice matrix and faster settling due to their increased size.

6.2.2.2. Effect of Irradiance on Sea Ice Algae Uptake Dynamics

The effect of light conditions on sea ice algae uptake dynamics was assessed by comparing the experiments with the same ocean temperature of -1.8°C at different light conditions of 0 $\mu mol.m^{-2}.s^{-1}$ (no light) and 30 $\mu mol.m^{-2}.s^{-1}$, respectively.

Table 6-8: Summary of p-values from single-factor ANOVA tests comparing normalised cell concentrations for differing light conditions on uptake dynamics.

Conditions	P-value
Flow	0.960
Microscopy: *Cocconeis sp.*	0.107
Microscopy: *Pseudo-nitzchia sp.*	0.0197

As shown in Figure 6-7, flow cytometry indicates negligible differences in mean normalised cell concentrations at different positions in the ice with the largest normalised cell concentration difference less than 0.200 cells/day 10 cells. This is supported by the p-value of 0.960, indicating normalised cell concentrations are closely matched. Flow cytometry and microscopy data resulted in the most sea ice algae cells occurring in the underlying seawater solution (refer to Figure D-24 and Figure D-25 in Appendix D.4 for normalised cell concentrations of the underlying seawater solution).

In contrast, microscopy observed significantly higher normalised cell concentrations within the ice compared to flow cytometry, with maximum concentrations of microscopy and flow cytometry of 0.606 cells/cells and 0.207 cells/cells, respectively. As shown in Figure 6-8 *Cocconeis sp.* displayed negligible variation across light conditions, whereas *Pseudo-nitzschia sp.* exhibited increased normalised cell concentrations under light conditions. This is supported by the p-values in Table 6-8, which indicate statistically significant differences in normalised cell concentrations for *Pseudo-nitzschia sp*. between light and no-light conditions. In contrast, the p-values suggest that light shows no statistically significant difference compared to the normalised cell concentrations of *Cocconeis sp.* However, as shown in Figure 6-8, the high variability among replicates in experiments with light may influence the observed effects of differing light conditions.

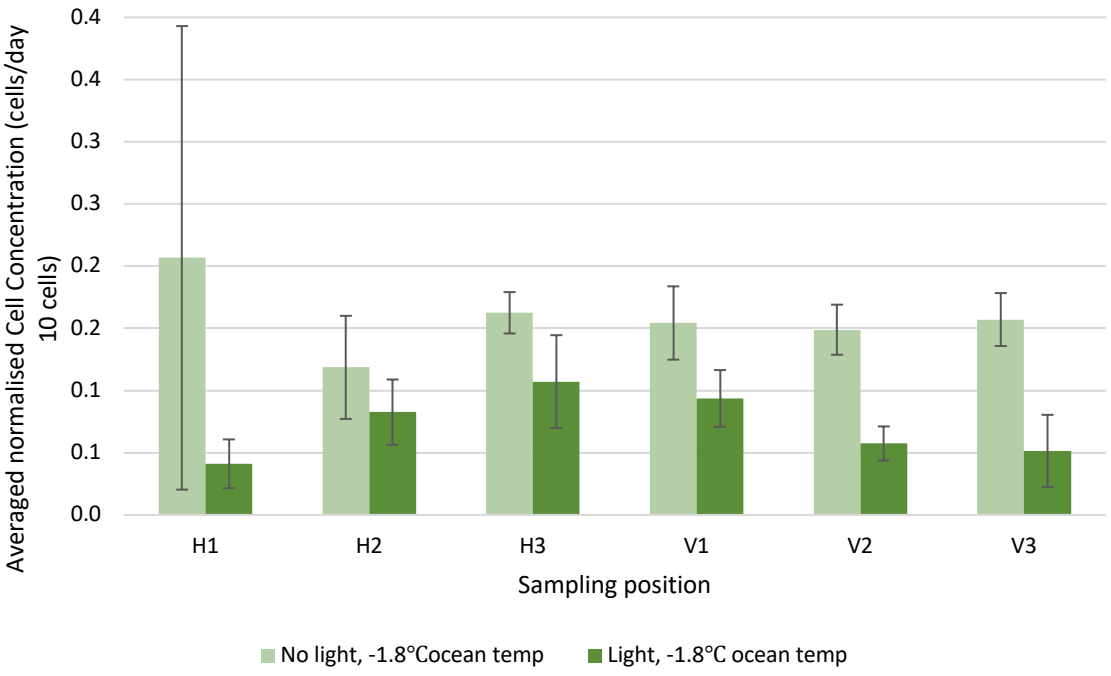

Figure 6-7: Averaged normalised cell concentrations comparing different light conditions during uptake dynamics for flow cytometry.

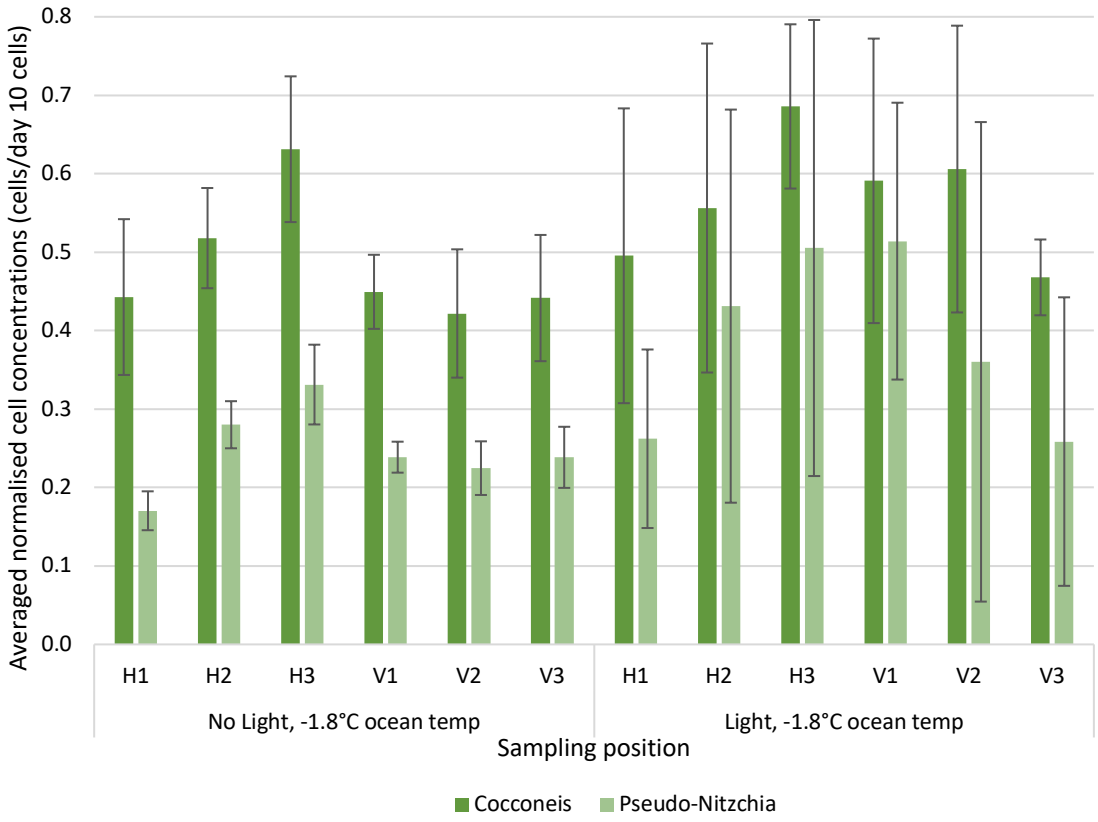

Figure 6-8: Averaged normalised cell concentrations comparing different light conditions during uptake dynamics for microscopy.

The microscopy results suggest that the response of sea ice algae was species-specific. However, the high variability in replicate samples for *Pseudo-nitzschia sp.* indicates that the statistical significance of the single-factor ANOVA test may be skewed. The general trend observed in both flow cytometry and microscopy data suggest that light had no significant impact on sea ice algae uptake dynamics. Rajanahally et al. (2014) found that increased light levels result in enhanced cell growth; however, the duration of each experiment may not have been sufficient for the algae populations to grow enough to produce measurable changes in uptake dynamics. Although, the higher surface to volume ratio of *Cocconeis sp.* results in *Cocconeis sp.* being more efficient at nutrient uptake and ability to harvest light (Al-Handal et al., 2019). This evident by the higher concentrations of *Cocconeis sp.* (Figure 6-8).

6.2.2.3. Effect of Ocean Warming on Sea Ice Algae Uptake Dynamics

The effect of ocean temperature on sea ice algae uptake dynamics was assessed by comparing the experiments with the same light conditions of 30 $\mu mol.m^{-2}.s^{-1}$ at differing ocean temperatures of -1.8°C and 0°C, respectively.

Table 6-9: Summary of p-values from single-factor ANOVA tests comparing normalised cell concentrations for ocean temperatures on uptake dynamics.

Conditions	P-value
Flow	0.121
Microscopy: *Cocconeis sp.*	0.625
Microscopy: *Pseudo-nitzchia sp.*	0.407

As shown in Figure 6-9, the flow cytometry data shows no general trends in normalised cell concentrations within the ice across different ocean temperatures. This is supported by a p-value of 0.121, indicating no statistically significant differences in normalised cell concentrations at the 5% significance level. Similarly, the p-values in Table 6-9 indicate no statistical significance in differences in normalised cell concentrations between ocean temperatures for both species in the microscopy data. However, trends in Figure 6-10, especially for *Pseudo-nitzchia sp.,* suggest a reduction in normalised cell concentrations at the 0°C ocean temperature. This trend may be influenced by the high variability in replicate samples at 0°C.

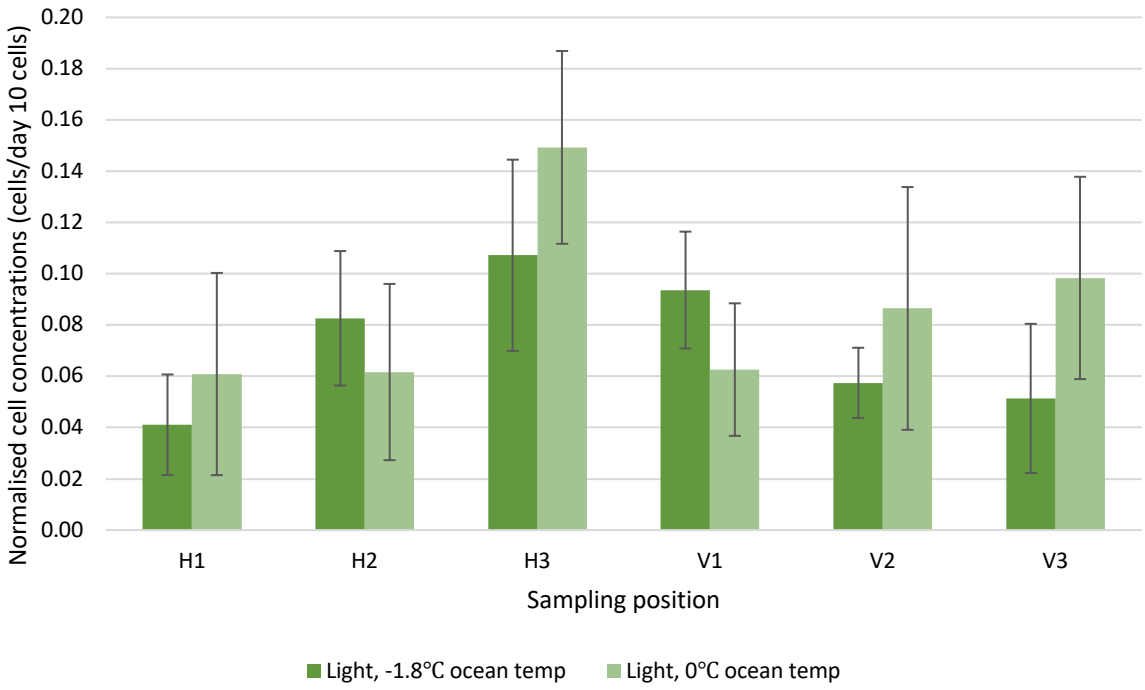

Figure 6-9: Averaged normalised cell concentrations comparing different ocean temperatures during uptake dynamics for flow cytometry.

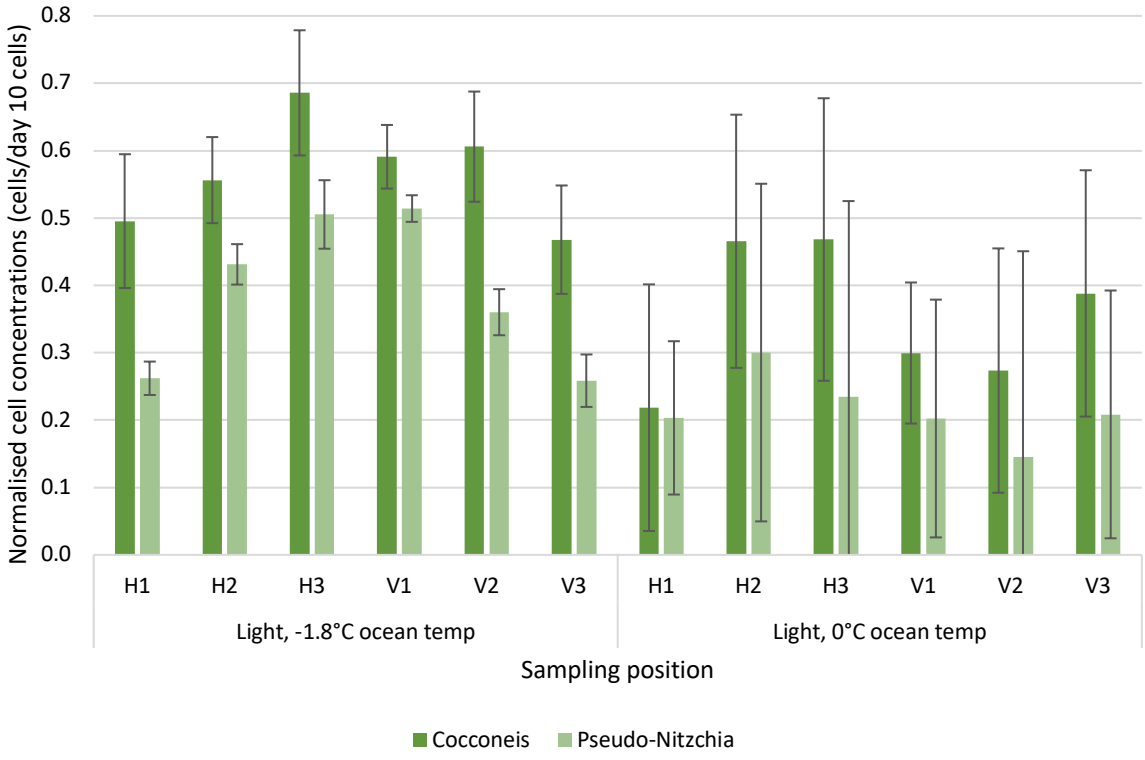

Figure 6-10: Averaged normalised cell concentrations comparing different ocean temperatures during uptake dynamics for microscopy.

The highly variable samples with an ocean temperature of 0°C, is likely due to reduced ice extent of -5°C (refer to Table D-1 and Table D-2 in Appendix D.4 for ice growth times and diameters). The reduced ice extent is a result of slower growth rates caused by decreased heat transfer. The cold finger, which drives ice formation, diminishes as the ice thickens, due to the reduction in the temperature gradient. Eventually, the temperature gradient becomes insufficient to overcome the heat of ice formation, leading to a limitation of ice growth that can occur for certain atmospheric temperatures. Since the ice formation period (winter) remains fixed, slower ice growth rates will lead to a smaller ice extent. This reduced ice extent will ultimately affect the available habitat for algae, resulting in less algae uptake.

6.2.2.4. Effect of Ice Growth Dynamics on Sea Ice Algae Uptake Dynamics

The effect of ice growth dynamics was investigated through the horizontal and vertical positions of ice samples within the ice. The average normalised cell concentrations for both vertical and horizontal ice sections was relatively similar as shown in Figure 6-11 and Figure 6-12. This was expected as each half of ice was expected to have relatively the same cell concentrations.

Table 6-10: Summary of p-values from single-factor ANOVA tests comparing normalised cell concentrations for different sampling positions within the ice.

Conditions	P-value	
	Vertical	Horizontal
Flow cytometry	0.932	7.39E-05
Microscopy: *Cocconeis sp.*	0.419	0.00147
Microscopy: *Pseudo-nitzchia sp.*	0.0781	0.428

The trends in Figure 6-11 illustrates negligible variation in normalised cell concentrations across vertical positions, supported by p-values in Table 6-10. For horizontal positions, the highest flow cytometry normalised cell concentrations were observed at the bottom position (H3), followed by the top (H1) and middle (H2) positions. However, high variability among replicate samples in the top position (H1) makes it difficult to draw definitive conclusions. However, p-values in Table 6-10 suggest statistically significant differences in normalised cell concentrations across horizontal positions.

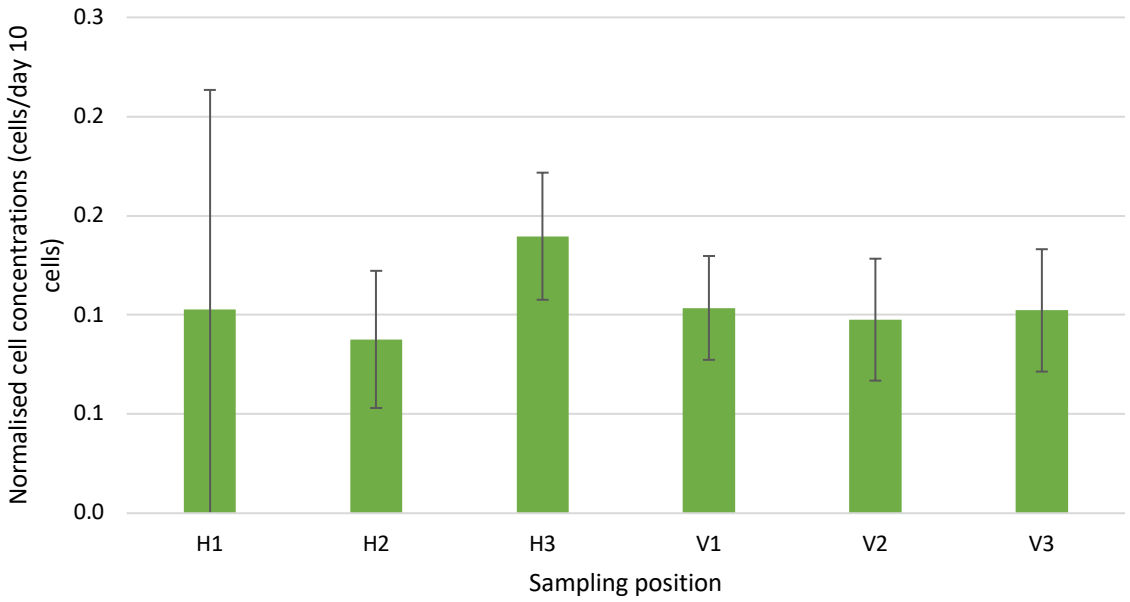

Figure 6-11: Averaged normalised cell concentrations comparing different sampling positions during uptake dynamics for flow cytometry.

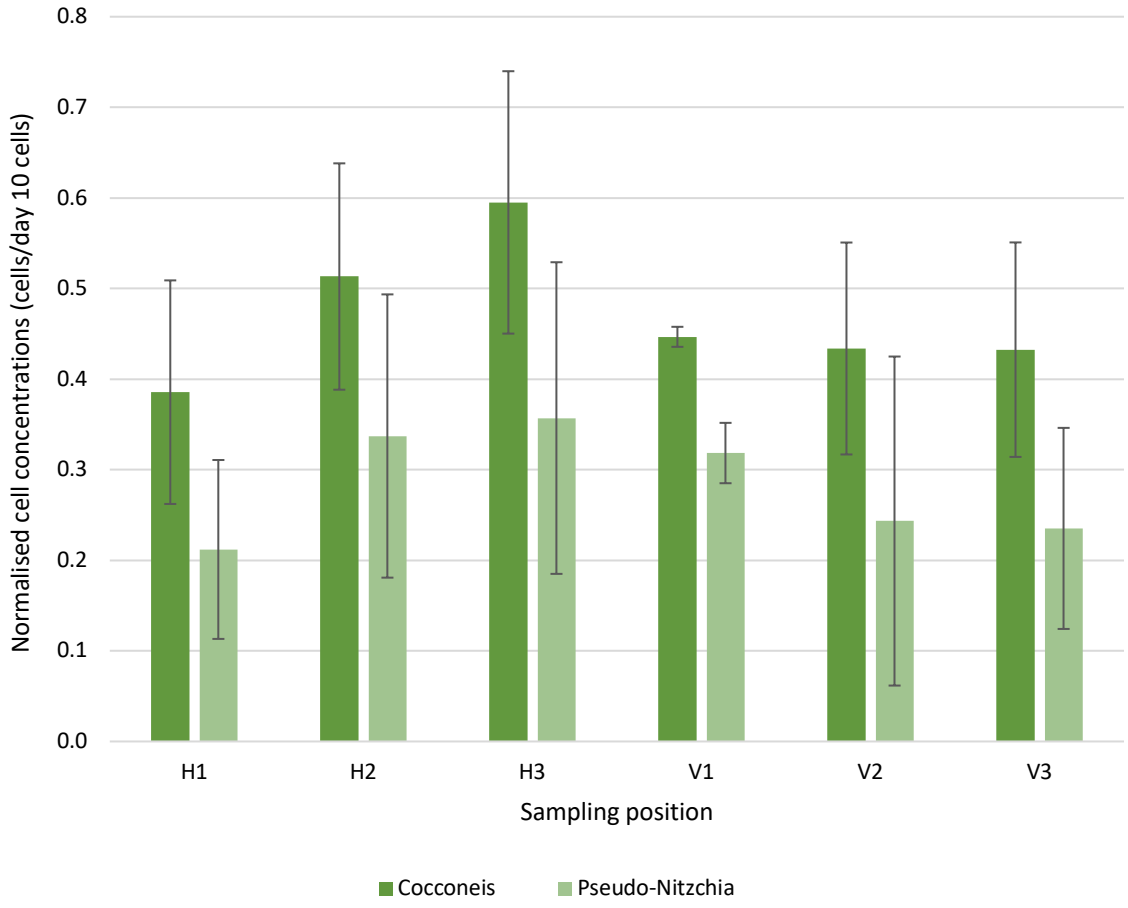

Figure 6-12: Averaged normalised cell concentrations comparing different sampling positions during uptake dynamics for microscopy.

The vertical distribution of *Cocconeis sp*. aligns with the trends observed in flow cytometry, showing relatively uniform normalised cell concentrations across vertical positions (Figure 6-11). *Cocconeis sp*. displayed the highest normalised cell concentrations in the bottom horizontal position (H3) and exhibited a clear trend of increasing concentrations with ice depth. The p-values in Table 6-10 confirm the statistical significance of these horizontal and vertical trends. In contrast, the p-values for *Pseudo-nitzchia sp.* indicate no statistically significant differences in normalised cell concentrations across either horizontal or vertical positions. However, the bottom horizontal position (H3) also exhibited the highest normalised cell concentrations for *Pseudo-nitzchia sp.,* consistent with general trends of increasing normalised cell concentrations with ice depth.

The general distribution of sea ice algae in the ice indicates that the radial direction of ice growth had no significant influence on the up-take dynamics of ice, as observed in both flow and microscopy data. However, the horizontal position showed a trend of increasing cell concentration for both species with increasing ice depth. This can be attributed to the non-motile nature of algae, causing them to settle to the bottom of the 1-litre aquaria (Miklasz & Denny, 2010). *Pseudo-nitzchia sp.,* being larger, settle faster and were therefore less likely to be incorporated into the growing ice matrix. Additionally, *Pseudo-nitzchia sp.* forms long chains, which further increases their settling rate (Miklasz & Denny, 2010). As a result, larger normalised concentrations of *Pseudo-nitzchia sp.* were found in the underlying seawater solution, while *Cocconeis sp.* exhibited higher normalized cell concentrations within the sea ice matrix. This may not accurately reflect real-world conditions, as turbulence would likely keep these cells suspended in the water column.

As discussed in Section 4, the cold finger facilitates the formation of vertically slanted brine inclusions from the horizontal plane of ice growth. Desalination of sea ice promotes the convective overturning of brine within these inclusions, causing algae to move downward toward the bottom of the ice matrix (Notz & Worster, 2009). The combined effect of the diatoms' non-motile nature and desalination results in the highest concentrations of algae at the bottom of the ice and in the underlying seawater solution (Miklasz & Denny, 2010). The horizontal and vertical salinity profiles across the experiments further support the desalination of sea ice in this study, demonstrating an increase in salinity with ice depth while

remaining uniform across radial profiles (refer to in Table D-6, Table D-7 and Table D-8 in Appendix D.3 for detailed salinity measurements). As nutrients behave similarly to salts in abiotic conditions, nutrient concentrations were likely highest at increased ice depths, enhancing algae growth in these sections. Therefore, the highest abundance of sea ice algae was observed where salinity, and consequently nutrient concentrations were highest. This aligns with literature observing the highest abundance of sea ice algae communities typically at the bottom of the sea ice matrix (Arrigo, 2016).

6.3. Summary of Key Findings

Table 6-11: A summary of key findings from the results of varying environmental conditions on sea ice algae growth and uptake dynamics.

Aspect	Key Findings
Comparison of analysis methods	Significant differences between microscopy and flow cytometry indicate the methods are not directly comparable and should be assessed independently.
Impact of light on growth	Light conditions significantly affected sea ice algae growth: populations decreased under no-light conditions, while in light conditions they declined toward the end, likely due to photo-inhibition.
Impact of ocean temperature on growth	Ocean warming significantly impacted growth by enhancing metabolic activity and nutrient uptake, promoting algae proliferation; in closed systems, this led to eventual nutrient depletion.
Atmospheric temperature effect on uptake	Ice grown at -10°C showed the highest algae uptake, likely due to more interconnected brine channels and greater nutrient availability compared to other temperatures.
Light effect on uptake dynamics	Light had negligible overall effect on uptake dynamics, with Pseudo-nitzschia sp. showing some species-specific increases under light, while Cocconeis sp. remained largely unaffected.
Ocean temperature effect on uptake dynamics	Ocean temperature influenced uptake: slower ice growth rates at 0°C resulted in smaller ice extent and reduced algae incorporation.
Species-specific distribution	Cocconeis sp. was more abundant in the ice, likely due to its smaller size, while Pseudo-nitzschia sp., settling faster due to its larger size, was more abundant in the underlying seawater.
Distribution in sea ice matrix	No significant radial variation was observed, but cell concentrations increased with ice depth, correlating with higher bulk salinities (and thus higher inferred nutrient concentrations), supporting enhanced algae growth deeper in the ice.

7. Overall Discussion

The current alternative techniques to atmospheric freezing include cold finger apparatus and cold plates (Cox & Weeks, 1975; Notz, Wettlaufer & Worster, 2005; Ewert & Deming, 2011; Schulson, Renshaw & Snyder, 2012). However, cold finger apparatus was preferred within this investigation because it fosters faster and more effective ice growth by enabling simultaneous ice formation at multiple depths within the aquaria. This evident in a previous study where ice growth occurred along the cold finger forming a hemisphere (Ewert & Deming, 2011). Sea ice algae tend to sink in the absence of agitation; therefore, the use of a cold finger would allow for greater inclusion of algae with depth in the aquaria. Cold finger ice growth dynamics differs from top-down growth of natural sea ice (Petrich & Eicken, 2017). Instead, the cold finger apparatus induced radial ice growth in horizontal plane (Ewert & Deming, 2011). This resulted in downward-slanted brine inclusions from the horizontal growth plane, potentially altering the desalination process and affecting the natural convective nutrient flows within the ice.

The developed system enabled the simulation of sea ice algae uptake dynamics under differing environmental conditions (that can be related to global warming effects). This work focused on effects of changes in irradiance, ocean warming (acclimatisation and cold finger experiments), and increase in atmospheric temperature (cold finger experiments). The results indicate that higher irradiance and warmer ocean temperatures initially promoted an increase in sea ice algae populations, followed by a decline. Swadling et al. (2023) reported increased metabolic activity at higher irradiance and ocean temperatures, leading to increased nutrient uptake. However, in the closed system used here, limited nutrient availability likely resulted in nutrient depletion, which may be the major contributor to the observed population decline. Al-Handal et al. (2019) noted smaller diatoms exhibit more efficient nutrient uptake and light harvesting due to their higher surface area-to-volume ratio. This characteristic likely attributes to the observed decrease in cell size with increasing temperature (Montagnes & Franklin, 2001). This study observed higher normalised concentrations of *Cocconeis sp.* compared to *Pseudo-nitzschia sp.,* which is consistent with literature.

The results of algae uptake into the ice in this study show that fluctuations in irradiance level, ocean temperature and atmospheric temperature had a negligible effect on sea ice algae uptake into the ice, likely due to the short duration of the ice growth periods. Instead, algae uptake in this study was postulated to be dictated by two primary factors, gravity and ice extent. Sea ice algae were found in higher concentrations in the lower portions of sea ice, as they are non-motile and the absence of turbulence impeded them from staying suspended in the solution. Additionally, in the -5°C experiment at an ocean temperature of 0°C, there was a reduced algae uptake into the ice. This was attributed to reduced temperature gradient driving heat transfer and led to a decrease in ice extent, which in turn limited the uptake of algae into the ice.

8. Conclusions and Recommendations

A system was developed within the scope of this study to allow for the dynamic relationship between sea ice and sea ice algae to be investigated. The system was used to investigate the dynamic relationship under various irradiances, oceanic and atmospheric temperatures. The following conclusions were drawn from this investigation:

- A cold finger apparatus was designed to grow artificial sea ice radially in the horizontal plane in 1-litre aquaria at -5°C, -10°C and -15°C. This limitation of radial growth is that it differs from top-down growth of natural sea ice and resulted in brine inclusions downward slanted off the horizontal plane.

- A rudimentary thermodynamic model was developed to predict the allowable ice growth time to limit undesired wall effects on ice growth dynamics. The model demonstrated a prediction accuracy within a 5% error range. The model's predictive accuracy was limited for ocean temperatures above seawater's freezing point due to considering only conductive heat transfer.

- The methodology (experimental and sampling) for investigating the dynamic relationship between sea ice and sea ice algae represents a novel approach. A draw back from the developed sampling protocol was the limited sampling frequency for microscopy during the acclimatisation phase, which may hinder the of the observed trends.

- Irradiance conditions significantly affected the growth and uptake of sea ice algae. Under no light conditions, both species had initial changes in cell concentrations before concentrations stabilised. At an irradiance of 30 $\mu mol.m^{-2}.s^{-1}$, algae populations exhibited a decrease in growth towards the end of the growth, likely due to photon inhibition.

- Ocean temperature significantly influenced both the growth and uptake dynamics of sea ice algae. Sea ice algae populations initially increased but then significantly declined. The overall decline was likely attributed to nutrient depletion from increased metabolic activity

at warmer temperatures. Reduced ice extent was observed at cold finger temperature of -5°C, resulting from a lower temperature gradient and therefore diminished heat transfer capabilities. A reduced ice extent due to warmer ocean temperatures will lead to decreased sea ice algae uptake, as less habitat would be available.

- Atmospheric temperature had no statically significant effect on the uptake dynamics of sea ice algae. However, results illustrated a general trend where uptake was highest at ice growth temperatures of-10°C followed by -15°C and then -5°C. General trends indicated no significant changes in concentrations radially (vertical sections), however concentrations increased with ice depth (horizontal sections), which is attributed primarily to settling of algae and desalination within the downward-slanted brine channels. The nutrient distribution followed a similar trend, with higher nutrient concentrations at increased ice depths. This enhanced nutrient availability at increased ice depth would have supported the increased algae concentrations observed, further indicating the relationship between brine inclusion dynamics and nutrient incorporation within the ice matrix.

The study had limitations and therefore recommendations aim to address such inefficiencies to improve future work. The following recommendations are proposed:

- The number of species used in experimentation should be increased. Additionally, this study could benefit from the inclusion of motile species of algae such as Dinoflagellates. This will allow for better understanding of broader community response to changing climate conditions. This expansion could provide insights into how sea ice algae might behave in the natural sea ice environment, including interactions within a full community in response to factors like nutrient availability and environmental stressors.

- The thermodynamic model should be modified to include convective heat transfer. This improvement will enable better predictive capabilities for scenarios where ocean temperatures are above the freezing point (-1.8°C).

- Sampling frequency, particularly for microscopy samples, should be increased. A higher frequency of sampling will provide a more robust foundation for analysing and discussing observed trends. This approach would support a better understanding of the dynamics of algae growth and community interactions, helping future studies to investigate how these behaviours change under long-term climate variations.

- Future research could benefit from inclusion of turbulence using the likes of shake tables, aeration or pumps to simulate natural ecological turbulence. The inclusion of turbulence in the sea ice formation model would introduce a new level of complexity, affecting heat transfer, temperature and salinity gradients, and the distribution of materials within the water column. Turbulence enhances mixing at the ice-water interface, which could influence ice growth rates, crystal structure, and algal incorporation into the sea ice matrix. This is crucial for understanding how algae communities behave under conditions of ocean wave dynamics and nutrient suspension. Incorporating turbulence will help model how ocean warming, changing ice dynamics, and increased wave action might impact sea ice algae communities in natural settings, thus contributing to the larger picture of climate change impacts on sea ice ecosystems.

- Results could be strengthened by incorporating additional statistical tools. For example, applying Monte Carlo simulations to the dataset would allow for error propagation, determining the level of certainty that can associated with the final results. Additionally, performing sensitivity analysis would enable a more comprehensive assessment of the key parameters driving the observed trends, ensuring that conclusions are well-supported and robust.

References

Abraham, J.P., Baringer, M., Bindoff, N.L., Boyer, T., Cheng, L.J., Church, J.A., Conroy, J.L., Domingues, C.M., et al. 2013. A review of global ocean temperature observations: Implications for ocean heat content estimates and climate change. *Reviews of Geophysics*. 51(3):450–483. DOI: 10.1002/rog.20022.

Ackley, S.F. & Sullivan, C.W. 1994. *Physical controls on the development and characteristics of Antarctic sea ice biological communities-a review and synthesis*.

Al-Handal, A., Riaux-Gobin, C., Jahn, R., Katarina Wulff, A. & Minerovic, A. 2019. Two new marine species of Cocconeis (Bacillariophyceae) from the west coast of Sweden. *Journal of Taxonomy*. 497(497):1–16. DOI: 10.5852/ejt.2019.497ï.

Almandoz, G.O., Ferreyra, G.A., Schloss, I.R., Dogliotti, A.I., Rupolo, V., Paparazzo, F.E., Esteves, J.L. & Ferrario, M.E. 2008. Distribution and ecology of Pseudo-nitzschia species (Bacillariophyceae) in surface waters of the Weddell Sea (Antarctica). *Polar Biology*. 31(4):429–442. DOI: 10.1007/s00300-007-0369-9.

Anderson, N.J. 2019. *Miniview : Diatoms, temperature and climatic change*. Available: https://www.cambridge.org/core/terms.

Anderson, P. 2010. Filtering – calcofluor staining – quantitative epifluorescence microscopy for phytoplankton analysis. In *Microscopic And Molecular Methods For Quantitative Phytoplankton Analysis*. 31–36.

Arrigo, K.B. 2016. Sea ice as a habitat for primary producers. In *Sea Ice: Third Edition*. Wiley Blackwell. 352–369. DOI: 10.1002/9781118778371.

Arrigo, K.R. & Thomas, D.N. 2004. Large scale importance of sea ice biology in the Southern Ocean. *Antarctic Science*. 16(4):471–486. DOI: 10.1017/S0954102004002263.

Arrigo, K.R., Mock, T. & Lizotte, M.P. 2010. Primary Producers and Sea Ice. In *Sea Ice*. 2nd ed. D.N. Thomas & G.S. Dieckmannt, Eds. Blackwell Publishing Ltd. 283–326.

AZO Materials. 2012. *AISI 1053 Carbon Steel (UNS G10530)*. Available: https://www.azom.com/article.aspx?ArticleID=6535 [2024, April 18].

BD Biosciences. 2023.

Beans, C., Hecq, J.H., Koubbi, P., Vallet, C., Wright, S. & Goffart, A. 2008. A study of the diatom-dominated microplankton summer assemblages in coastal waters from Terre Adélie to the

Mertz Glacier, East Antarctica (139°E-145°E). *Polar Biology*. 31(9):1101–1117. DOI: 10.1007/s00300-008-0452-x.

Bejan, A. & Kraus, A.D. 2003. Heat Transfer Handbook. Available: www.wiley.com. [2024, April 16].

Brandt, R.E., Warren, S.G., Worby, A.P. & Grenfell, T.C. 2005. *Surface Albedo of the Antarctic Sea Ice Zone*.

Campbell, K., Mundy, C.J., Juhl, A.R., Dalman, L.A., Michel, C., Galley, R.J., Else, B.E., Geilfus, N.X., et al. 2019. Melt procedure affects the photosynthetic response of sea ice algae. *Frontiers in Earth Science*. 7. DOI: 10.3389/feart.2019.00021.

Cefarelli, A.O., Ferrario, M.E. & Vernet, M. 2016. Diatoms (Bacillariophyceae) associated with free-drifting Antarctic icebergs: taxonomy and distribution. *Polar Biology*. 39(3):443–459. DOI: 10.1007/s00300-015-1791-z.

Cembella, A. & Rafuse, C. 2010. The filter - transfer - freeze method for quantitative phytoplankton analysis. In *Microscopic And Molecular Methods For Quantitative Phytoplankton Analysis*. 41–46.

Cengel, Y.A. & Cimbala, J.M. 2014. *Fluid Mechanics: Fundamentals And Applications, Third Edition*.

Cheah, Y.T. & Chan, D.J.C. 2022. DOI: 10.1111/jam.15455.

Costa, O.Y.A., Raaijmakers, J.M. & Kuramae, E.E. 2018. DOI: 10.3389/fmicb.2018.01636.

Cox, G.F.N. & Weeks, W.F. 1975. *Brine Drainage And Initial Salt Entrapment In Sodium Chloride Ice Cold Regions Research And Engineering Laboratory*.

Crabeck, O., Delille, B., Rysgaard, S., Thomas, D.N., Geilfus, N.X., Else, B. & Tison, J.L. 2014. First in situ'' determination of gas transport coefficients (DO2, DAr, and DN2) from bulk gas concentration measurements (O2, N2, Ar) in natural sea ice. *Journal of Geophysical Research: Oceans*. 119(10):6655–6668. DOI: 10.1002/2014JC009849.

Dahl, E. & Nautsvoll, L.-J. 2010. Filtering – semitransparent filters for for quantitative phytoplankton analysis. In *Microscopic And Molecular Methods For Quantitative Phytoplankton Analysis*. 37–40.

Demir-Yilmaz, I., Novosel, N., Levak Zorinc, M., Mišić Radić, T., Ftouhi, M.S., Guiraud, P., Ivošević DeNardis, N. & Formosa-Dague, C. 2023. Investigation of the role of cell hydrophobicity and EPS production in the aggregation of the marine diatom Cylindrotheca

closterium under hypo-saline conditions. *Marine Environmental Research*. 188:106020. DOI: 10.1016/J.MARENVRES.2023.106020.

Doble, M.J., Coon, M.D. & Wadhams, P. 2003. Pancake ice formation in the Weddell Sea. *Journal of Geophysical Research: Oceans*. 108(C7):3209. DOI: 10.1029/2002JC001373.

Dumont, I., Schoemann, V., Lannuzel, D., Chou, L., Tison, J.L. & Becquevort, S. 2009. Distribution and characterization of dissolved and particulate organic matter in Antarctic pack ice. *Polar Biology*. 32(5):733–750. DOI: 10.1007/s00300-008-0577-y.

Edler, L. & Elbrächter, M. 2010. The Utermöhl method for quantitative phytoplankton analysis. In *Microscopic And Molecular Methods For Quantitative Phytoplankton Analysis*. 13–20.

European Space Agency. 2016. Available: https://earth.esa.int/eogateway/documents/20142/1227611/Introduction-sea-ice-Process-Observations-and-Model.pdf [2025, January 15].

Ewert, M. & Deming, J.W. 2011. Selective retention in saline ice of extracellular polysaccharides produced by the cold-adapted marine bacterium Colwellia psychrerythraea strain 34H. *Annals of Glaciology*. 52(57):111–117. DOI: 10.3189/172756411795931868.

Ewert, M. & Deming, J.W. 2013. Sea ice microorganisms: Environmental constraints and extracellular responses. *Biology*. 2(2):603–628. DOI: 10.3390/biology2020603.

Fenchel, T. 1988. MARINE PLANKTON FOOD CHAINS. *Annual Review of Ecology and Systematics*. 19(1):19–38. DOI: 10.1146/annurev.es.19.110188.000315.

Fogg, G.E. & Calvario-Martinez, O. 1989. *Production and Pathways of Freshly Produced Organic Matter within the Pelagic Zone Effects of bottle size in determinations of primary productivity by phytoplankton*.

Forgereau, Z.L., Lange, B.A. & Campbell, K. 2023. *The Stressful Life of Sea Ice Algae*.

Forgereau, Z.L., Lange, B.A., Gradinger, R., Assmy, P., Osanen, J.E., García, L.M., Søreide, J.E., Granskog, M.A., et al. 2023. Photophysiological responses of bottom sea-ice algae to fjord dynamics and rapid freshening. *Frontiers in Marine Science*. 10. DOI: 10.3389/fmars.2023.1221639.

Gadiyar, H.S. & Shibad, P.R. 1980. Titanium For Salt Water Service.

Van Gassen, S., Callebaut, B., Van Helden, M.J., Lambrecht, B.N., Demeester, P., Dhaene, T. & Saeys, Y. 2015. FlowSOM: Using self-organizing maps for visualization and interpretation of cytometry data. *Cytometry Part A*. 87(7):636–645. DOI: 10.1002/CYTO.A.22625.

Gow, A.J. & Iii, W.B.T. 1991. AD-A256 303 Physical and Dynamic Properties of Sea Ice in the Polar Oceans.

Graco. 2013. Available: https://www.graco.com/content/dam/graco/ipd/literature/misc/chemical-compatibility-guide/Graco_ChemCompGuideEN-B.pdf [2024, April 16].

Guni, F. 2022. *Heat transfer analysis on the growth of artificial sea ice using dynamic temperature profiles in an idealised environment*.

Hall, B.M. 2019. Design of a Small-Scale System for the Growth of Artificial Sea Ice. University of Cape Town.

Hall, B., Johnson, S., Thomas, M. & Rampai, T. 2023. Review of the design considerations for the laboratory growth of sea ice. *Journal of Glaciology*. 69(276):953–965. DOI: 10.1017/jog.2022.115.

Hancke, K., Lund-Hansen, L.C., Lamare, M.L., Højlund Pedersen, S., King, M.D., Andersen, P. & Sorrell, B.K. 2018. Extreme Low Light Requirement for Algae Growth Underneath Sea Ice: A Case Study From Station Nord, NE Greenland. *Journal of Geophysical Research: Oceans*. 123(2):985–1000. DOI: 10.1002/2017JC013263.

Himmelblau, D.M. & Riggs, J.B. 2013. *Basic Principles and Calculations in Chemical Engineering*. 8th ed. B. Goodwin, Ed.

Hyka, P., Lickova, S., Přibyl, P., Melzoch, K. & Kovar, K. 2013. Flow cytometry for the development of biotechnological processes with microalgae. *Biotechnology Advances*. 31(1):2–16. DOI: 10.1016/J.BIOTECHADV.2012.04.007.

Jiao, Y., Cody, G.D., Harding, A.K., Wilmes, P., Schrenk, M., Wheeler, K.E., Banfield, J.F. & Thelen, M.P. 2010. Characterization of extracellular polymeric substances from acidophilic microbial biofilms. *Applied and Environmental Microbiology*. 76(9):2916–2922. DOI: 10.1128/AEM.02289-09/FORMAT/EPUB.

Johnson, S. 2020. Evaluation of the Changes in the Crystal Structure of Antarctic Sea Ice from the Marginal Ice Zone during Winter and Spring. University of Cape Town.

Johnson, S., Audh, R.R., De Jager, W., Matlakala, B., Vichi, M., Womack, A. & Rampai, T. 2023. Physical and morphological properties of first-year Antarctic sea ice in the spring marginal ice zone of the Atlantic-Indian sector. *Journal of Glaciology*. 69(277):1351–1364. DOI: 10.1017/jog.2023.21.

Jonsson, T. 2013. On the one dimensional Stefan problem with some numerical analysis.

Karlson, B., Godhe, A., Cusack, C. & Bresnan, E. 2010. Introduction to methods for quantitative phytoplankton analysis. In *Microscopic And Molecular Methods For Quantitative Phytoplankton Analysis*. 5–12.

Katam, K., Ananthula, R., Anumala, S., Sriariyanun, M. & Bhattacharyya, D. 2022. The impact of light intensity and wavelength on the performance of algal-bacterial culture treating domestic wastewater. In *E3S Web of Conferences*. V. 355. EDP Sciences. DOI: 10.1051/e3sconf/202235502003.

Kim, K., Park, J., Jo, N., Park, S., Yoo, H., Kim, J. & Lee, S.H. 2021. Monthly Variation in the Macromolecular Composition of Phytoplankton Communities at Jang Bogo Station, Terra Nova Bay, Ross Sea. *Frontiers in Microbiology*. 12. DOI: 10.3389/fmicb.2021.618999.

Kim, K., Ha, S.Y., Shin, K.H., Kim, J.H., Mundy, C.J., Dalman, L.A., Kim, B.K., Lee, D., et al. 2023. Vertical distributions of organic matter components in sea ice near Cambridge Bay, Dease Strait, Canadian Archipelago. *Frontiers in Marine Science*. 10. DOI: 10.3389/fmars.2023.1231083.

Kingston, J.C. 2003. *Araphid and Monoraphid Diatoms*. DOI: 10.1016/B978-0-12-741550-5.50017-9.

Krembs, C., Gradinger, R. & Spindler, M. 2000. *Implications of brine channel geometry and surface area for the interaction of sympagic organisms in Arctic sea ice*. Available: www.elsevier.nl/locate/jembe.

Krembs, C., Eicken, H., Junge, K. & Deming, J.W. 2002. High concentrations of exopolymeric substances in Arctic winter sea ice: implications for the polar ocean carbon cycle and cryoprotection of diatoms. *Deep-Sea Research I*. 49:2163–2181.

Krembs, C., Eicken, H. & Deming, J.W. 2011. Exopolymer alteration of physical properties of sea ice and implications for ice habitability and biogeochemistry in a warmer Arctic. *Proceedings of the National Academy of Sciences of the United States of America*. 108(9):3653–3658. DOI: 10.1073/pnas.1100701108.

Kuiper, M.J., Lankin, C., Gauthier, S.Y., Walker, V.K. & Davies, P.L. 2003. Purification of antifreeze proteins by adsorption to ice. *Biochemical and Biophysical Research Communications*. 300(3):645–648. DOI: 10.1016/S0006-291X(02)02900-5.

Kumadiro, L. 2023. *Antarctic Sea Ice phytoplankton growth rates and survival mechanisms CHEMICAL ENGINEERING*.

Lange, M.A. & Eicken, H. 1991. Textural characteristics of sea ice and the major mechanisms of ice growth in the Weddell Sea. DOI: 10.3189/1991AoG15-1-210-215.

Lange, M.A., Ackley, S.F., Dieck Mann, G.S. & Eicken, H. 1989. Development Of Sea Ice In The Weddell Sea. DOI: 10.3189/S0260305500007023.

van Leeuwe, M.A., Webb, A.L., Venables, H.J., Visser, R.J.W., Meredith, M.P., Elzenga, J.T.M. & Stefels, J. 2020. Annual patterns in phytoplankton phenology in Antarctic coastal waters explained by environmental drivers. *Limnology and Oceanography*. 65(7):1651–1668. DOI: 10.1002/LNO.11477.

LeGresley, M. & McDermott, G. 2010. Counting chamber methods for quantitative phytoplankton analysis - haemocytometer, Palmer-Maloney cell and Sedgewick-Rafter cell. 25–30.

Lindsey, R. & Scott, M. 2010. What are Phytoplankton. *NASA Earth Observatory*. (June, 13).

Louw, S.D.V., Walker, D.R. & Fawcett, S.E. 2022. Factors influencing sea-ice algae abundance, community composition, and distribution in the marginal ice zone of the Southern Ocean during winter. *Deep Sea Research Part I: Oceanographic Research Papers*. 185:103805. DOI: 10.1016/J.DSR.2022.103805.

Lu, X., Zhang, Y., Liu, Y. & Fan, Y. 2022. Differences in planktonic and benthic diatoms reflect water quality during a rainstorm event in the Songhua River Basin of northeast China. *Ecological Indicators*. 144:109547. DOI: 10.1016/J.ECOLIND.2022.109547.

Lund-Hansen, L.C., Gradinger, R., Hassett, B., Jayasinghe, S., Kennedy, F., Martin, A., McMinn, A., Søgaard, D.H., et al. 2024. DOI: 10.1007/s00300-024-03296-z.

Lundholm, N., Christensen, A.L., Olesen, A.K.J., Beszteri, B., Eggers, S.L., Krock, B. & Altenburger, A. 2024. Diversity, toxicity, and distribution of potentially toxic diatoms in Antarctic waters—With description of Pseudo-nitzschia meridionalis sp. nov. and P. glacialis sp. nov. *Harmful Algae*. 139. DOI: 10.1016/j.hal.2024.102724.

Maciej Serda, Becker, F.G., Cleary, M., Team, R.M., Holtermann, H., The, D., Agenda, N., Science, P., et al. 2013. Synteza i aktywność biologiczna nowych analogów tiosemikarbazonowych chelatorów żelaza. *Uniwersytet śląski*. 7(1):343–354. DOI: 10.2/JQUERY.MIN.JS.

Majewska, R., Gambi, M.C., Totti, C.M. & De Stefano, M. 2013. Epiphytic diatom communities of Terra Nova Bay, Ross Sea, Antarctica: Structural analysis and relations to algal host. *Antarctic Science*. 25(4):501–513. DOI: 10.1017/S0954102012001101.

Maksimov, V. & Amer, S. 2017. Convection influence on ice formation process on the evaporator heat pump pipes. DOI: 10.1051/matecconf/201714101001.

Maksym, T. 2025. Arctic and Antarctic Sea Ice Change: Contrasts, Commonalities, and Causes. *Downloaded from www.annualreviews.org. Guest (guest*. 11:42. DOI: 10.1146/annurev-marine-010816.

Malik, A.U., Ahmad, S., Andijani, I. & Al-Fouzan, S. 1999. Corrosion behavior of steels in Gulf seawater environment. *Desalination*. 123(2–3):205–213. DOI: 10.1016/S0011-9164(99)00078-8.

Maltsev, Y., Maltseva, K., Kulikovskiy, M. & Maltseva, S. 2021. DOI: 10.3390/biology10101060.

Mangoni, O., Carrada, G.C., Modigh, M., Catalano, G. & Saggiomo, V. 2009. Photoacclimation in Antarctic bottom ice algae: An experimental approach. *Polar Biology*. 32(3):325–335. DOI: 10.1007/s00300-008-0517-x.

Marks, A.A., Lamare, M.L. & King, M.D. 2017. Optical properties of laboratory grown sea ice doped with light absorbing impurities (black carbon). *The Cryosphere Discussion*. (May, 16). DOI: 10.5194/tc-2017-76.

Matlakala, B. 2022. Factors Influencing The Morphology Of Sea Ice. University of Cape Town.

McDermott, G. & Raine, R. 2010. Settlement bottle method for quantitative phytoplankton analysis. In *Microscopic And Molecular Methods For Quantitative Phytoplankton Analysis*. 21–24.

Meredith, M., Sommerkorn, M., Cassotta, S., Derksen, C., Ekaykin, A., Hollowed, A., Kofinas, G., Mackintosh, G., et al. 2022. Polar Regions. In *The Ocean and Cryosphere in a Changing Climate: Special Report of the Intergovernmental Panel on Climate Change*. Cambridge University Press. 203–320. DOI: 10.1017/9781009157964.005.

Mettler Toledo. n.d. Available: https://www.scribd.com/document/89464293/Weigh-Module-System-Handbook-Def-En [2024, April 16].

Miklasz, K.A. & Denny, M.W. 2010. Diatom sinkings speeds: Improved predictions and insight from a modified Stokes' law. *Limnology and Oceanography*. 55(6):2513–2525. DOI: 10.4319/LO.2010.55.6.2513.

Moncheva, S. 2010. Manual for Phytoplankton Sampling and Analysis in the Black Sea.

Montagnes, D.J.S. & Franklin, D.J. 2001. Effect of temperature on diatom volume, growth rate, and carbon and nitrogen content: Reconsidering some paradigms. *Limnology and Oceanography*. 46(8):2008–2018. DOI: 10.4319/lo.2001.46.8.2008.

Morawetz, K., Thoms, S. & Kutschan, B. 2017. Formation of brine channels in sea ice. (March, 3). DOI: 10.1140/epje/i2017-11512-x.

Morel, F.M.M., Milligan, A.J. & Saito, M.A. 2003. *6.05 Marine Bioinorganic Chemistry: The Role of Trace Metals in the Oceanic Cycles of Major Nutrients*.

Morrow, M. n.d. *A Photographic Atlas for Botany*. Available: https://bio.libretexts.org/Bookshelves/Botany/A_Photographic_Atlas_for_Botany_(Morrow)/04%3A_Protists/4.04%3A_Diatoms [2024, December 07].

Nagayach, N. kumar & Agrawal, A.B. 2012. *Review Of Heat Transfer Augmentation In Circular And Non-Circular Tube*. Available: www.ijera.com.

Naumann, A.K., Notz, D., Håvik, L. & Sirevaag, A. 2012. Laboratory study of initial sea-ice growth: properties of grease ice and nilas. *The Cryosphere*. 6:729–741. DOI: 10.5194/tc-6-729-2012.

North, N. & MacLeod, I. 1987. Corrosion of metals.

Notz, D. & Worster, M.G. 2009. Desalination processes of sea ice revisited. *Journal of Geophysical Research: Oceans*. 114(5). DOI: 10.1029/2008JC004885.

Notz, D., Wettlaufer, J.S. & Worster, M.G. 2005. A non-destructive method for measuring the salinity and solid fraction of growing sea ice in situ. *Journal of Glaciology*. 51(172):159–166. DOI: 10.3189/172756505781829548.

Passow, U. & Alldredge, A.L. 1995. A dye-binding assay for the spectrophotometric measurement of transparent exopolymer particles (TEP). *Limnology and Oceanography*. 40(7):1326–1335. DOI: 10.4319/LO.1995.40.7.1326.

Peperzak, L., Zetsche, E.M., Gollasch, S., Artigas, L.F., Bonato, S., Creach, V., de Vré, P., Dubelaar, G.B.J., et al. 2020. Comparing flow cytometry and microscopy in the quantification of vital aquatic organisms in ballast water. *Journal of Marine Engineering and Technology*. 19(2):68–77. DOI: 10.1080/20464177.2018.1525806.

Perovich, D.K. & Grenfell, T.C. 1981. Laboratory Studies of the Optical Properties of Young Sea Ice. *Journal of Glaciology*. 27(96):331–346. DOI: 10.3189/s0022143000015410.

Pesjak, L., McMinn, A., Chase, Z. & Bostock, H. 2023. Sea ice and productivity changes over the last glacial cycle in the Adélie Land region, East Antarctica, based on diatom assemblage variability. *Climate of the Past*. 19(2):419–437. DOI: 10.5194/cp-19-419-2023.

Petrich, C. & Eicken, H. 2017. Overview of sea ice growth and proiperties. In *Sea Ice Third Edition*. D. Thomas, Ed. Wiley-Blackwell. 1–41. Available: https://www.wiley.com/en-us/Sea+Ice%2C+3rd+Edition-p-9781118778388 [2024, April 23].

Rajanahally, M.A., Sim, D., Ryan, K.G. & Convey, P. 2014. Can bottom ice algae tolerate irradiance and temperature changes? *Journal of Experimental Marine Biology and Ecology*. 461:516–527. DOI: 10.1016/j.jembe.2014.10.005.

Romero, O.E. 2011. Morphological study of the genus Cocconeis Ehrenberg (Bacillariophyceae) collected during the 1897-1899 Belgian Antarctic Expedition. *Botanica Marina*. 54(2):179–188. DOI: 10.1515/BOT.2011.020.

Rösler, J., Harders, H. & Bäker, M. 2007. *Mechanical Behaviour of Engineering Materials*.

San Marchi, C., Somerday, B.P., Tang, X. & Schiroky, G.H. 2008. Effects of alloy composition and strain hardening on tensile fracture of hydrogen-precharged type 316 stainless steels. *International Journal of Hydrogen Energy*. 33(2):889–904. DOI: 10.1016/J.IJHYDENE.2007.10.046.

Schneider, C.A., Rasband, W.S. & Eliceiri, K.W. 2012. DOI: 10.1038/nmeth.2089.

Schulson, E.M., Renshaw, C.E. & Snyder, S.A. 2012. The Effect of Deformation Damage on the Mechanical Behavior of Sea Ice: Ductile-to-Brittle Transition, Elastic Modulus, and Brittle Compressive Strength.

Semih Genculu, P.E. n.d. Cast Irons-Properties and Applications.

Sparrow, E.M., Chevalier, P.W. & Abraham, J.P. 2006. The Design of Cold Plates for the Thermal Management of Electronic Equipment. *Heat Transfer Engineering*. 27(7):6–16. DOI: 10.1080/01457630600742308.

Stoecker, D.K., Gustafson, D.E., D Black, M.M. & Baier, C.T. 1997. *Excystment And Growth Of Chrysophwes And Dinoflagellates At Low Temperatures And High Salinities In Antarctic Sea-Ice'*.

Sunda, W.G. 2012. Feedback interactions between trace metal nutrients and phytoplankton in the ocean. *Frontiers in Microbiology*. 3(JUN). DOI: 10.3389/fmicb.2012.00204.

Swadling, K.M., Constable, A.J., Fraser, A.D., Massom, R.A., Borup, M.D., Ghigliotti, L., Granata, A., Guglielmo, L., et al. 2023. Biological responses to change in Antarctic sea ice habitats. *Frontiers in Ecology and Evolution*. 10. DOI: 10.3389/fevo.2022.1073823.

Swait, H. 2024. Investigating Brine and Air Porosity from Sea Ice Samples from the Marginal Ice Zone of Antarctica. Masters Thesis. University of Cape Town.

Tedesco, L. & Vichi, M. 2014. Sea ice biogeochemistry: A guide for modellers. *PLoS ONE*. 9(2). DOI: 10.1371/JOURNAL.PONE.0089217.

Tetzner, D.R., Allen, C.S. & Thomas, E.R. 2022. Regional variability of diatoms in ice cores from the Antarctic Peninsula and Ellsworth Land, Antarctica. *Cryosphere*. 16(3):779–798. DOI: 10.5194/tc-16-779-2022.

Underwood, G.J.C., Fietz, S., Papadimitriou, S., Thomas, D.N. & Dieckmann, G.S. 2010. Distribution and composition of dissolved extracellular polymeric substances (EPS) in Antarctic sea ice. *Marine Ecology Progress Series*. 404:1–19. DOI: 10.3354/meps08557.

Vancoppenolle, M., Goosse, H., De Montety, A., Fichefet, T., Tremblay, B. & Tison, J.L. 2010. Modeling brine and nutrient dynamics in Antarctic sea ice: The case of dissolved silica. *Journal of Geophysical Research: Oceans*. 115(2). DOI: 10.1029/2009JC005369.

Vaulot, D., Bilcke, G., Chaerle, P., Falciatore, A., Gourvil, P., Lomas, M.W., Probert, I. & Vyverman, W. 2023. *Culturing Diatoms 1 Chapter prepared for: 18 Diatom Photosynthesis: From Primary Production to High Value Molecules*.

Venegas, R.M., Acevedo, J. & Treml, E.A. 2023. Three decades of ocean warming impacts on marine ecosystems: A review and perspective. *Deep-Sea Research Part II: Topical Studies in Oceanography*. 212. DOI: 10.1016/j.dsr2.2023.105318.

Vihma, T. 2014. Effects of Arctic Sea Ice Decline on Weather and Climate: A Review Timo Vihma. 35:1175–1214. DOI: 10.1007/s10712-014-9284-0.

Weeks, W.F. 1962. Tensile Strength of NaCl Ice. *Journal of Glaciology*. 4(31):25–52. DOI: 10.3189/s0022143000018190.

Weeks, W.F. & Ackley, S.F. 1982. *The Growth Structure And Properties Of Sea Ice(U) Cold.*

Wolfenbarger, N., Buffo, J., Soderlund, K., Blankenship, D., Wolfenbarger, N.S., Buffo, J.J., Soderlund, K.M. & Pickle Research Campus, J. 2022. Ice Shell Structure and Composition of Ocean Worlds: Insights from Accreted Ice on Earth. DOI: 10.1002/essoar.10507059/v3.

Yen, Y.-C. 1981. *Review Of Thermal Properties Of Snow, Ice And Sea Ice*. Hanover.

Zwaan, D., Jacobs, P. & Van Houcke, J. 2023. *EFFECTS OF DIFFERENT LIGHT WAVELENGTHS AND INTENSITIES ON DIATOM AND FLAGELLATE MICROALGAE PRODUCTION*.

Appendices:

A. Cold Finger Engineering Drawings

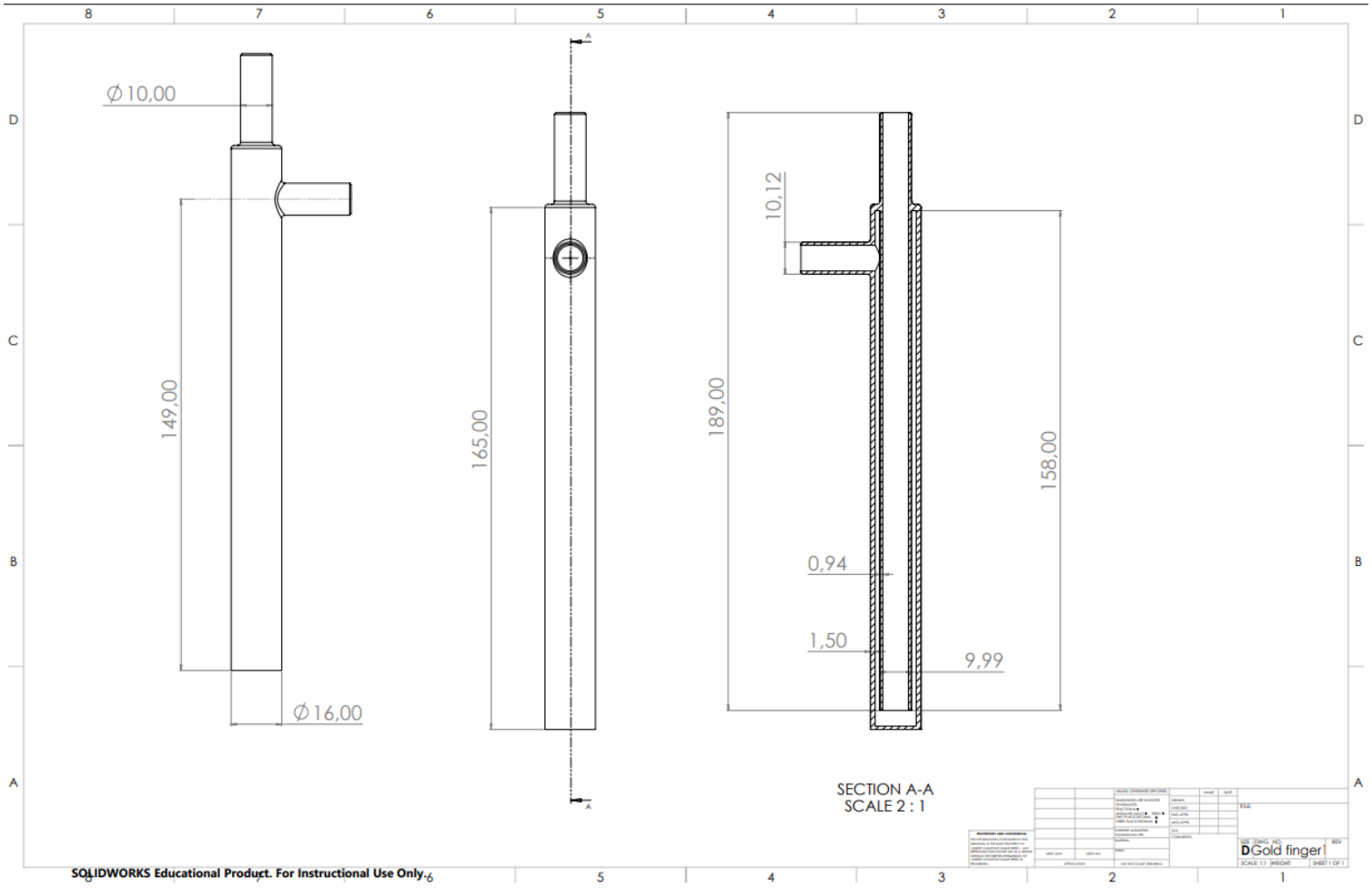

Figure A-1: Cold finger internal and external drawings with dimensions.

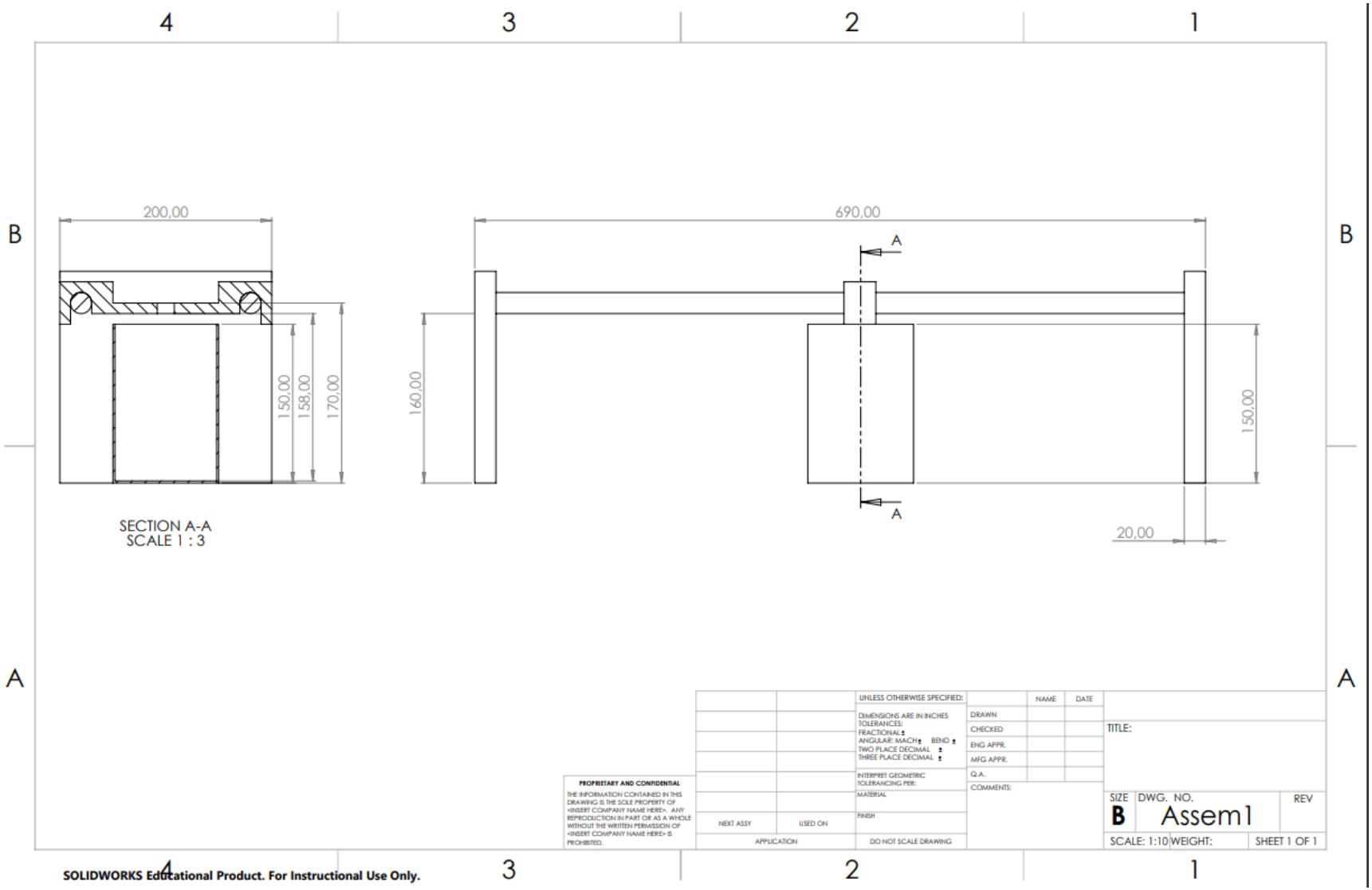

Figure A-2: Cold finger scaffolding design with dimensions part 2.

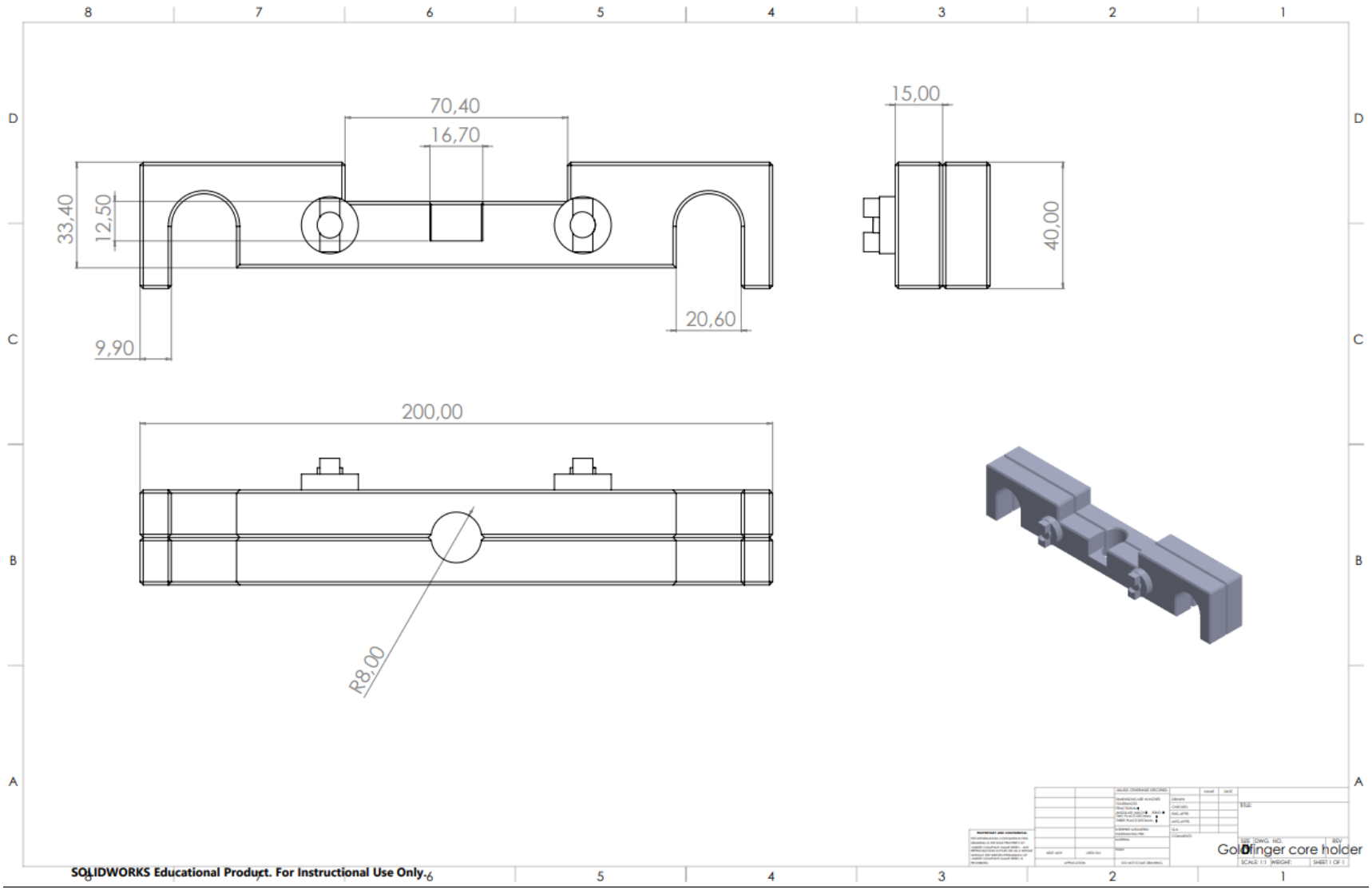

Figure A-3: Cold finger scaffolding design with dimensions part 2.

B. Thermodynamic Model and Ice Growth Dynamics

B.1. Thermodynamic Model Development

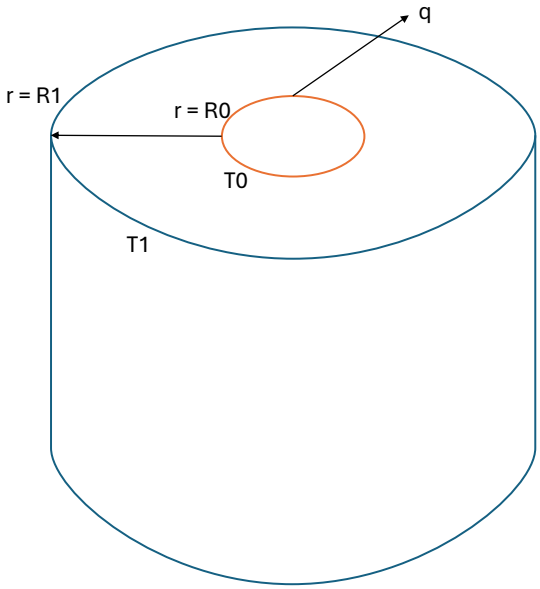

Figure B-1: Radial conduction through a semi-hollow cylinder adapted from Bejan & Kraus (2003).

The following key assumptions were made:

1. The coolant is cold enough to maintain a constant temperature along the cold finger length, which is pre-set to a desired level.
2. One-dimensional heat transfer is assumed with an infinitely cold finger.
3. Chiller maintains constant brine temperature of -1.8°C, aligning with the freezing point of the solution.
4. Ice properties are assumed to remain constant: bulk density remains constant despite variations in salinity, and thermal conductivity is considered constant since ice is treated as isotropic within the temperature range of 0°C to -30°C (Yen, 1981).
5. In the context of phase transition with a dynamic boundary, the Stefan problem is assumed, thus establishing a pseudo-steady state within the ice (Jonsson, 2013). This implies that the heat flux is rapid compared to ice growth and therefore the temperature profile is linear in respect to the inverse of the radius.
6. There is no heat transfer resistance between the cold finger and the formation of ice, nor between the brine and the ice formation process.

7. Apart from the phase change process, no heat is either lost or consumed and therefore the heat flux is equal to the rate of ice formation.

The development of the model used Fourier's Law, which describes conductive heat flux through area per unit time as linearly proportional to the temperature gradient (Bejan & Kraus, 2003).

Equation B-1: $$q_n = -k_n \frac{\partial T}{\partial n}$$

Fourier's law is given by the Equation B-1 in the n direction where q_n is the heat transfer rate per unit area, k_n is the thermal conductivity and $\frac{\partial T}{\partial n}$ is temperature gradient. Given the radial heat transfer induced by the cold finger, an adaptation of the Fourier equation was necessary to accommodate its application within an annulus. Hence, Equation B-2, describing heat conduction within a cylindrical coordinate system, is derived through performing an energy balance (Bejan & Kraus, 2003).

Equation B-2: $$\frac{1}{r}\frac{\partial}{\partial r}\left(kr\,\frac{\partial T}{\partial r}\right)+\frac{1}{r^2}\,\frac{\partial}{\partial \emptyset}\left(k\frac{\partial T}{\partial \emptyset}\right)+\frac{\partial}{\partial z}\left(k\,\frac{\partial T}{\partial z}\right)+q=\rho c\frac{\partial T}{\partial t}$$

Given the underlying assumptions, we can apply the concept of steady state one-dimensional conduction. This can be effectively modelled like heat conduction in a hollow cylinder, as discussed in (Bejan & Kraus, 2003). Typically, heat transfer in a hollow cylinder is considered from its centre origin with a radius of zero. However, in this modified "semi-hollow" cylinder, heat transfer occurs from the radius of a cold finger. In the context of one-dimensional conduction in the radial direction, Equation B-2 simplifies to Equation B-3.

Equation B-3: $$\frac{d}{dr}\left(r\,\frac{dT}{dr}\right)=0$$

Integrating Equation B-3 between the boundary conditions. The boundary conditions are the temperature (T0) and radius (R0) of the cold finger, and the temperature (T1) and radius (R1) at any specific stage of ice growth.

Equation B-4: $$q = \frac{2\pi kL(T_0 - T_1)}{ln\,(\frac{r_1}{r_0})}$$

Therefore, by applying one-dimensional radial conduction as described in Equation B-3 along with the application of Fourier's law in Equation B-1, the heat flux (q) within the semi-hollow cylinder can be expressed by Equation B-4, where k represents the thermal conductivity of the saline solution and L signifies the length of the hollow (cold finger). As per the assumptions the energy generated during ice formation is directly proportional to the heat flux.

Equation B-5: $$Q_{phase\ change} = m_{ice} \times \Delta H_{fusion}$$

The energy released during formation can be expressed as the product of mass of ice forming and the latent heat of formation as denoted by Equation B-5, where $Q_{\text{phase change}}$ is the energy released to form a specific mass of ice (m_{ice}) and ΔH_{fusion} is the latent heat of fusion required for the conversion of the saline solution to ice. Since no other energy transfer occurs other than from the phase change from the saline solution to ice, differentiating Equation B-5 with respect to time yields the rate of energy release, which is equivalent to the heat flux, as demonstrated in Equation B-6.

Equation B-6: $$\frac{dQ_{phase\ change}}{dt} = q$$

The rate of energy release during the phase change is directly linked to the variation in ice mass, as the latent heat of fusion remains constant. Considering that the models objective is to predict ice growth as a function of time, it becomes practical to express mass in terms of ice density and volume, and subsequently, in relation to the ice radius. Therefore, Equation B-6 can be rearranged to derive Equation B-7. Equation B-7 provides the rudimentary model predicting ice growth as a function of time.

Equation B-7: $$\frac{dr}{dt} = \frac{k(T0 - T1)}{\rho \Delta H_{fusion}(r - R0)\,ln\left(\frac{R0}{r}\right)}$$

B.2. Thermodynamic Model Code

```
clear
clc
//  a.  solve the steady state conduction in an anulus at any instant in time
//  b.  obtain an ode for r vs t by setting the rate of growth of a differential
//      element dr of ice at time t equal to the rate of energy that has passed
//      through the ice in a time step dt in which the ice interface moved from
//      r(t) to r(t)+dr using the difference between two equations from (a)
//---------------------------------------------------------------------------
function f=stick(t,r)
   f(1)=-k*(T1-T2)./(density*dH*r(1).*log(R1./r(1))^2)  //model
//    disp([t,r])
endfunction
k=2.3  //varies from 2.2....2.4
dH=333000   //J/kg
density=917   //kg/m3
T1=-15 // cold finger temp
T2=-1.8 // EC temp
R1=0.008   //m
r0=R1+R1*0.01  //m
t=logspace(log10(1e-5),log10(60*60*12),201)';t(1)=0  //sec

r=ode([r0;r0],t(1),t,stick)'
scf(1)
gcf.figure_size=[500 500]
clf
gca.font_size=3
gca.thickness=2
plot(t/(60*60),(r-R1)*1000,"-")
xlabel("time [h]","fontsize",4)
```

```
ylabel("radial growth of ice [mm]","fontsize",4)
legend("Model",1)
xs2svg(1,"IceStickProblem_fig1.svg")
```

B.3. Experimental Output of Thermodynamic Model Performance

Table B-1: Theoretical and experimental ice growth measurements at different experimental durations.

Temperature	-5°C	-10°C	-15°C
Growth Time	15h 4min	5h 53min	3h 39min
Theoretical Model Growth (mm)	32	32	32
Experimental Ice Growth 1 (mm)	28	33	29
Model Performance 1 (%)	-14.3	3.0	-10.3
Experimental Ice Growth 2 (mm)	34	34	33
Model Performance 2 (%)	5.9	5.9	3
Experimental Ice Growth 3 (mm)	30	34	31
Model Performance 3 (%)	-10.3	5.9	-3.2
Experimental Ice Growth Average (mm)	30.7	33.7	31.0
Model Performance Average (%)	-4.3	5.0	-3.2

Table B-2: Fraction of each ice texture and corresponding crystal size with varying EPS concentrations.

	Granular		Intermediate		Columnar	
EPS Concentration	%	Crystal Size (mm)	%	Crystal Size (mm)	%	Crystal Size (mm)
0 mg/l	21	1.06 ± 0.12	79	4.04 ± 1.22	-	-
1 mg/l	8	0.87 ± 0.14	11	1.02 ± 0.40	81	9.12 ± 0.95
10 mg/l	9	0.56 ± 0.10	37	2.82 ± 0.64	54	7.58 ± 0.65
1000 mg/l	-	-	-	-	100	14.93 ± 1.36
95% Confidence	$0.60 \leq x \leq 1.47$		$2.48 \leq x \leq 4.08$		$10.42 \leq x \leq 12.39$	

Table B-3: Comparison of EPS concentrations, salinity (initial, underlying, and ice), and ice growth parameters (diameter and rate) across samples

Sample	EPS (mg/l)	Initial salinity (PSU)		Underlying seawater salinity (PSU)		Ice salinity (PSU)		Ice growth	
		Actual	Normalised	Actual	Normalised	Actual	Normalised	Diameter (mm)	Rate (mm/h)
SW 1	0	35.5	1.00	39.8	1.12	14.6	0.410	66.8	22.3
SW 2	0	34.2	1.00	44.4	1.30	13.4	0.390	70.7	23.6
SW 3	0	33.5	1.00	43.8	1.31	14.1	0.420	69.7	23.2
SW average	0	34.4	1.00	42.7	1.24	14.0	0.410	69.1	23.0
EPS 1.1	1	35.0	1.00	38.3	1.09	14.6	0.420	69.8	23.3
EPS 1.2	1	35.1	1.00	45.5	1.30	14.2	0.400	70.6	23.5
EPS 1.3	1	34.5	1.00	45.3	1.31	13.6	0.390	67.1	22.4
EPS 1 average	1	34.9	1.00	43.0	1.23	14.1	0.410	69.2	23.1
EPS 10.1	10	34.4	1.00	42.0	1.22	12.2	0.350	68.7	22.9
EPS 10.2	10	35.1	1.00	40.3	1.15	15.5	0.440	68.2	22.7
EPS 10.3	10	34.9	1.00	45.9	1.32	14.7	0.420	70.4	23.5
EPS 10 average	10	34.8	1.00	42.7	1.23	14.1	0.410	69.1	23.0
EPS 1000.1	1000	34.8	1.00	36.3	1.04	27.7	0.800	73.9	24.7
EPS 1000.2	1000	35.3	1.00	36.4	1.03	30.4	0.860	74.5	24.8
EPS 1000.3	1000	34.7	1.00	36.5	1.05	34.3	0.990	74.0	24.7
EPS 1000 average	1000	34.9	1.00	36.4	1.04	30.8	0.880	74.1	24.7

Table B-4: Cross polarised image of all sea ice sample replicates at different EPS concentrations.

Replicate	EPS Concentration			
	0 mg/l	1 mg/l	10 mg/l	1000 mg/l
1	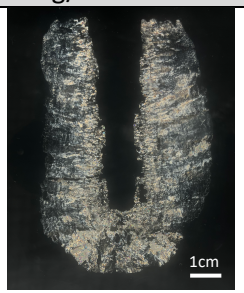	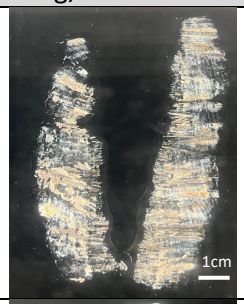	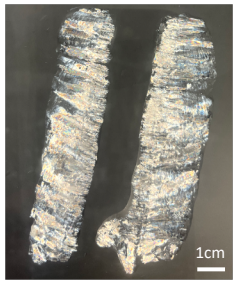	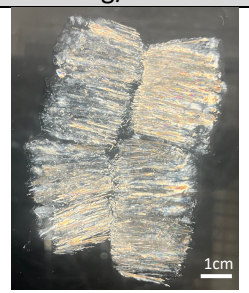
2	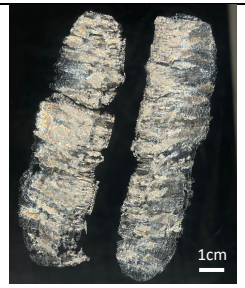	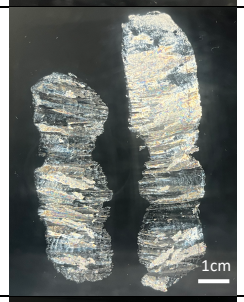	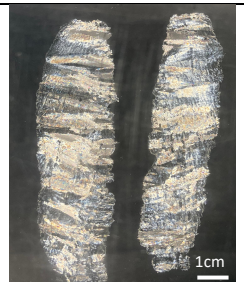	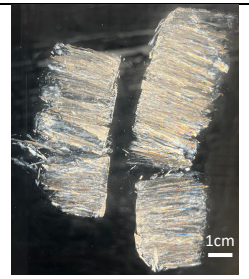
3	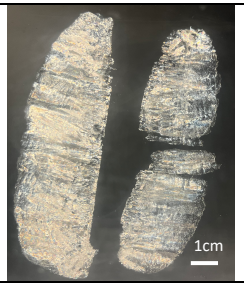	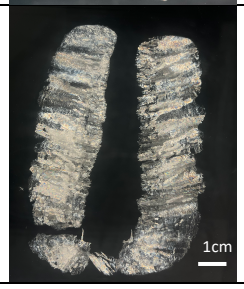	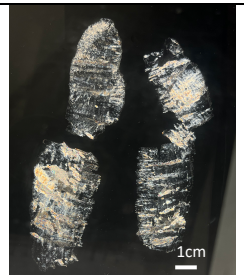	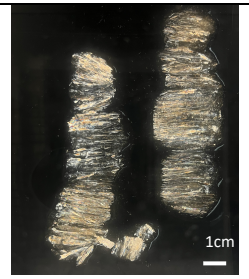

Table B-5: Visual output from Micro-CT scanning analysis at varying EPS concentrations.

	EPS Concentration			
	0 mg/l	1 mg/l	10 mg/l	1000 mg/l
2D greyscale image slice (scale bars at bottom of each image)	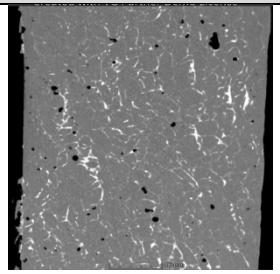	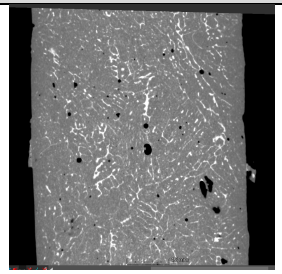	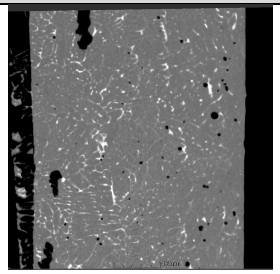	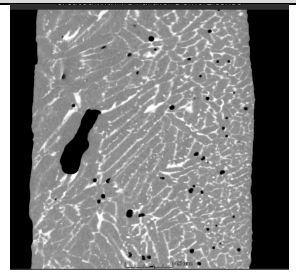
3D brine phase reconstruction Tubes Pockets	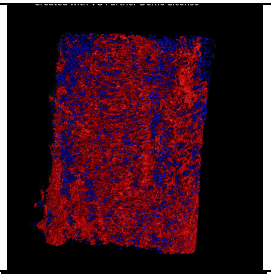	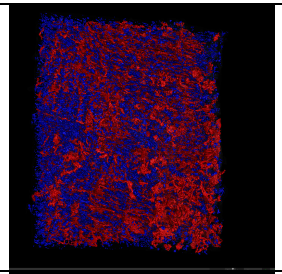	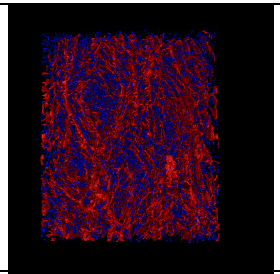	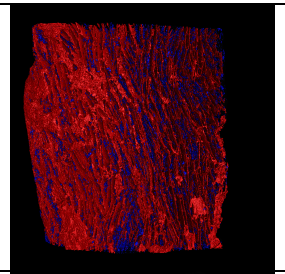
3D air phase reconstructions Micro Large Macro	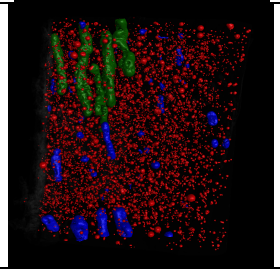	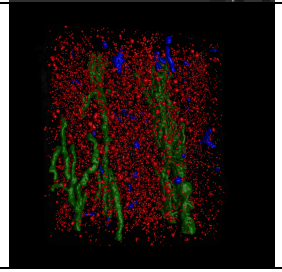	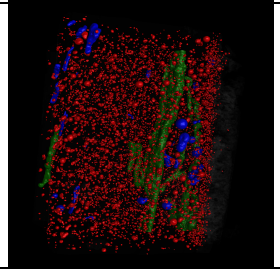	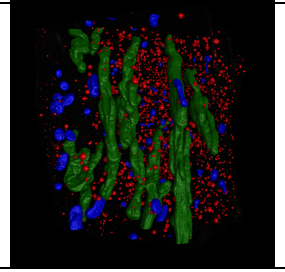

C. Preliminary Output of the Optimisation of the Experimental Methodology

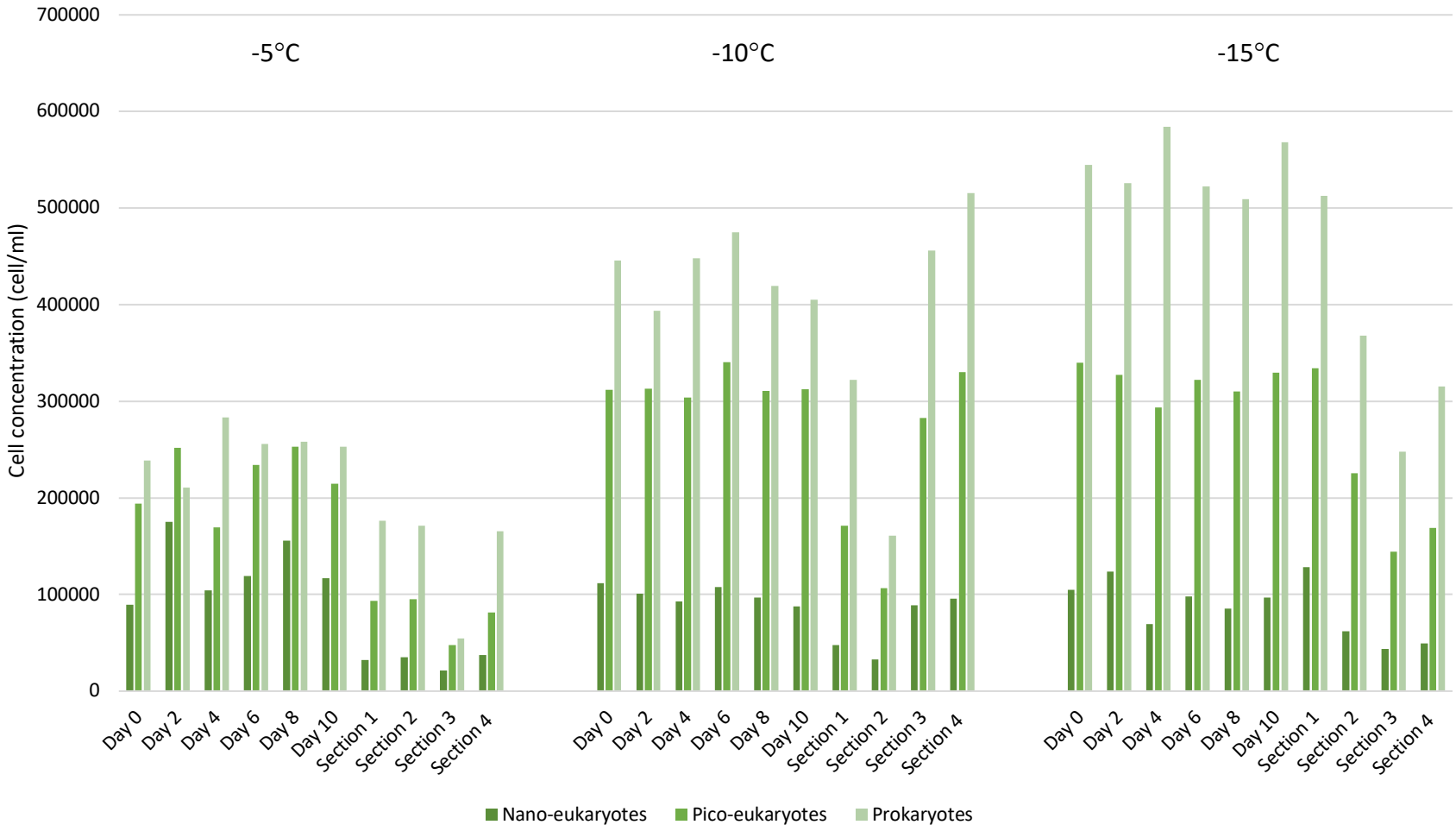

Figure C-1: Preliminary results for the initial experiment.

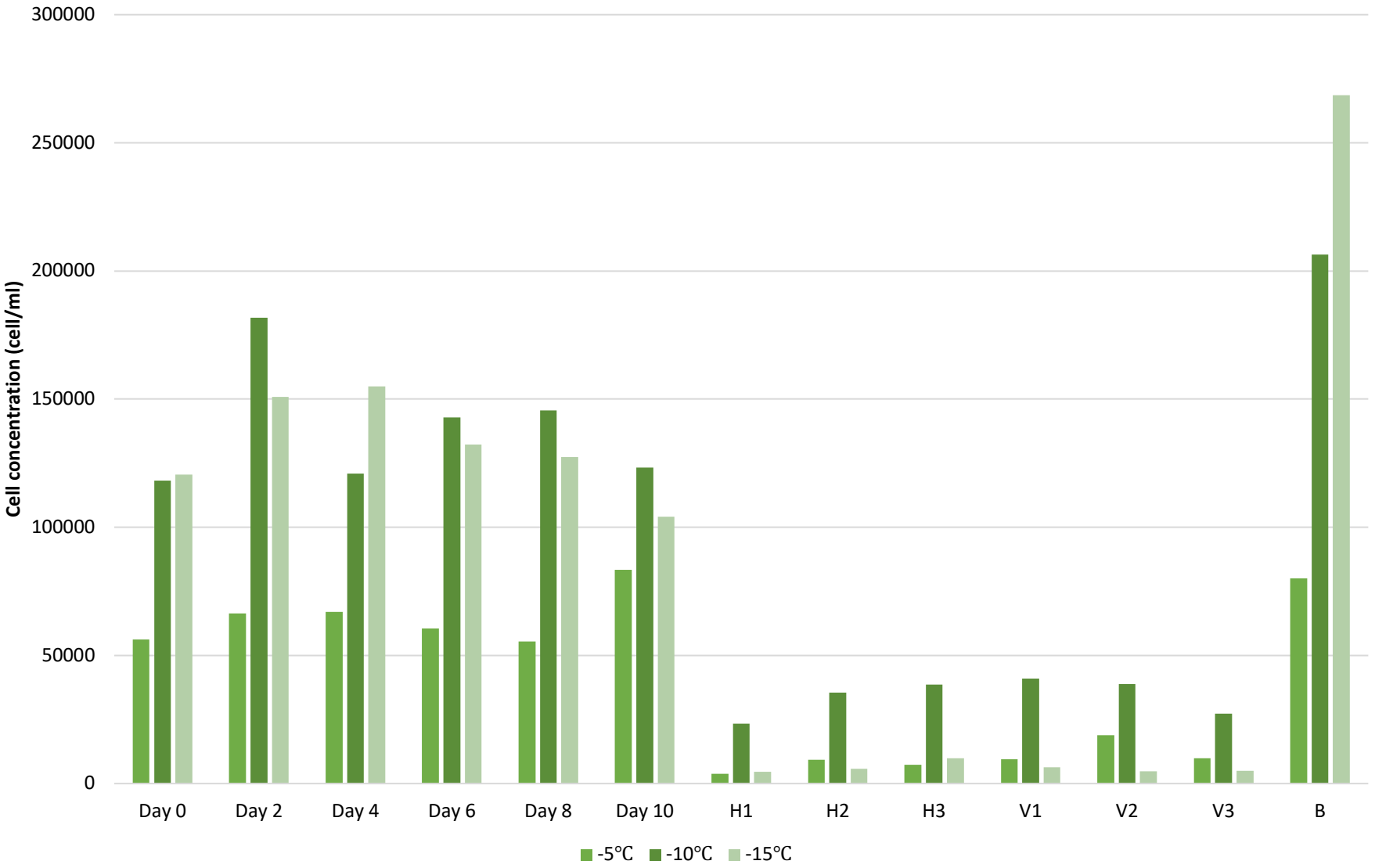

Figure C-2: Preliminary flow cytometry results for the first optimisation experiment.

M

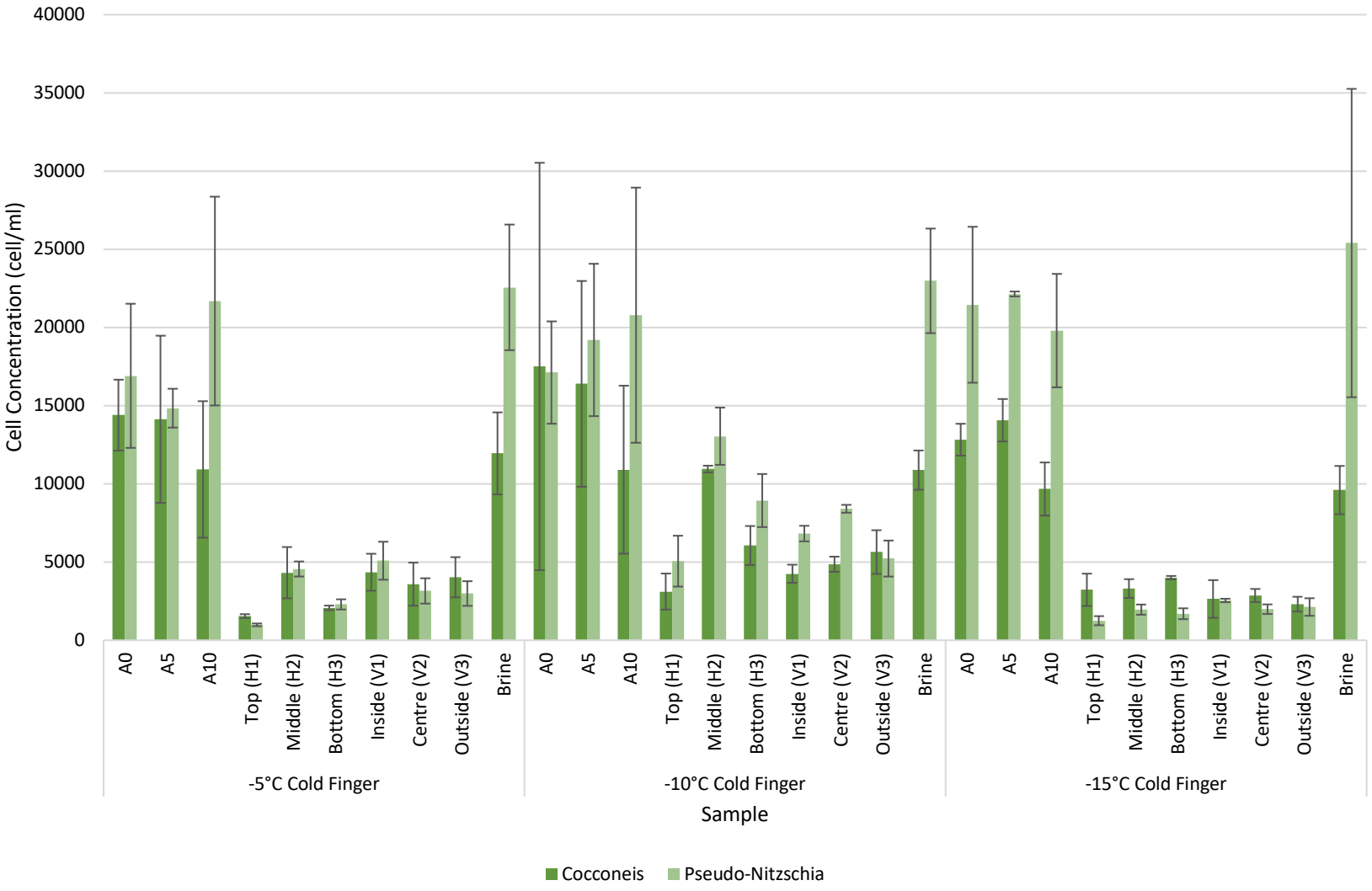

Figure C-3: Preliminary microscopy results for the first optimisation experiment.

N

D. Experimental Output of Fully Optimised Experiment

D.1. Light Data

For the experiment conducted at light with an ocean temperature of -1.8°C, 1-litre aquaria were placed adjacent to the par sensor for the first 7 days, indicating the true irradiance (light exposure with no Perspex tank over sensor) (Figure D-2). This is important as approximately 92% of light is let through by Perspex. For the remainder of the experiment, tanks were placed on top of the par sensor and hence the apparent drop in light exposure. However, this is also a result of the increased cell density on the bottom of the 1-litre aquaria due to settling of algae and debris. For the experiments conducted at light with an ocean temperature of 0°C and no light with an ocean temperature of -1.8°C, aquaria were placed over par sensors for the duration of the experiments.

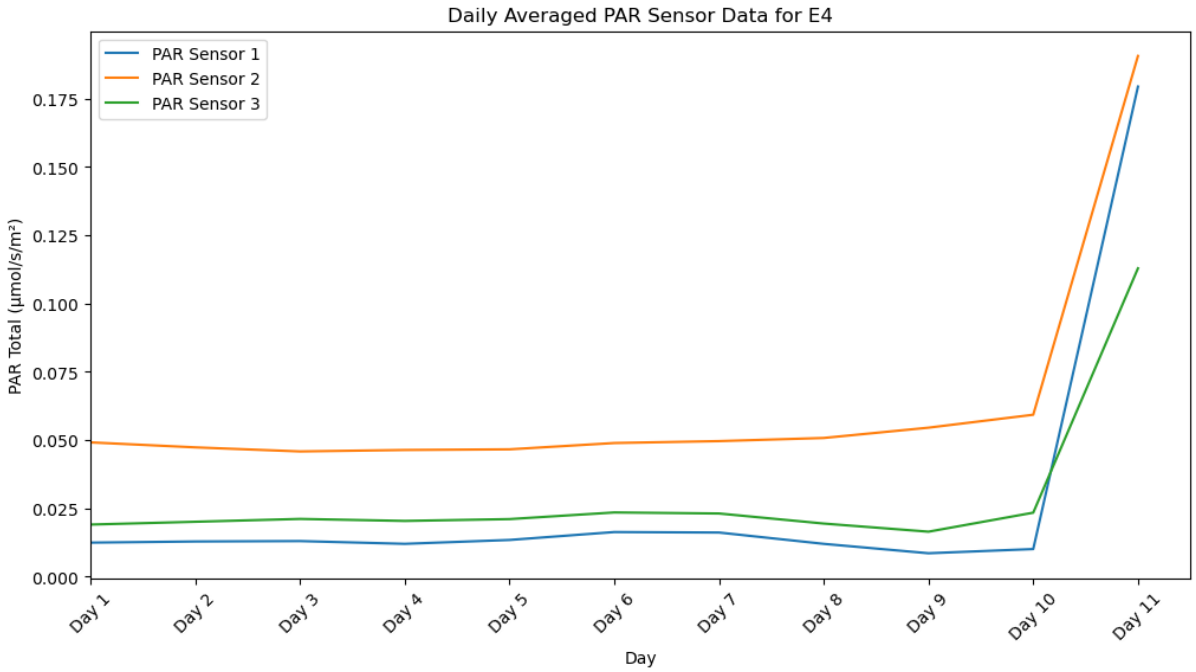

Figure D-1: Daily averaged par sensor data for the experiment conducted with no light and an ocean temperature of -1.8C.

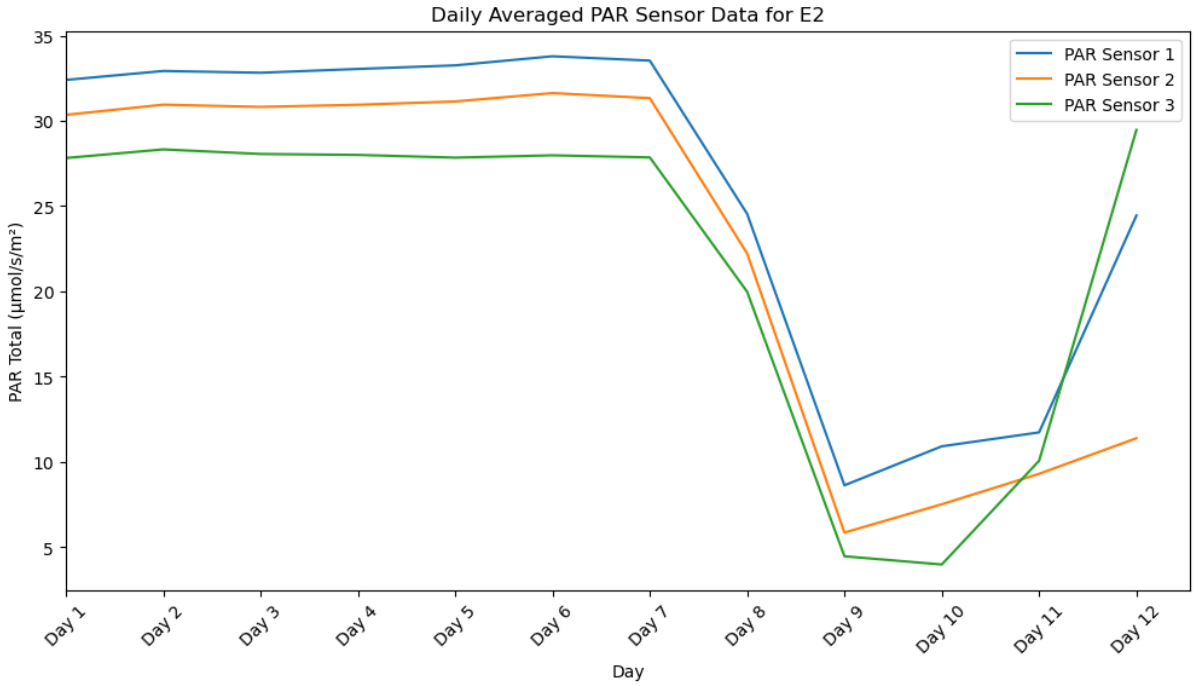

Figure D-2: Daily averaged par sensor data for the experiment conducted with light and an ocean temperature of -1.8℃.

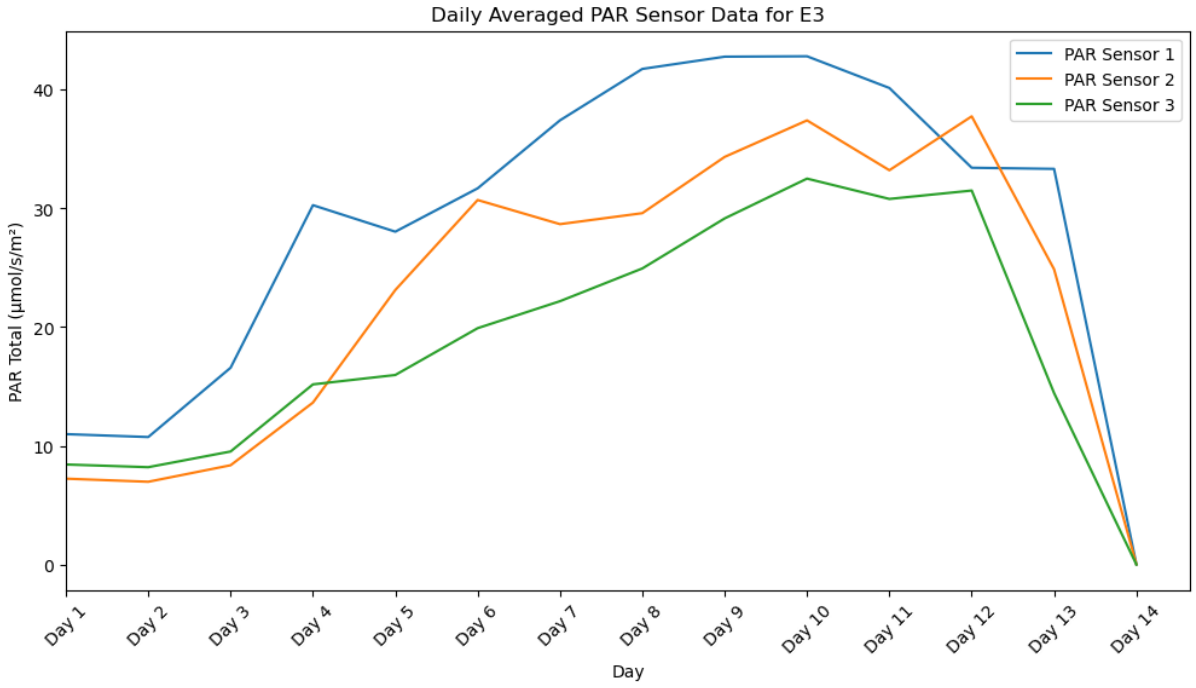

Figure D-3: Daily averaged par sensor data for the experiment conducted with light and an ocean temperature of 0℃.

D.2. Growth Dynamics

Table D-1: Summary of growth times for each experiment.

Experiments	Ice growth times		
Cold Finger Temperature (°C)	-5	-10	-15
No light, -1.8°C ocean temp	15h 5min	6h 5min	3h 45min
Light, -1.8°C ocean temp	20h 1min	5h 57min	3h 39min
Light, 0°C ocean temp	31h 55min	7h 31min	4h 36min

Table D-2: Summary of ice diameters for each experiment.

Experiments	Ice diameter (mm)		
Cold Finger Temperature (°C)	-5	-10	-15
No light, -1.8°C ocean temp	80.0	81.4	81.6
Light, -1.8°C ocean temp	77.6	78.5	78.2
Light, 0°C ocean temp	66.2	80.2	77.6

D.3. Physical Properties

Table D-3: Summary of measured ice volumes for the experiment conducted with no light and an ocean temperature of -1.8℃.

Section	Volume (ml)		
Cold Finger Temperature (°C)	-5	-10	-15
H1	72	73	69
H2	58	62	72
H3	40	42	61
V1	55	64	67
V2	39	74	52
V3	60	12	63
B (underlying seawater solution)	470	400	425

Table D-4: Summary of measured ice volumes for the experiment conducted with light and an ocean temperature of -1.8℃.

Section	Volume (ml)		
Cold Finger Temperature (°C)	-5	-10	-15
H1	54	80	78
H2	48	60	70
H3	30	48	60
V1	47	50	82
V2	43	61	48
V3	38	71	55
B (underlying seawater solution)	539	469	400

Table D-5: Summary of measured ice volumes for the experiment conducted with light and an ocean temperature of 0℃.

Section	Volume (ml)		
Cold Finger Temperature (°C)	-5	-10	-15
H1	38	50	69
H2	46	55	72
H3	23	40	61
V1	26	50	67
V2	24	48	52
V3	48	75	63
B (underlying seawater solution)	616	432	460

Table D-6: Summary of measured ice salinities for the experiment conducted with no light and an ocean temperature of -1.8℃.

Section	Salinity (PSU)		
Cold Finger Temperature (°C)	-5	-10	-15
Starting salinity	36.3	36.3	36.3
H1	9.53	10.6	12.2
H2	10.6	13.6	14.6
H3	14.3	15.7	17.1
V1	8.03	13.6	14.3
V2	7.30	11.3	11.2
V3	9.40	11.4	13.1
B (underlying seawater solution)	54.5	56.5	57.5

Table D-7: Summary of measured ice salinities for the experiment conducted with light and an ocean temperature of -1.8 ℃.

Section	Salinity (PSU)		
Cold Finger Temperature (°C)	-5	-10	-15
Starting salinity	36.8	36.8	36.8
H1	10.3	12.9	13.8
H2	10.6	15.1	14.9
H3	12.3	17.5	17.6
V1	7.8	13.5	15.5
V2	8.3	12.5	11.6
V3	9.3	11.6	12.2
B (underlying seawater solution)	53.5	59.0	59.5

Table D-8: Summary of measured ice salinities for the experiment conducted with light and an ocean temperature of 0 ℃.

Section	Salinity (PSU)		
Cold Finger Temperature (°C)	-5	-10	-15
Starting salinity	36.8	36.8	36.8
H1	6.80	13.7	13.9
H2	7.90	14.9	15.0
H3	7.30	16.8	16.4
V1	4.60	11.4	14.5
V2	3.43	11.3	13.4
V3	6.30	13.3	14.1
B (underlying seawater solution)	51.0	59.0	57.5

D.4. Graphs Displaying Normalised Cell Concentrations

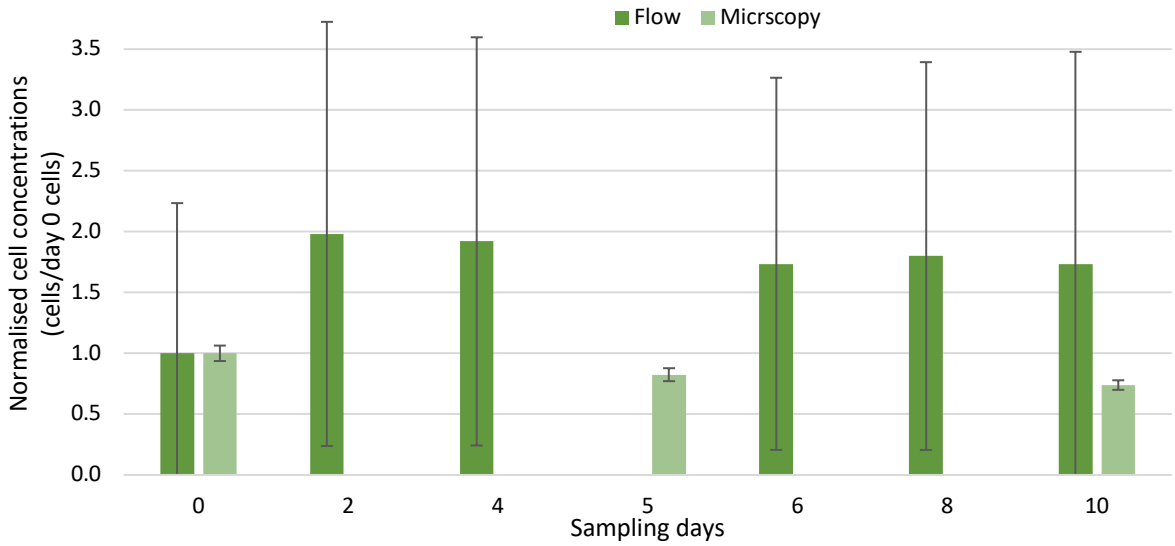

Figure D-4: Normalised cell concentrations in the -5 ℃ tank comparing flow cytometry and microscopy during acclimatisation with no light and ocean temperature of -1.8 ℃.

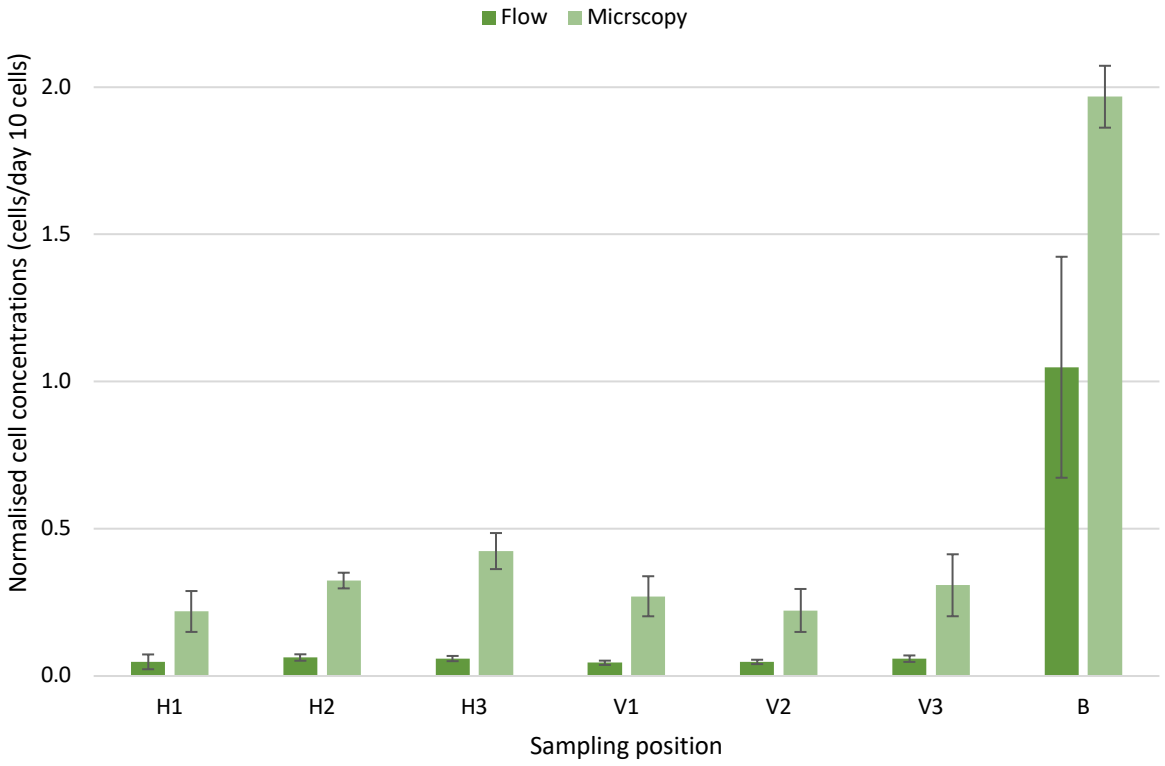

Figure D-5: Normalised cell concentrations for atmospheric temperature of -5 ℃ comparing flow cytometry and microscopy uptake dynamics with no light and ocean temperature of -1.8 ℃.

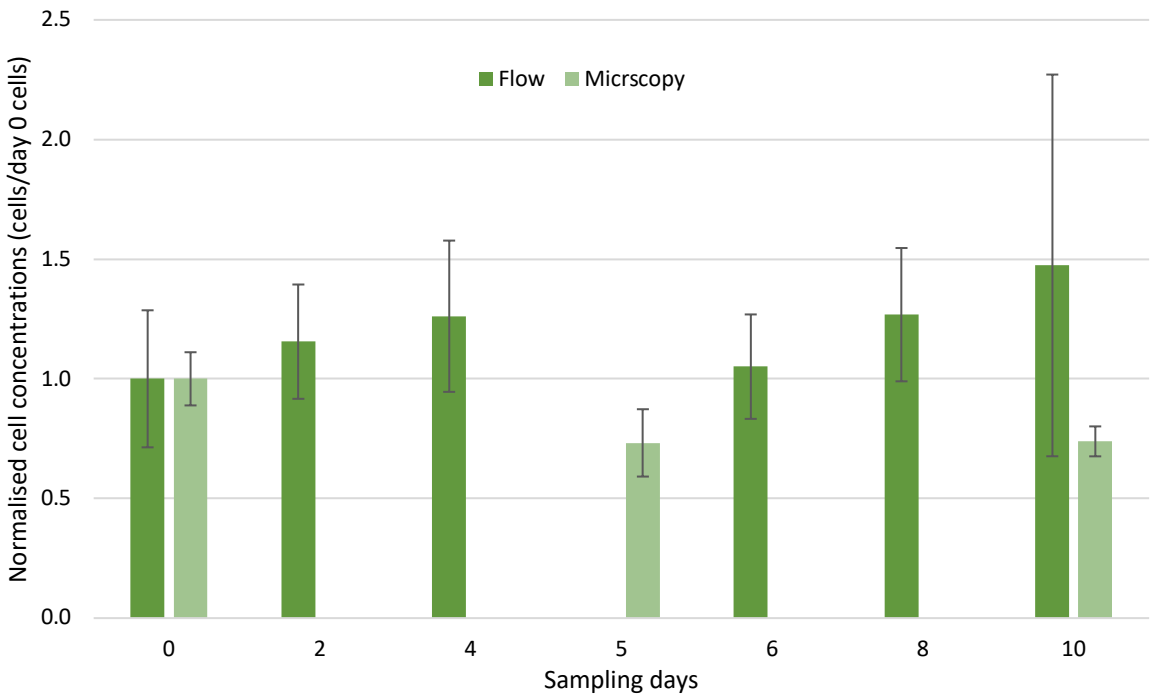

Figure D-6: Normalised cell concentrations in the -15 ℃ tank comparing flow cytometry and microscopy during acclimatisation with no light and ocean temperature of -1.8 ℃.

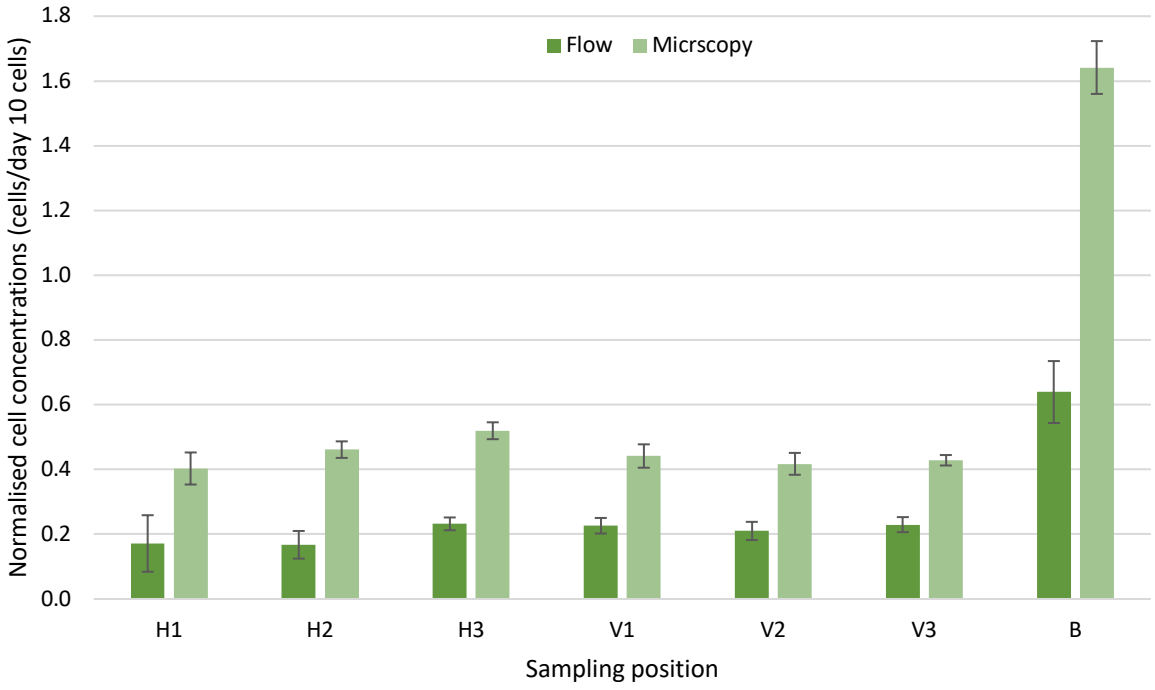

Figure D-7: Normalised cell concentrations for atmospheric temperature of -15 ℃ comparing flow cytometry and microscopy uptake dynamics with no light and ocean temperature of -1.8 ℃.

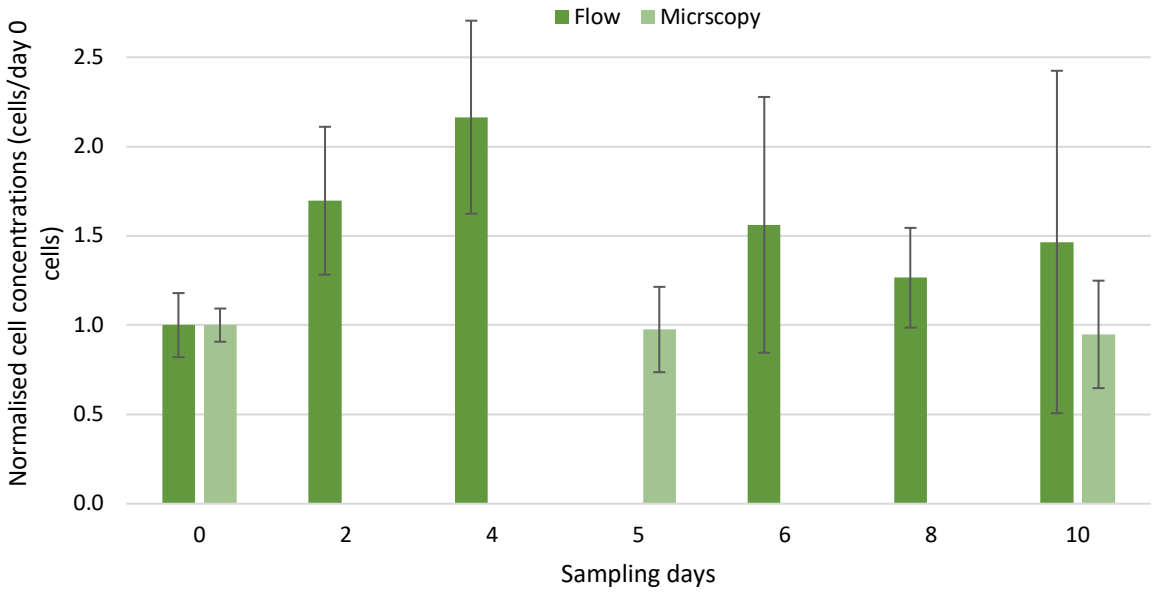

Figure D-8: Normalised cell concentrations in the -5 ℃ tank comparing flow cytometry and microscopy during acclimatisation with light and ocean temperature of -1.8 ℃.

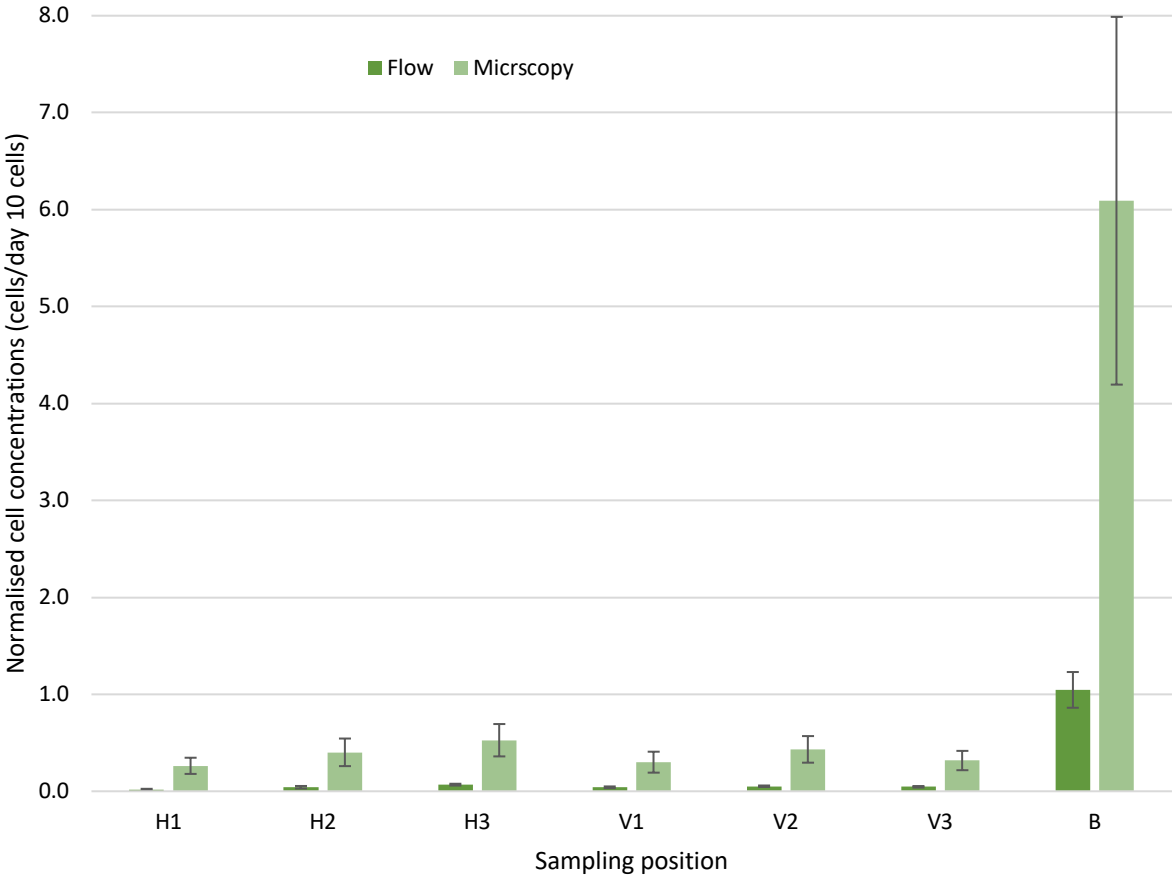

Figure D-9: Normalised cell concentrations for atmospheric temperature of -5 ℃ comparing flow cytometry and microscopy uptake dynamics with light and ocean temperature of -1.8 ℃.

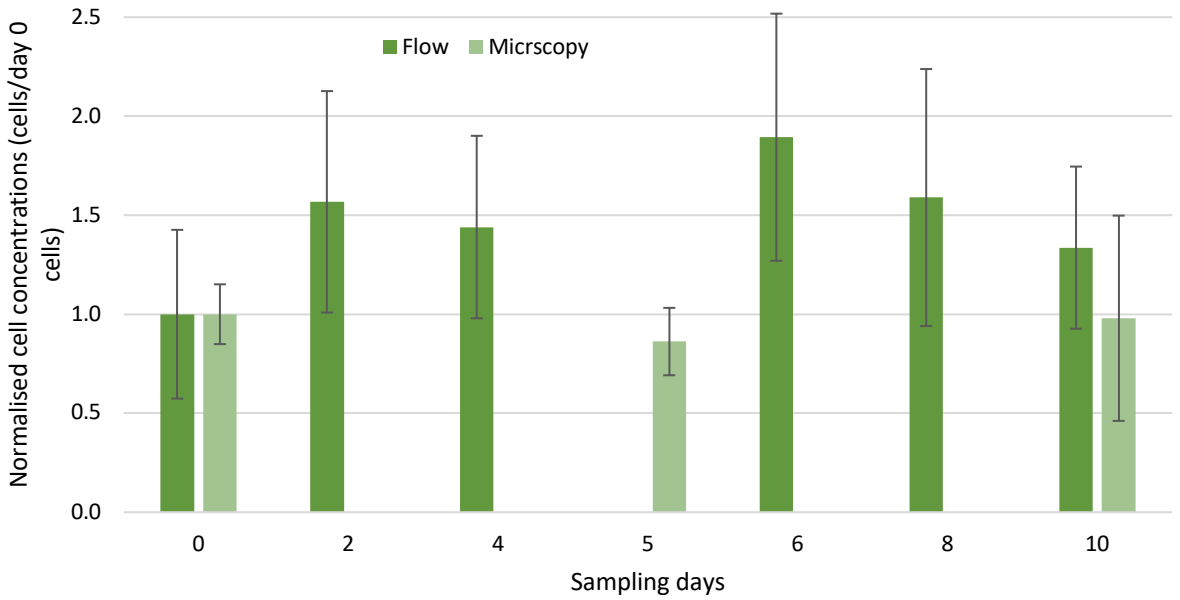

Figure D-10: Normalised cell concentrations in the -10℃ tank comparing flow cytometry and microscopy during acclimatisation with light and ocean temperature of -1.8℃.

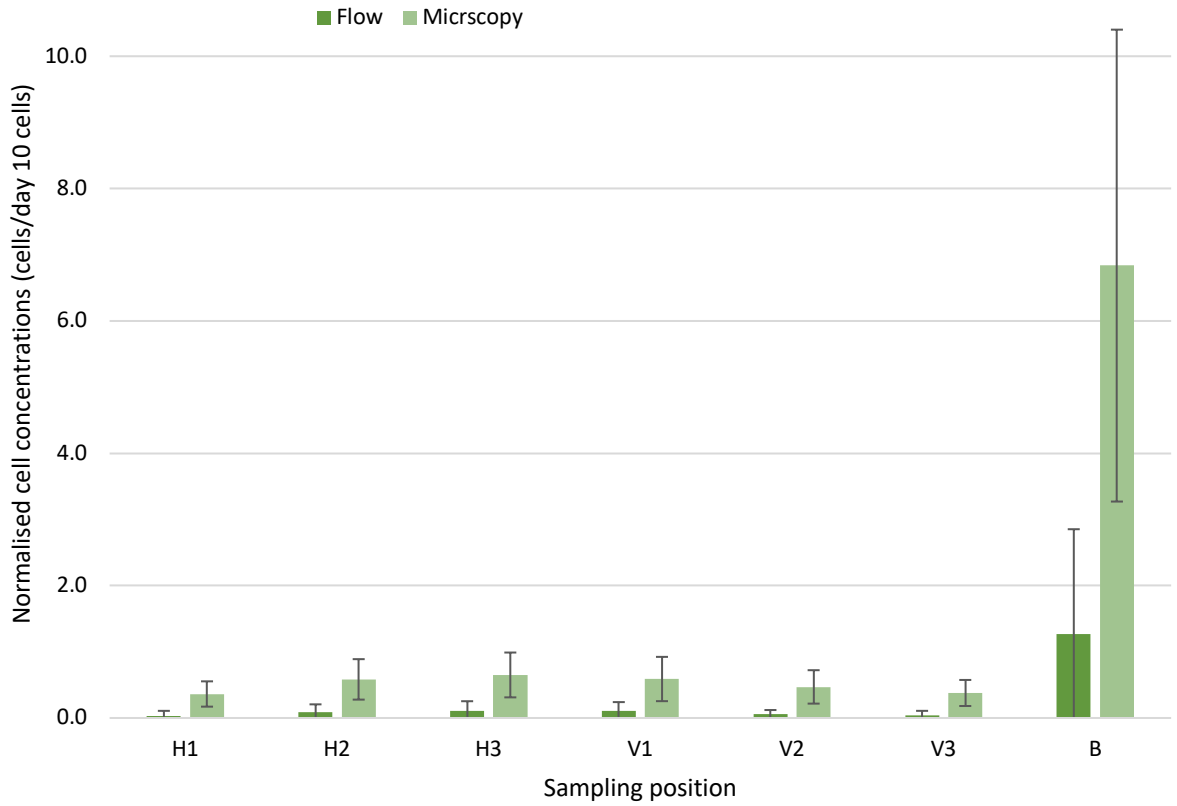

Figure D-11: Normalised cell concentrations for atmospheric temperature of -10℃ comparing flow cytometry and microscopy uptake dynamics with light and ocean temperature of -1.8℃.

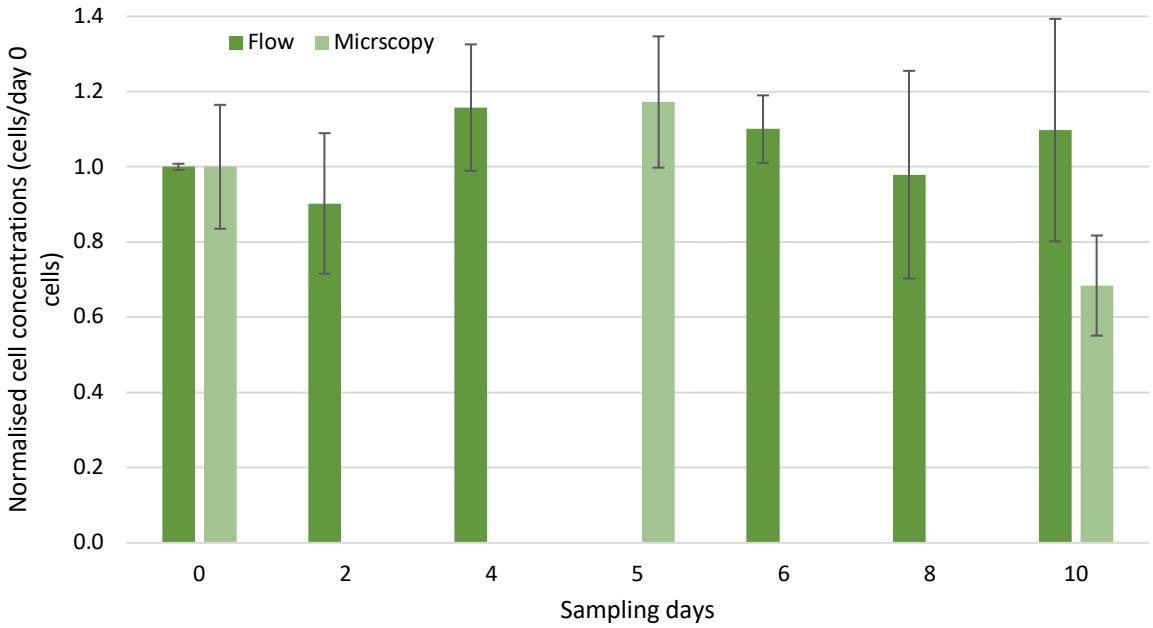

Figure D-12: Normalised cell concentrations in the -15℃ tank comparing flow cytometry and microscopy during acclimatisation with light and ocean temperature of -1.8℃.

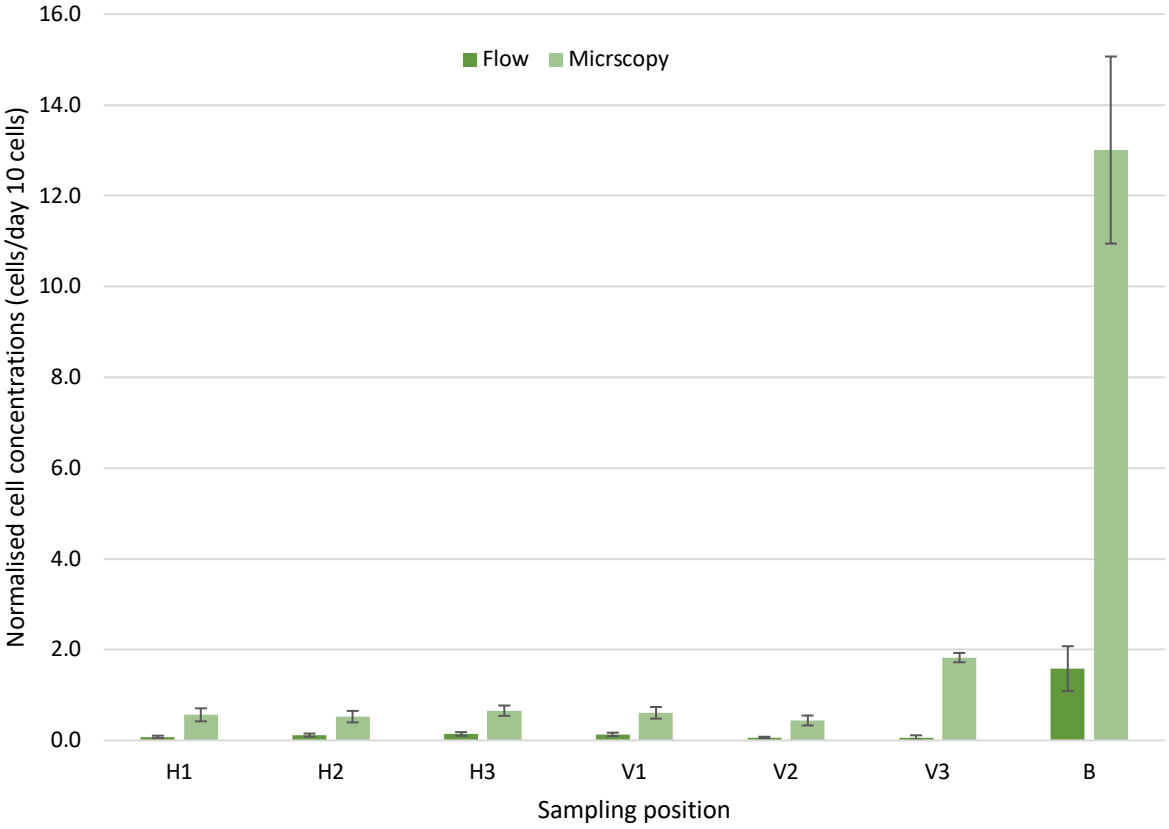

Figure D-13: Normalised cell concentrations for atmospheric temperature of -15℃ comparing flow cytometry and microscopy uptake dynamics with light and ocean temperature of -1.8℃.

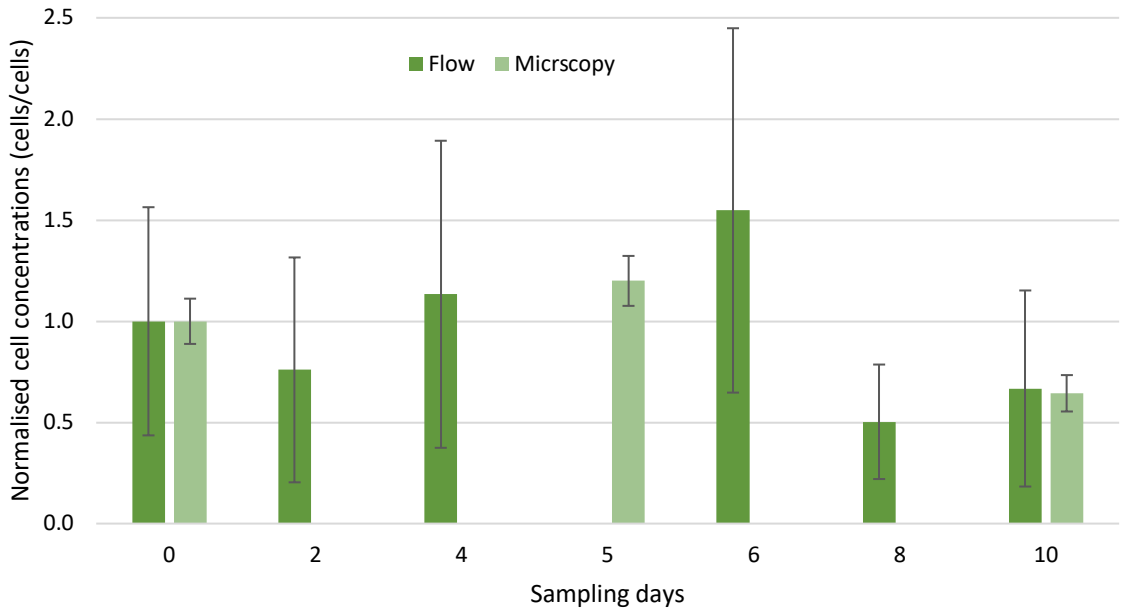

Figure D-14: Normalised cell concentrations in the -5 ℃ tank comparing flow cytometry and microscopy during acclimatisation with light and ocean temperature of 0 ℃.

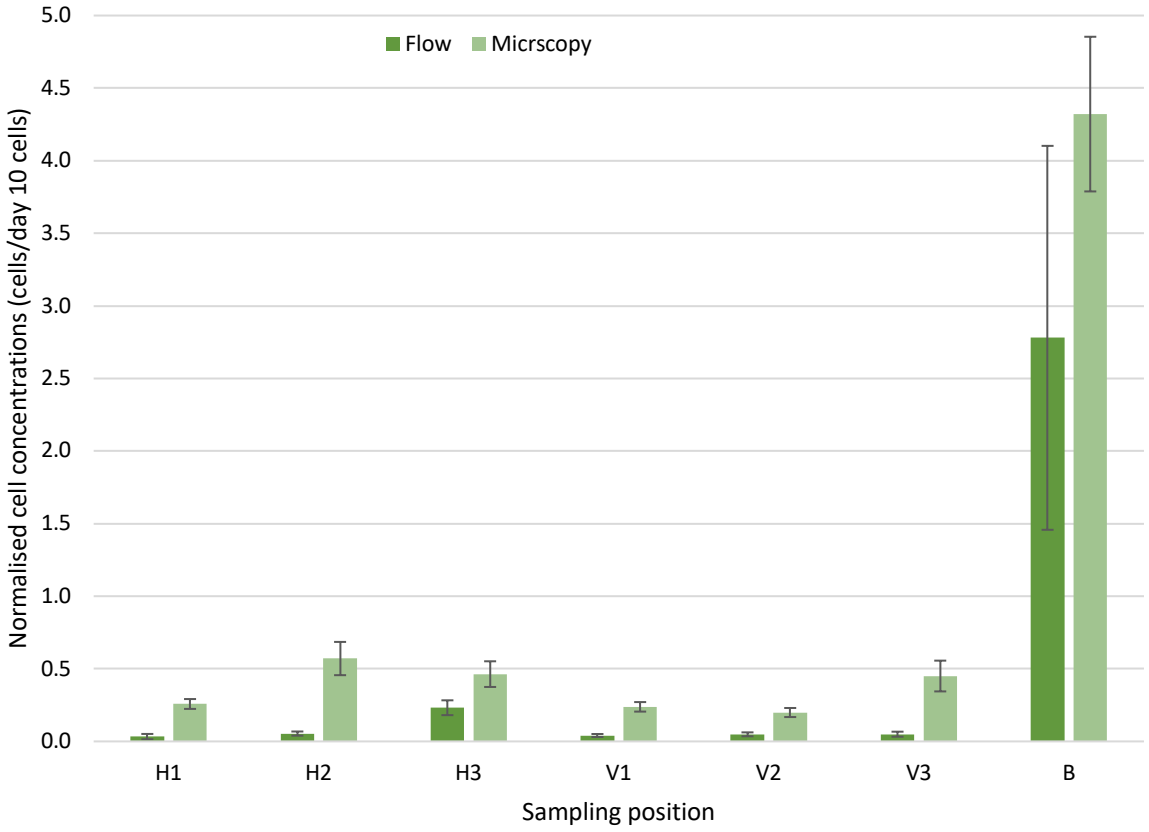

Figure D-15: Normalised cell concentrations for atmospheric temperature of -5 ℃ comparing flow cytometry and microscopy uptake dynamics with light and ocean temperature of 0 ℃.

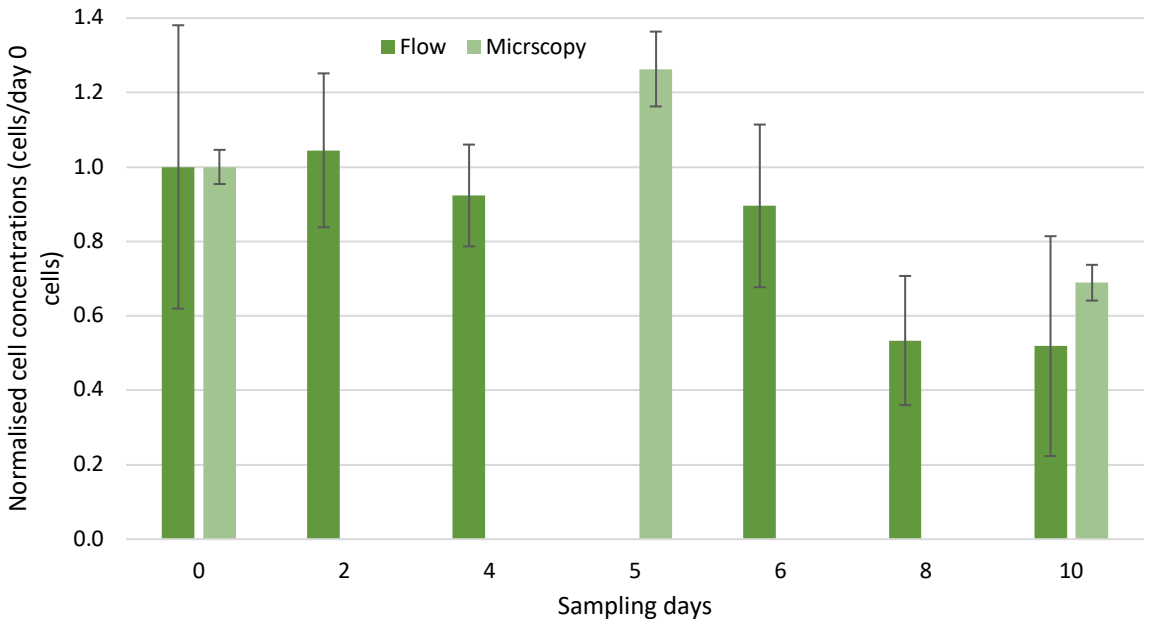

Figure D-16: Normalised cell concentrations in the -10℃ tank comparing flow cytometry and microscopy during acclimatisation with light and ocean temperature of 0℃.

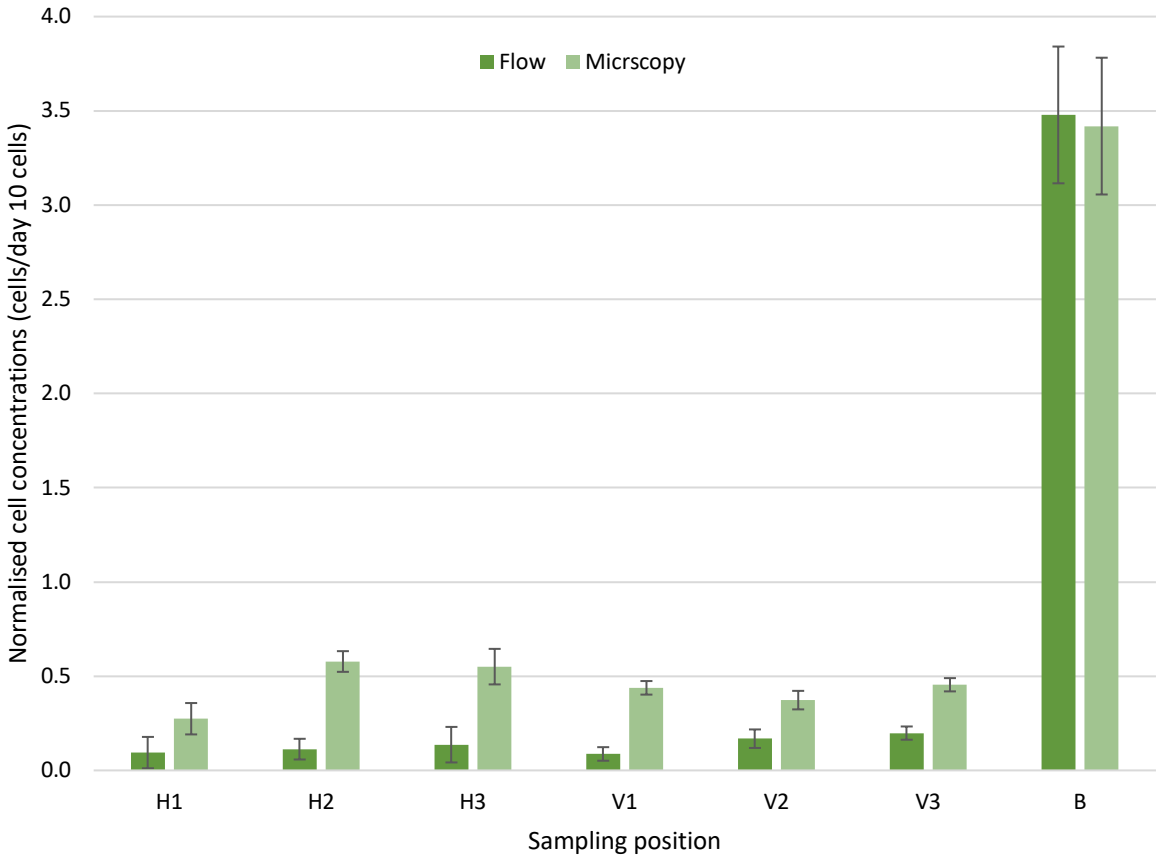

Figure D-17: Normalised cell concentrations for atmospheric temperature of -10℃ comparing flow cytometry and microscopy uptake dynamics with light and ocean temperature of 0℃.

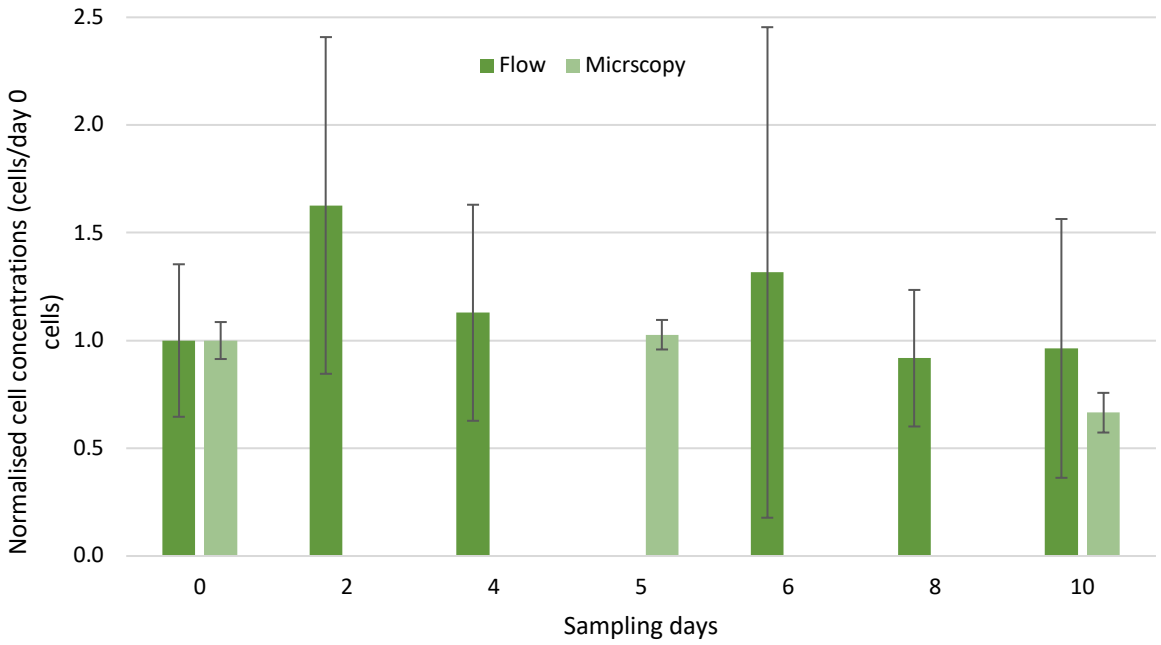

Figure D-18: Normalised cell concentrations in the -15℃ tank comparing flow cytometry and microscopy during acclimatisation with light and ocean temperature of 0℃.

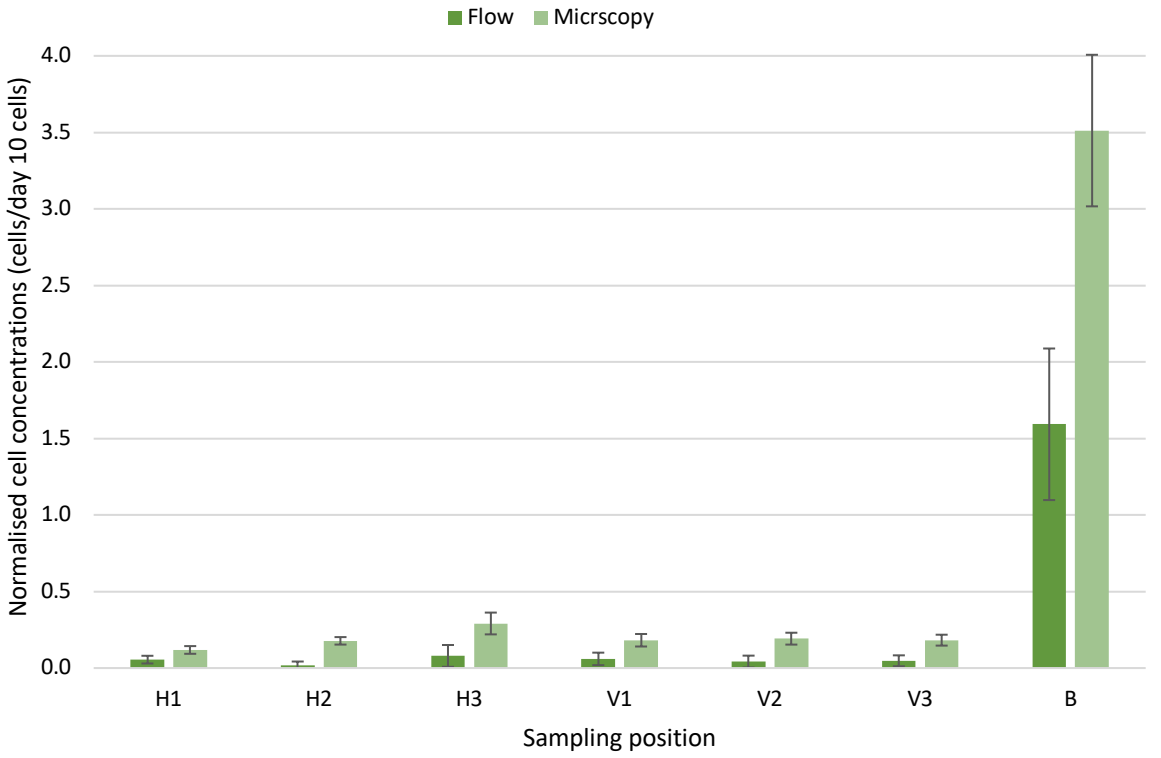

Figure D-19: Normalised cell concentrations for atmospheric temperature of -15℃ comparing flow cytometry and microscopy uptake dynamics with light and ocean temperature of 0℃.

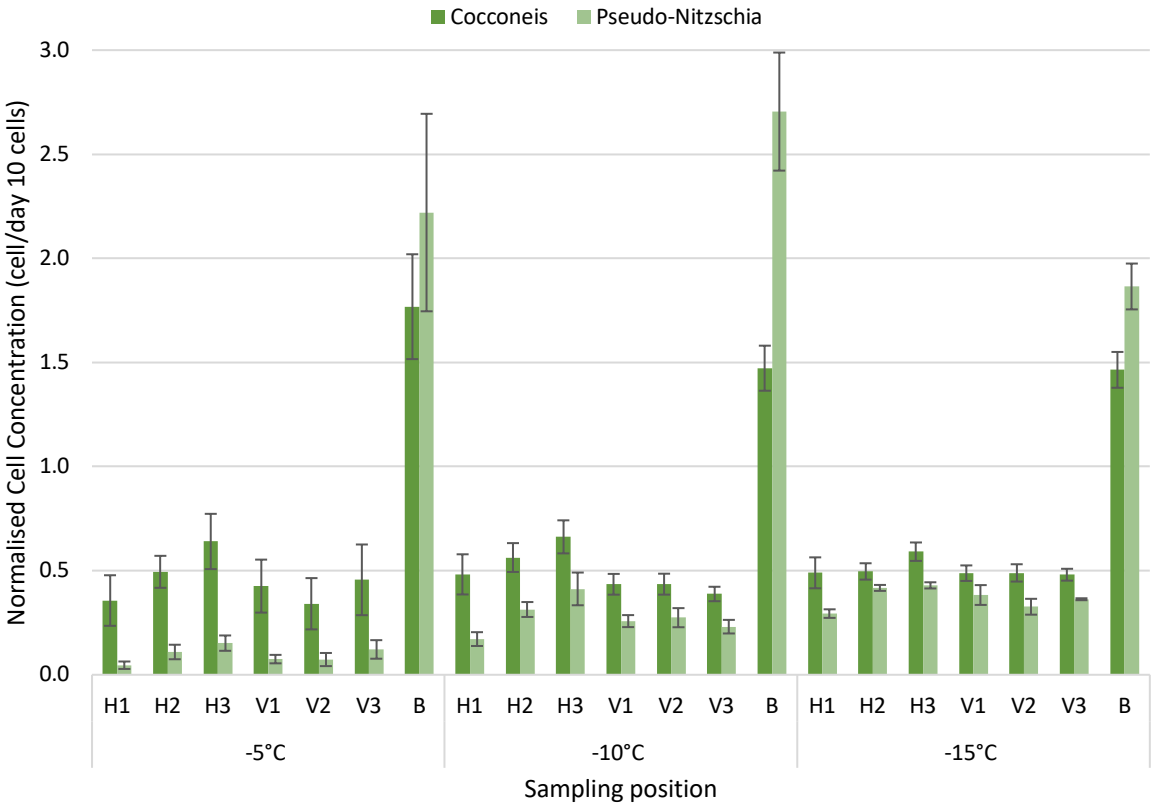

Figure D-20: Normalised cell concentrations comparing atmospheric temperatures with no light conditions and ocean temperature of -1.8 ℃ during the cold finger procedure for microscopy (including underlying seawater solution).

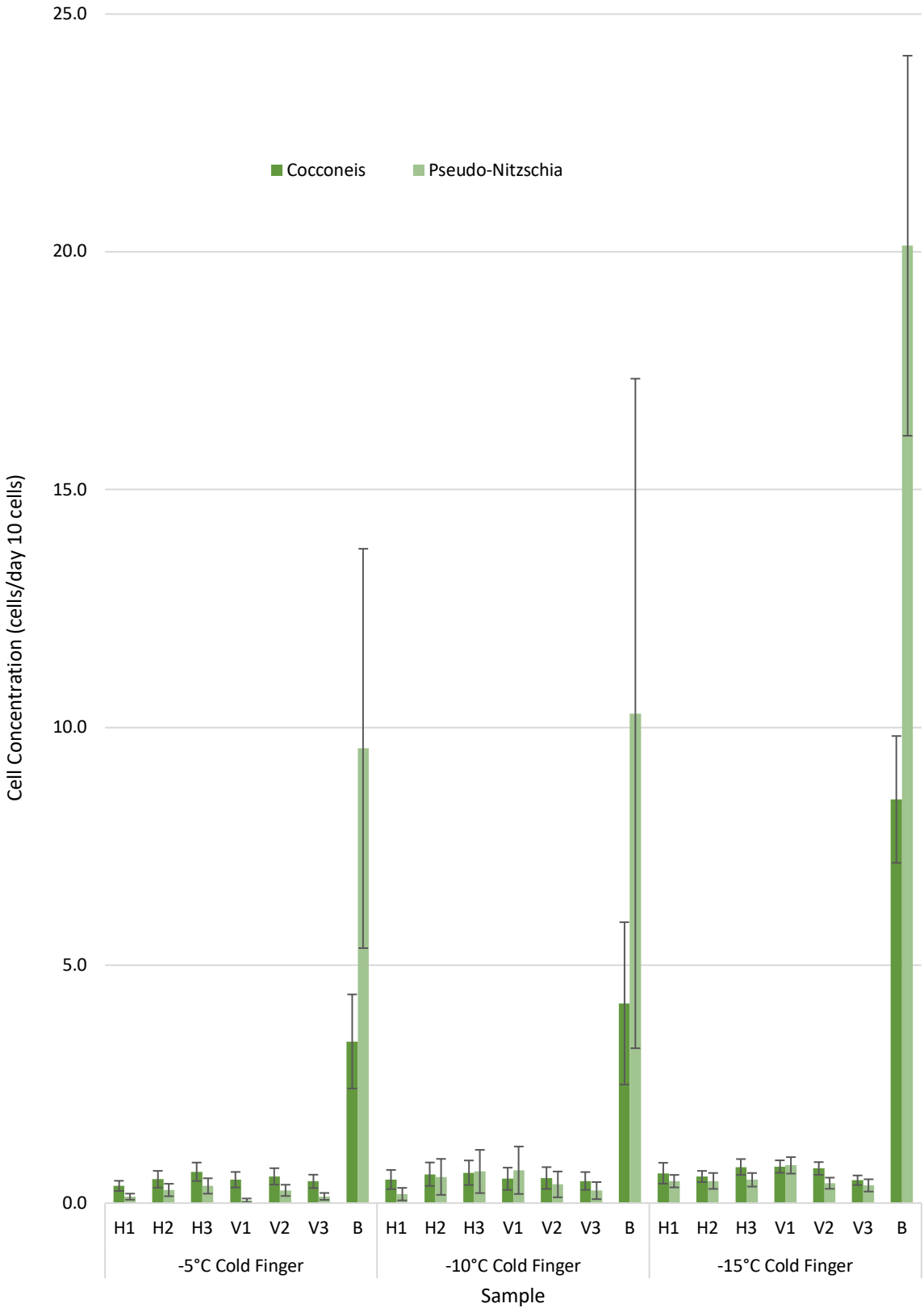

Figure D-21: Normalised cell concentrations comparing atmospheric temperatures with light conditions and ocean temperature of -1.8 ℃ during the cold finger procedure for microscopy (including underlying seawater solution).

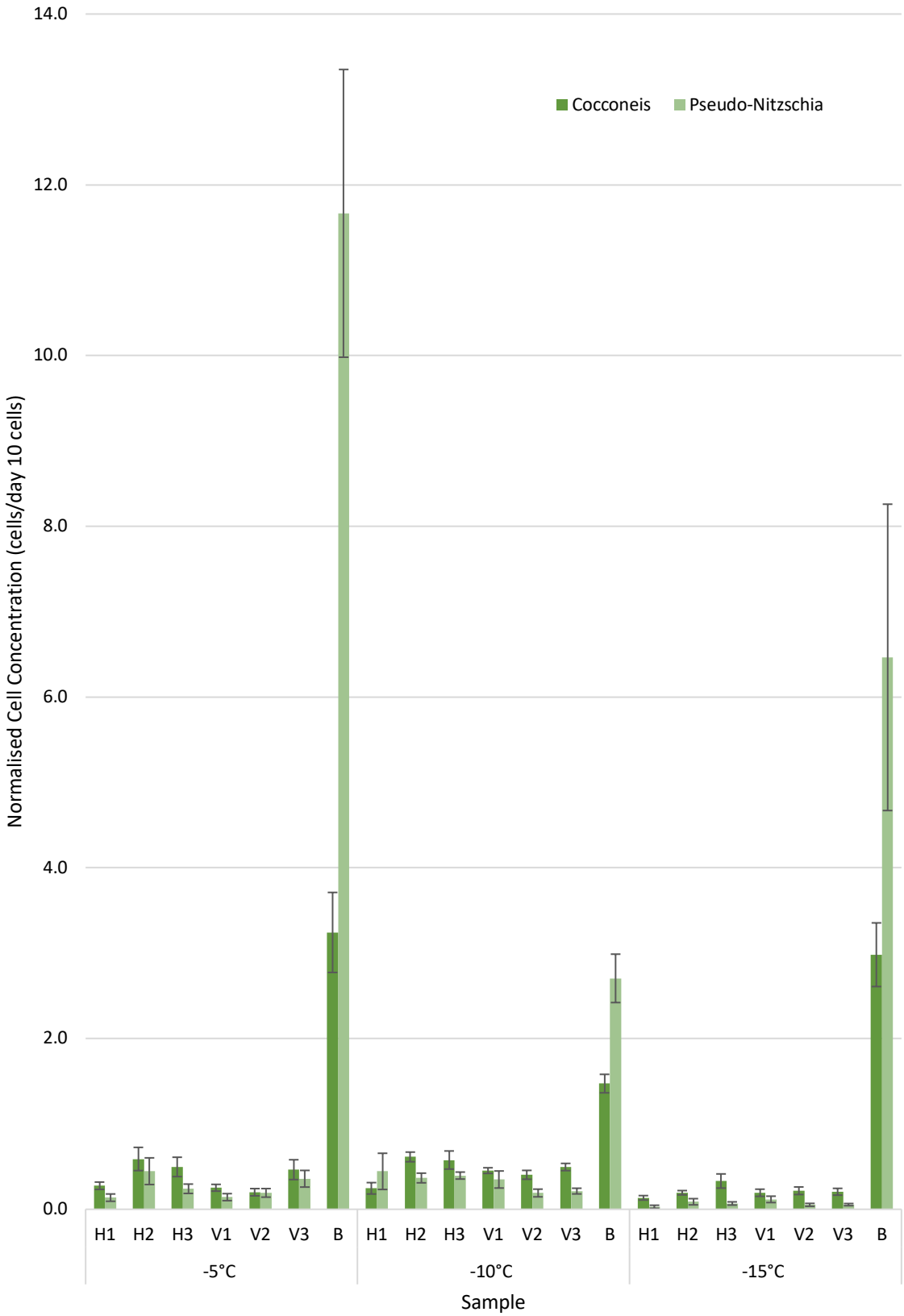

Figure D-22: Normalised cell concentrations comparing atmospheric temperatures with light conditions and ocean temperature of 0℃ during the cold finger procedure for microscopy (including underlying seawater solution).

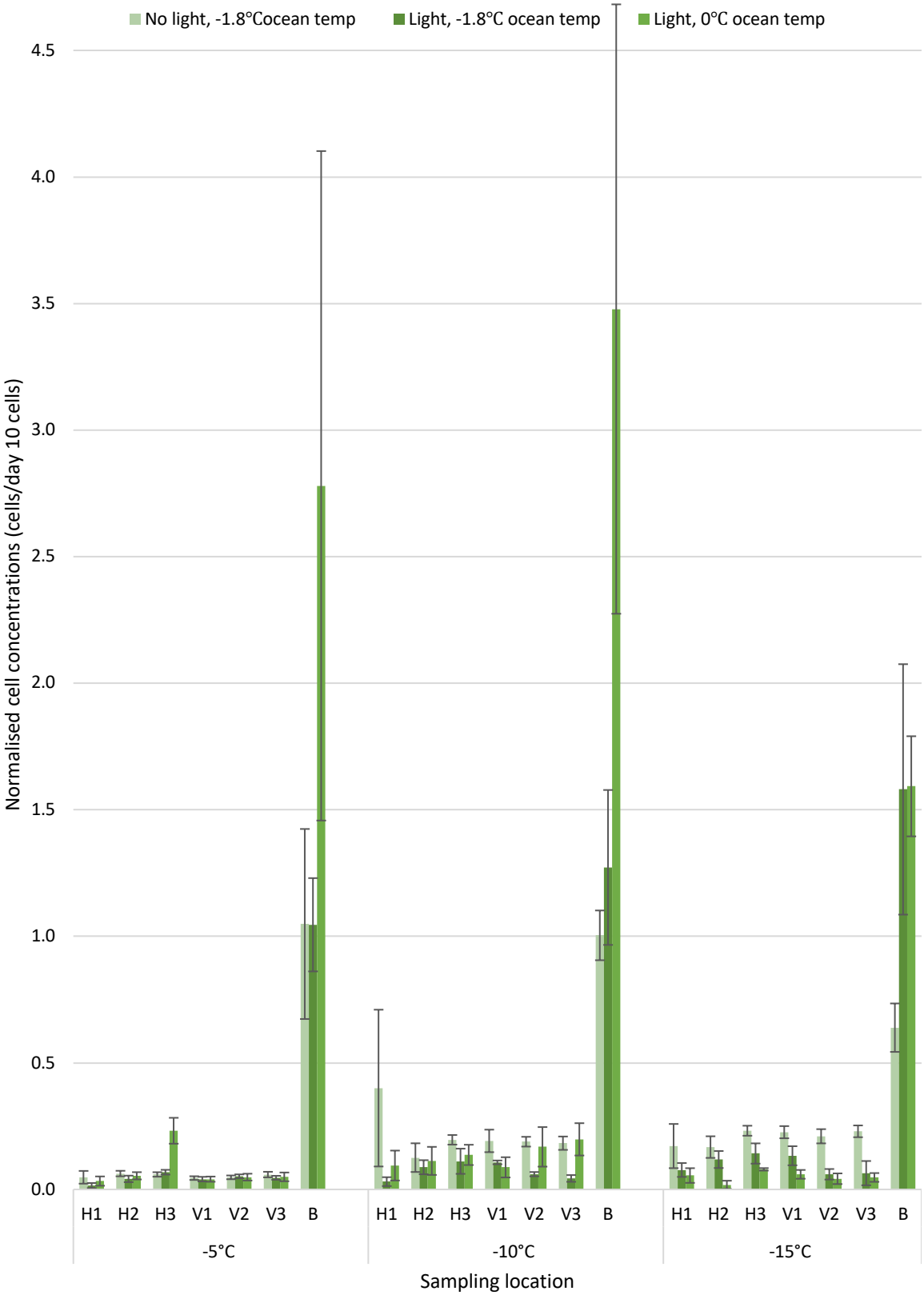

Figure D-23: Normalised cell concentrations comparing atmospheric temperatures for different light conditions and ocean temperatures during the cold finger procedure for flow cytometry (including underlying brine solution).

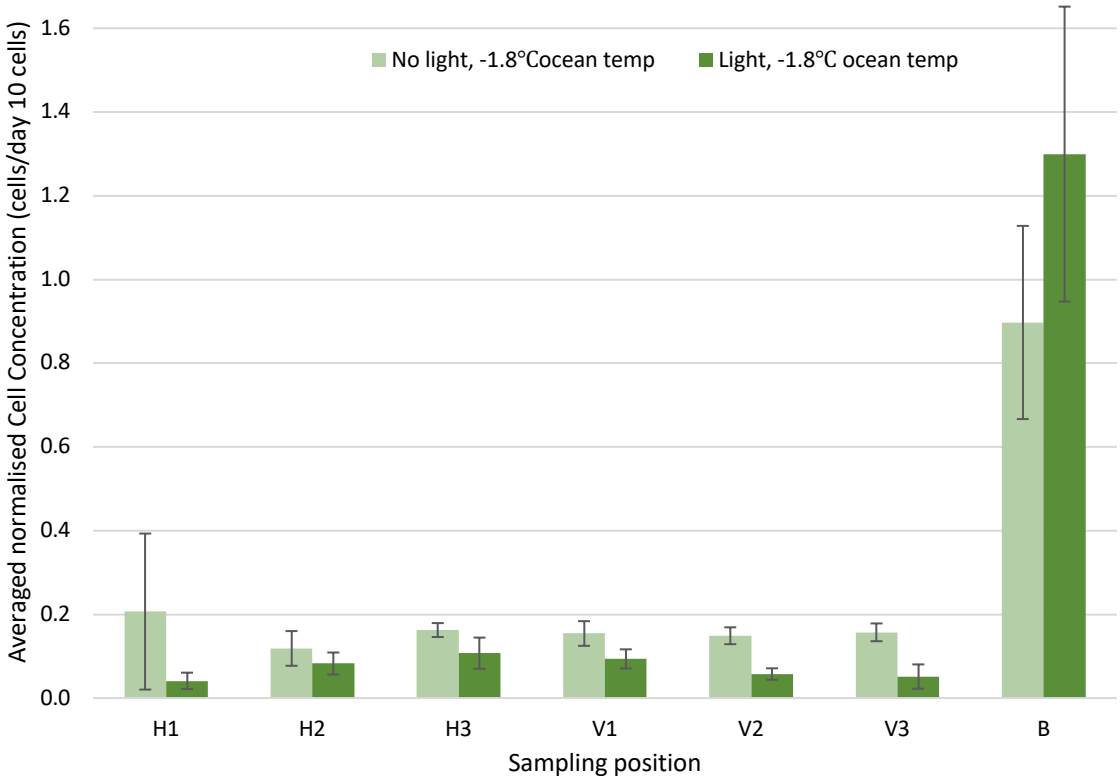

Figure D-24: Averaged normalised cell concentrations comparing different light conditions during the cold finger procedure for flow cytometry (including underlying brine solution).

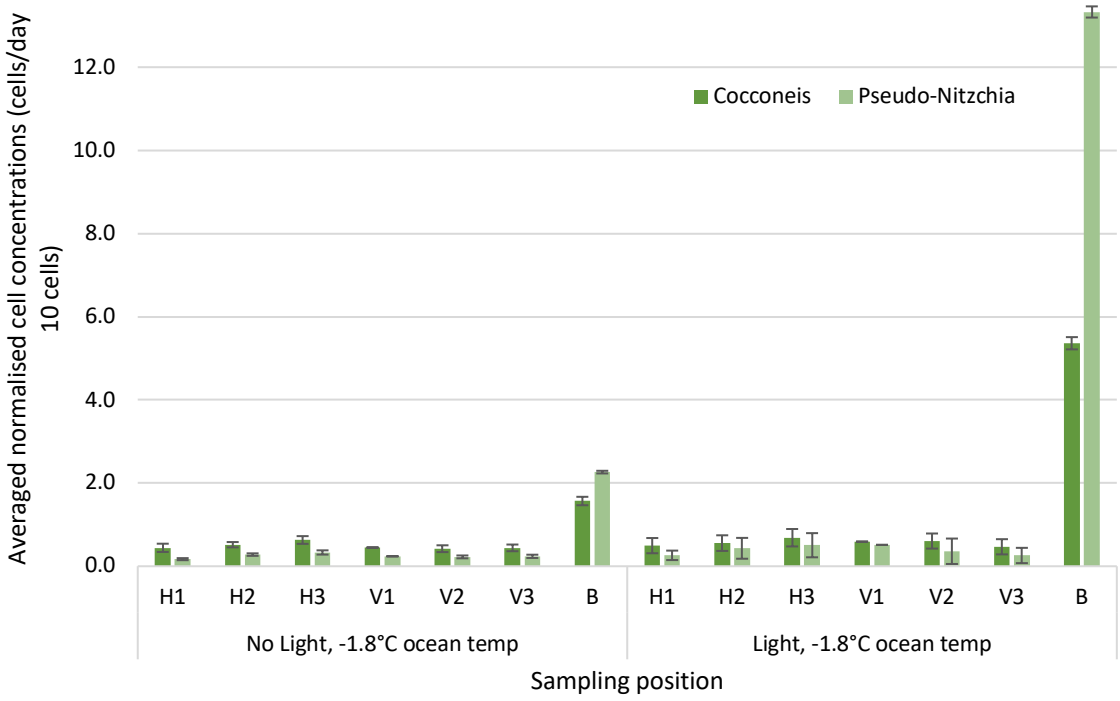

Figure D-25: Averaged normalised cell concentrations comparing different light conditions during the cold finger procedure for microscopy (including underlying brine solution).

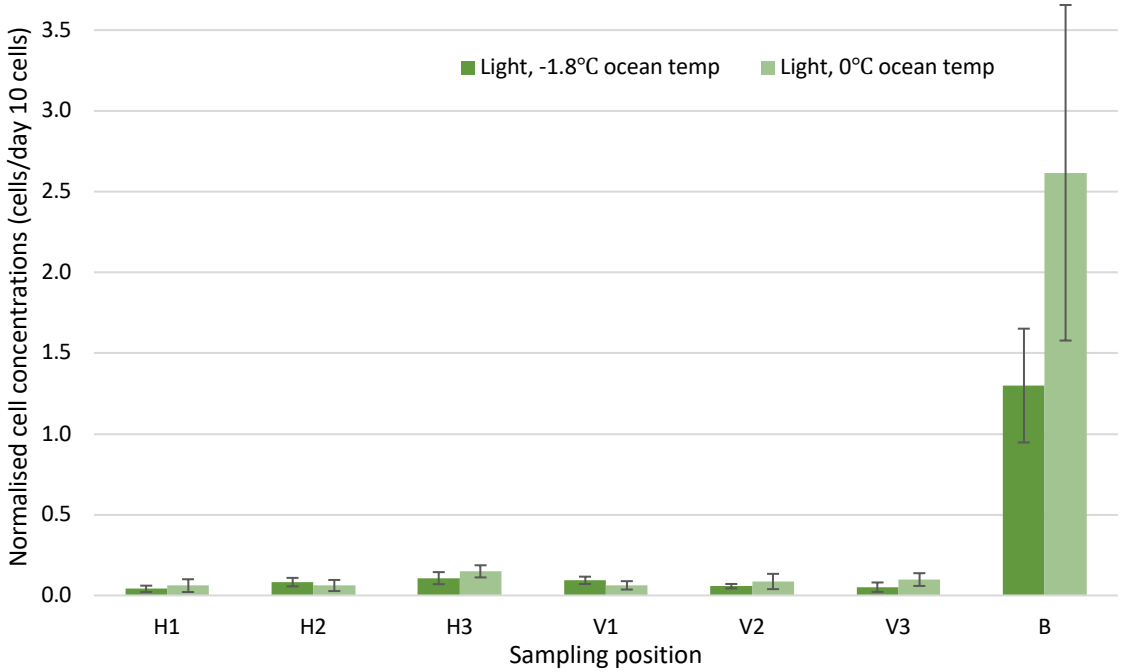

Figure D-26: Averaged normalised cell concentrations comparing different ocean temperatures during the cold finger procedure for flow cytometry (including underlying brine solution).

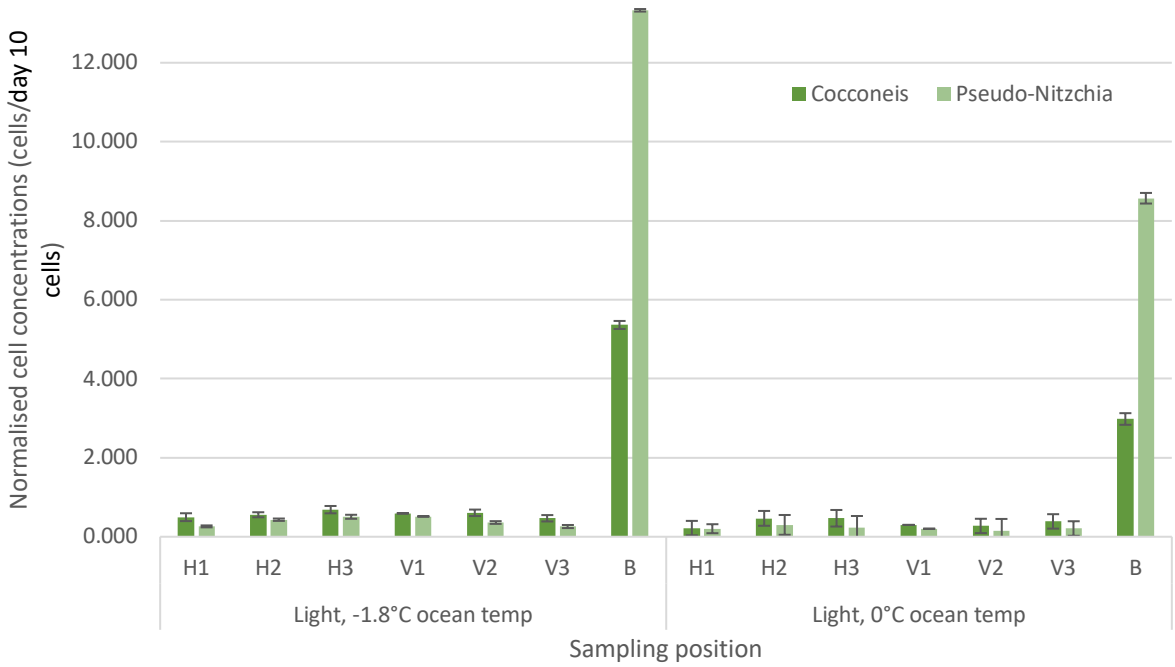

Figure D-27: Averaged normalised cell concentrations comparing different ocean temperatures during the cold finger procedure for microscopy (including underlying brine solution).

E. Parametric Statistical Testing Output

Table E-1: Summary of F-test comparing variances between microscopy and flow cytometry cell concentrations during acclimatisation.

F-Test Two-Sample for Variances	Microscopy	Flow
Mean	0.875	3.71
Variance	0.0391	4.84
Observations	54.0	54.0
df	53.0	53.0
F	0.00808	
P(F<=f) one-tail	0	
F Critical one-tail	0.634	

Table E-2: Summary of t-test comparing variances between microscopy and flow cytometry cell concentrations during acclimatisation.

t-Test: Two-Sample Assuming Unequal Variances	Microscopy	Flow
Mean	0.875	3.71
Variance	0.0391	4.84
Observations	54.0	54.0
Hypothesized Mean Difference	0	
df	54.0	
t Stat	-9.43	
P(T<=t) one-tail	2.63E-13	
t Critical one-tail	1.67	
P(T<=t) two-tail	5.26E-13	
t Critical two-tail	2.00	

Table E-3: Summary of F-test comparing variances between microscopy and flow cytometry cell concentrations during the cold finger procedure.

F-Test Two-Sample for Variances	Microscopy	Flow
Mean	0.203	0.0922
Variance	0.0569	0.0244
Observations	189	189
df	188	188
F	2.33	
P(F<=f) one-tail	5.38E-09	
F Critical one-tail	1.27	

Table E-4: Summary of t-test comparing variances between microscopy and flow cytometry cell concentrations during the cold finger procedure.

t-Test: Two-Sample Assuming Unequal Variances	Microscopy	Flow
Mean	0.203	0.0922
Variance	0.0569	0.0244
Observations	189	189
Hypothesized Mean Difference	0	
df	324	
t Stat	5.33	
P(T<=t) one-tail	9.29E-08	
t Critical one-tail	1.65	
P(T<=t) two-tail	1.86E-07	
t Critical two-tail	1.97	

Table E-5: Summary of statistics used in single factor ANOVA comparing flow cytometry cell concentrations on different sampling days with no light and ocean temperature of -1.8℃.

Groups	Count	Sum	Average	Variance
Day 0	9	9	1	0.0274
Day 2	9	11.5	1.28	0.0272
Day 4	9	11.4	1.26	0.024
Day 6	9	10.7	1.19	0.0327
Day 8	9	11.1	1.23	0.0161
Day 10	9	12.1	1.34	0.0427

Table E-6: Summary of single factor ANOVA results comparing flow cytometry cell concentrations on different sampling days with no light and ocean temperature of -1.8℃.

Source of Variation	SS	df	MS	F	P-value	F crit
Between Groups	0.625	5	0.125	4.41	0.00221	2.41
Within Groups	1.36	48	0.0284			
Total	1.99	53				

Table E-7: Summary of statistics used in single factor ANOVA comparing flow cytometry cell concentrations on different sampling days with light and ocean temperature of -1.8℃.

Groups	Count	Sum	Average	Variance
Day 0	9	9	1	0.023
Day 2	9	12.5	1.39	0.189
Day 4	9	14.3	1.59	0.254
Day 6	9	13.7	1.52	0.139
Day 8	9	11.5	1.28	0.209
Day 10	9	11.7	1.30	0.0600

Table E-8: Summary of single factor ANOVA results comparing flow cytometry cell concentrations on different sampling days with light and ocean temperature of -1.8℃

Source of Variation	SS	df	MS	F	P-value	F crit
Between Groups	1.95	5	0.389	2.68	0.0330	2.41
Within Groups	6.99	48	0.146			
Total	8.94	53				

Table E-9:Summary of statistics used in single factor ANOVA comparing flow cytometry cell concentrations on different sampling days with light and ocean temperature of 0℃.

Groups	Count	Sum	Average	Variance
Day 0	9	9	1	0.0464
Day 2	9	10.3	1.14	0.267
Day 4	9	9.56	1.06	0.0954
Day 6	9	11.3	1.25	0.104
Day 8	9	5.86	0.652	0.181
Day 10	9	6.45	0.717	0.0505

Table E-10: Summary of single factor ANOVA results comparing flow cytometry cell concentrations on different sampling days with light and ocean temperature of 0℃

Source of Variation	SS	df	MS	F	P-value	F crit
Between Groups	2.57	5	0.513	4.14	0.00330	2.41
Within Groups	5.95	48	0.124			
Total	8.52	53				

Table E-11: Summary of statistics used in single factor ANOVA comparing Cocconeis microscopy cell concentrations on different sampling days with no light and ocean temperature of -1.8℃.

Groups	Count	Sum	Average	Variance
Day 0	9	9	1	0.0132
Day 5	9	6.92	0.768	0.00596
Day 10	9	6.44	0.715	0.00316

Table E-12: Summary of single factor ANOVA results comparing Cocconeis microscopy cell concentrations on different sampling days with no light and ocean temperature of -1.8℃.

Source of Variation	SS	df	MS	F	P-value	F crit
Between Groups	0.413	2	0.206	27.8	5.63E-07	3.4
Within Groups	0.178	24	0.00742			
Total	0.591	26				

Table E-13:Summary of statistics used in single factor ANOVA comparing Cocconeis microscopy cell concentrations on different sampling days with light and ocean temperature of -1.8℃.

Groups	Count	Sum	Average	Variance
Day 0	9	9	1	0.0111
Day 5	9	8.61	0.956	0.0282
Day 10	9	7.2	0.800	0.0611

Table E-14: Summary of single factor ANOVA results comparing Cocconeis microscopy cell concentrations on different sampling days with light and ocean temperature of -1.8℃.

Source of Variation	SS	df	MS	F	P-value	F crit
Between Groups	0.2	2	0.1	2.98	0.0697	3.4
Within Groups	0.803	24	0.0335			
Total	1.002	26				

Table E-15: Summary of statistics used in single factor ANOVA comparing Cocconeis microscopy cell concentrations on different sampling days with light and ocean temperature of -0℃.

Groups	Count	Sum	Average	Variance
Day 0	9	9	1	0.00298
Day 5	9	10.88	1.21	0.0168
Day 10	9	8.42	0.936	0.00918

Table E-16: Summary of single factor ANOVA results comparing Cocconeis microscopy cell concentrations on different sampling days with light and ocean temperature of 0℃.

Source of Variation	SS	df	MS	F	P-value	F crit
Between Groups	0.365	2	0.183	18.9	1.18E-05	3.40
Within Groups	0.232	24	0.00966			
Total	0.597	26				

Table E-17: Summary of statistics used in single factor ANOVA comparing Pseudo-Nitzchia microscopy cell concentrations on different sampling days with no light and ocean temperature of -1.8℃.

Groups	Count	Sum	Average	Variance
Day 0	9	9	1	0.00833
Day 5	9	6.97	0.774	0.0281
Day 10	9	6.45	0.716	0.0143

Table E-18: Summary of single factor ANOVA results comparing Pseudo-Nitzchia microscopy cell concentrations on different sampling days with no light and ocean temperature of -1.8℃.

Source of Variation	SS	df	MS	F	P-value	F crit
Between Groups	0.404	2	0.202	11.96	0.000249	3.40
Within Groups	0.406	24	0.0169			
Total	0.81	26				

Table E-19: Summary of statistics used in single factor ANOVA comparing Pseudo-Nitzchia microscopy cell concentrations on different sampling days with light and ocean temperature of -1.8℃.

Groups	Count	Sum	Average	Variance
Day 0	9	8.69	0.965	0.0212
Day 5	9	8.69	0.966	0.157
Day 10	9	8.55	0.950	0.227

Table E-20: Summary of single factor ANOVA results comparing Pseudo-Nitzchia microscopy cell concentrations on different sampling days with light and ocean temperature of -1.8℃.

Source of Variation	SS	df	MS	F	P-value	F crit
Between Groups	0.00149	2	0.000744	0.00552	0.994	3.40
Within Groups	3.23	24	0.134			
Total	3.24	26				

Table E-21: Summary of statistics used in single factor ANOVA comparing Pseudo-Nitzchia microscopy cell concentrations on different sampling days with light and ocean temperature of 0℃.

Groups	Count	Sum	Average	Variance
Day 0	9	9	1	0.00493
Day 5	9	8.82	0.98	0.106
Day 10	9	2.18	0.242	0.00139

Table E-22: Summary of single factor ANOVA results comparing Pseudo-Nitzchia microscopy cell concentrations on different sampling days with light and ocean temperature of 0℃.

Source of Variation	SS	df	MS	F	P-value	F crit
Between Groups	3.36	2	1.68	44.7	8.04E-09	3.40
Within Groups	0.901	24	0.0375			
Total	4.26	26				

Table E-23: Summary of statistics used in single factor ANOVA comparing flow cytometry cell concentrations at different light conditions during acclimatisation.

Groups	Count	Sum	Average	Variance
No light	54	55.8	1.03	0.0413
Light	54	72.7	1.35	0.169

Table E-24: Summary of single factor ANOVA results comparing flow cytometry cell concentrations at different light conditions during acclimatisation.

Source of Variation	SS	df	MS	F	P-value	F crit
Between Groups	2.62	1	2.62	25.0	2.30E-06	3.93
Within Groups	11.1	106	0.105			
Total	13.7	107				

Table E-25: Summary of statistics used in single factor ANOVA comparing Cocconeis microscopy cell concentrations at different light conditions during acclimatisation.

Groups	Count	Sum	Average	Variance
No light	27	22.35	0.8279	0.0227
Light	27	24.8	0.9187	0.0386

Table E-26: Summary of single factor ANOVA results comparing Cocconeis microscopy cell concentrations at different light conditions during acclimatisation.

Source of Variation	SS	df	MS	F	P-value	F crit
Between Groups	0.1114	1	0.1114	3.6347	0.0621	4.0266
Within Groups	1.5936	52	0.0306			
Total	1.705	53				

Table E-27: Summary of statistics used in single factor ANOVA comparing Pseudo-Nitzchia microscopy cell concentrations at different light conditions during acclimatisation.

Groups	Count	Sum	Average	Variance
No light	27	22.4	0.83	0.0312
Light	27	25.9	0.96	0.124

Table E-28: Summary of single factor ANOVA results comparing Pseudo-Nitzchia microscopy cell concentrations at different light conditions during acclimatisation.

Source of Variation	SS	df	MS	F	P-value	F crit
Between Groups	0.229	1	0.229	2.94	0.0922	4.03
Within Groups	4.05	52	0.078			
Total	4.28	53				

Table E-29: Summary of statistics used in single factor ANOVA comparing flow cytometry cell concentrations at different ocean temperatures during acclimatisation.

Groups	Count	Sum	Average	Variance
-1.8°C	54	72.7	1.35	0.169
0°C	54	52.4	0.971	0.161

Table E-30: Summary of single factor ANOVA results comparing flow cytometry cell concentrations at different ocean temperatures during acclimatisation.

Source of Variation	SS	df	MS	F	P-value	F crit
Between Groups	3.78	1	3.78	23.0	5.39E-06	3.93
Within Groups	17.5	106	0.165			
Total	21.2	107				

Table E-31: Summary of statistics used in single factor ANOVA comparing Cocconeis microscopy cell concentrations at different ocean temperatures during acclimatisation.

Groups	Count	Sum	Average	Variance
-1.8°C	27	24.8	0.919	0.0386
0°C	27	28.3	1.05	0.0230

Table E-32: Summary of single factor ANOVA results comparing Cocconeis microscopy cell concentrations at different ocean temperatures during acclimatisation.

Source of Variation	SS	df	MS	F	P-value	F crit
Between Groups	0.226	1	0.226	7.35	0.00910	4.03
Within Groups	1.60	52	0.0308			
Total	1.83	53				

Table E-33: Summary of statistics used in single factor ANOVA comparing Pseudo-Nitzchia microscopy cell concentrations at different ocean temperatures during acclimatisation.

Groups	Count	Sum	Average	Variance
-1.8°C	27	25.9	0.960	0.124
0°C	27	20.0	0.741	0.164

Table E-34: Summary of single factor ANOVA results comparing Pseudo-Nitzchia microscopy cell concentrations at different ocean temperatures during acclimatisation.

Source of Variation	SS	df	MS	F	P-value	F crit
Between Groups	0.652	1	0.652	4.53	0.0381	4.03
Within Groups	7.49	52	0.144			
Total	8.15	53				

Table E-35: Summary of statistics used in single factor ANOVA comparing flow cytometry cell concentrations at different atmospheric temperatures with no light and ocean temperature of -1.8℃.

Groups	Count	Sum	Average	Variance
-5°C	21	4.01	0.191	0.0985
-10°C	21	5.75	0.274	0.0682
-15°C	21	6.04	0.288	0.0286

Table E-36: Summary of single factor ANOVA results comparing flow cytometry cell concentrations at different atmospheric temperatures with no light and ocean temperature of -1.8℃

Source of Variation	SS	df	MS	F	P-value	F crit
Between Groups	0.115	2	0.0574	0.882	0.419	3.15
Within Groups	3.91	60	0.0651			
Total	4.02	62				

Table E-37: Summary of statistics used in single factor ANOVA comparing flow cytometry cell concentrations at different atmospheric temperatures with light and ocean temperature of -1.8℃.

Groups	Count	Sum	Average	Variance
-5°C	21	3.93	0.187	0.131
-10°C	21	5.14	0.245	0.195
-15°C	21	6.53	0.311	0.290

Table E-38: Summary of single factor ANOVA results comparing flow cytometry cell concentrations at different atmospheric temperatures with light and ocean temperature of -1.8℃

Source of Variation	SS	df	MS	F	P-value	F crit
Between Groups	0.161	2	0.0803	0.392	0.678	3.15
Within Groups	12.3	60	0.205			
Total	12.5	62				

Table E-39: Summary of statistics used in single factor ANOVA comparing flow cytometry cell concentrations at different atmospheric temperatures with light and ocean temperature of 0℃.

Groups	Count	Sum	Average	Variance
-5°C	21	9.71	0.463	1.08
-10°C	21	12.0	0.574	1.23
-15°C	21	6.95	0.331	0.491

Table E-40: Summary of single factor ANOVA results comparing flow cytometry cell concentrations at different atmospheric temperatures with light and ocean temperature of 0℃.

Source of Variation	SS	df	MS	F	P-value	F crit
Between Groups	0.620	2	0.310	0.332	0.719	3.15
Within Groups	56.0	60	0.933			
Total	56.6	62				

Table E-41: Summary of statistics used in single factor ANOVA comparing Cocconeis microscopy cell concentrations at different atmospheric temperatures with no light and ocean temperature of -1.8℃.

Groups	Count	Sum	Average	Variance
-5°C	21	13.4	0.640	0.244
-10°C	21	13.2	0.629	0.136
-15°C	21	13.5	0.643	0.121

Table E-42: Summary of single factor ANOVA results comparing Cocconeis microscopy cell concentrations at different atmospheric temperatures with no light and ocean temperature of -1.8℃

Source of Variation	SS	df	MS	F	P-value	F crit
Between Groups	0.00211	2	0.00106	0.00632	0.994	3.15
Within Groups	10	60	0.167			
Total	10	62				

Table E-43: Summary of statistics used in single factor ANOVA comparing Cocconeis microscopy cell concentrations at different atmospheric temperatures with light and ocean temperature of -1.8℃.

Groups	Count	Sum	Average	Variance
-5°C	21	13.5	0.645	0.202
-10°C	21	16	0.764	0.332
-15°C	21	20.3	0.965	0.66

Table E-44: Summary of single factor ANOVA results comparing Cocconeis microscopy cell concentrations at different atmospheric temperatures with light and ocean temperature of -1.8℃

Source of Variation	SS	df	MS	F	P-value	F crit
Between Groups	1.1	2	0.549	1.38	0.260	3.15
Within Groups	23.9	60	0.398			
Total	24.98	62				

Table E-45: Summary of statistics used in single factor ANOVA comparing Cocconeis microscopy cell concentrations at different atmospheric temperatures with light and ocean temperature of 0℃.

Groups	Count	Sum	Average	Variance
-5°C	21	16.1	0.767	1.10
-10°C	21	16.5	0.787	0.679
-15°C	21	12.8	0.608	1.00

Table E-46: Summary of single factor ANOVA results comparing Cocconeis microscopy cell concentrations at different atmospheric temperatures with light and ocean temperature of 0℃.

Source of Variation	SS	df	MS	F	P-value	F crit
Between Groups	0.403	2	0.202	0.218	0.805	3.15
Within Groups	55.6	60	0.926			
Total	55.97	62				

Table E-47: Summary of statistics used in single factor ANOVA comparing Pseudo-Nitzchia microscopy cell concentrations at different atmospheric temperatures with no light and ocean temperature of -1.8℃.

Groups	Count	Sum	Average	Variance
-5°C	21	8.39	0.400	0.585
-10°C	21	12.9	0.615	0.748
-15°C	21	12.2	0.583	0.295

Table E-48: Summary of single factor ANOVA results comparing Pseudo-Nitzchia microscopy cell concentrations at different atmospheric temperatures with no light and ocean temperature of -1.8℃

Source of Variation	SS	df	MS	F	P-value	F crit
Between Groups	0.567	2	0.283	0.522	0.596	3.15
Within Groups	32.5	60	0.542			
Total	33.1	62				

Table E-49: Summary of statistics used in single factor ANOVA comparing Pseudo-Nitzchia microscopy cell concentrations at different atmospheric temperatures with light and ocean temperature of -1.8℃.

Groups	Count	Sum	Average	Variance
-5°C	21	18.2	0.866	2.70
-10°C	21	23.7	1.13	2.89
-15°C	21	29.1	1.39	4.98

Table E-50: Summary of single factor ANOVA results comparing Pseudo-Nitzchia microscopy cell concentrations at different atmospheric temperatures with light and ocean temperature of -1.8℃

Source of Variation	SS	df	MS	F	P-value	F crit
Between Groups	2.86	2	1.43	0.406	0.668	3.15
Within Groups	211	60	3.52			
Total	214	62				

Table E-51: Summary of statistics used in single factor ANOVA comparing Pseudo-Nitzchia microscopy cell concentrations at different atmospheric temperatures with light and ocean temperature of 0℃.

Groups	Count	Sum	Average	Variance
-5°C	21	45.9	2.19	16.9
-10°C	21	28.6	1.36	7.24
-15°C	21	20.6	0.982	5.68

Table E-52: Summary of single factor ANOVA results comparing Pseudo-Nitzchia microscopy cell concentrations at different atmospheric temperatures with light and ocean temperature of 0℃.

Source of Variation	SS	df	MS	F	P-value	F crit
Between Groups	15.9	2	7.95	0.800	0.454	3.15
Within Groups	596	60	9.94			
Total	612	62				

Table E-53: Summary of statistics used in single factor ANOVA comparing flow cytometry cell concentrations at different light conditions during the cold finger procedure.

Groups	Count	Sum	Average	Variance
No light	63	15.8	0.251	0.065
Light	63	15.6	0.248	0.201

Table E-54: Summary of single factor ANOVA results comparing flow cytometry cell concentrations at different light conditions during the cold finger procedure.

Source of Variation	SS	df	MS	F	P-value	F crit
Between Groups	0.000333	1	0.000333	0.00250	0.960	3.92
Within Groups	16.5	124	0.133			
Total	16.5	125				

Table E-55: Summary of statistics used in single factor ANOVA comparing Cocconeis microscopy cell concentrations at different light conditions during the cold finger procedure.

Groups	Count	Sum	Average	Variance
No light	63	40.2	0.637	0.162
Light	63	49.8	0.791	0.403

Table E-56: Summary of single factor ANOVA results comparing Cocconeis microscopy cell concentrations at different light conditions during the cold finger procedure.

Source of Variation	SS	df	MS	F	P-value	F crit
Between Groups	0.745	1	0.745	2.64	0.107	3.92
Within Groups	35.0	124	0.282			
Total	35.7	125				

Table E-57: Summary of statistics used in single factor ANOVA comparing Pseudo-Nitzchia microscopy cell concentrations at different light conditions during the cold finger procedure.

Groups	Count	Sum	Average	Variance
No light	63	33.5	0.532	0.534
Light	63	71.0	1.13	3.46

Table E-58: Summary of single factor ANOVA results comparing Pseudo-Nitzchia microscopy cell concentrations at different light conditions during the cold finger procedure.

Source of Variation	SS	df	MS	F	P-value	F crit
Between Groups	11.1	1	11.1	5.59	0.0197	3.92
Within Groups	247	124	2			
Total	259	125				

Table E-59: Summary of statistics used in single factor ANOVA comparing flow cytometry cell concentrations at different ocean temperatures during the cold finger procedure.

Groups	Count	Sum	Average	Variance
-1.8°C	63	15.6	0.248	0.201
0°C	63	28.7	0.455	0.914

Table E-60: Summary of single factor ANOVA results comparing flow cytometry cell concentrations at different ocean temperatures during the cold finger procedure.

Source of Variation	SS	df	MS	F	P-value	F crit
Between Groups	1.36	1	1.36	2.44	0.121	3.92
Within Groups	69.1	124	0.557			
Total	70.5	125				

Table E-61: Summary of single factor ANOVA results comparing Cocconeis microscopy cell concentrations at different ocean temperatures during the cold finger procedure.

Source of Variation	SS	df	MS	F	P-value	F crit
Between Groups	0.157	1	0.157	0.240	0.625	3.92
Within Groups	80.9	124	0.653			
Total	81.1	125				

Table E-62: Summary of statistics used in single factor ANOVA comparing Pseudo-Nitzchia microscopy cell concentrations at different ocean temperatures during the cold finger procedure.

Groups	Count	Sum	Average	Variance
-1.8°C	63	71.0	1.13	3.46
0°C	63	95.1	1.51	9.87

Table E-63: Summary of single factor ANOVA results comparing Pseudo-Nitzchia microscopy cell concentrations at different ocean temperatures during the cold finger procedure.

Source of Variation	SS	df	MS	F	P-value	F crit
Between Groups	4.62	1	4.62	0.693	0.407	3.92
Within Groups	826	124	6.66			
Total	831	125				

Table E-64: Summary of statistics used in single factor ANOVA comparing flow cytometry cell concentrations at different horizontal positions during the cold finger procedure.

Groups	Count	Sum	Average	Variance
H1	27	1.92	0.0711	0.00252
H2	27	2.99	0.111	0.00467
H3	27	4.1	0.152	0.00507

Table E-65: Summary of single factor ANOVA results comparing flow cytometry cell concentrations at different horizontal positions during the cold finger procedure.

Source of Variation	SS	df	MS	F	P-value	F crit
Between Groups	0.0881	2	0.0440	10.8	7.39E-05	3.11
Within Groups	0.319	78	0.00409			
Total	0.407	80				

Table E-66: Summary of statistics used in single factor ANOVA comparing Cocconeis microscopy cell concentrations at different horizontal positions during the cold finger procedure.

Groups	Count	Sum	Average	Variance
H1	27	10.4	0.385	0.0272
H2	27	12.7	0.469	0.0285
H3	27	14.9	0.55	0.0223

Table E-67: Summary of single factor ANOVA results comparing Cocconeis microscopy cell concentrations at different horizontal positions during the cold finger procedure.

Source of Variation	SS	df	MS	F	P-value	F crit
Between Groups	0.369	2	0.184	7.10	0.00147	3.11
Within Groups	2.03	78	0.026			
Total	2.39	80				

Table E-68: Summary of statistics used in single factor ANOVA comparing Pseudo-Nitzchia microscopy cell concentrations at different horizontal positions during the cold finger procedure.

Groups	Count	Sum	Average	Variance
H1	27	12.7	0.471	0.495
H2	27	8.96	0.332	0.0680
H3	27	9.04	0.335	0.0320

Table E-69: Summary of single factor ANOVA results comparing Pseudo-Nitzchia microscopy cell concentrations at different horizontal positions during the cold finger procedure.

Source of Variation	SS	df	MS	F	P-value	F crit
Between Groups	0.34	2	0.170	0.858	0.428	3.11
Within Groups	15.4	78	0.198			
Total	15.8	80				

Table E-70: Summary of statistics used in single factor ANOVA comparing flow cytometry cell concentrations at different vertical positions during the cold finger procedure.

Groups	Count	Sum	Average	Variance
V1	27	2.7	0.0999	0.00390
V2	27	2.56	0.0950	0.00442
V3	27	2.75	0.101	0.00567

Table E-71: Summary of single factor ANOVA results comparing flow cytometry cell concentrations at different vertical positions during the cold finger procedure.

Source of Variation	SS	df	MS	F	P-value	F crit
Between Groups	0.000660	2	0.00033	0.0710	0.932	3.11
Within Groups	0.364	78	0.00466			
Total	0.365	80				

Table E-72: Summary of statistics used in single factor ANOVA comparing Cocconeis microscopy cell concentrations at different vertical positions during the cold finger procedure.

Groups	Count	Sum	Average	Variance
V1	27	12.0	0.443	0.0280
V2	27	13.2	0.487	0.0398
V3	27	11.7	0.432	0.0111

Table E-73: Summary of single factor ANOVA results comparing Cocconeis microscopy cell concentrations at different vertical positions during the cold finger procedure.

Source of Variation	SS	df	MS	F	P-value	F crit
Between Groups	0.0463	2	0.0231	0.881	0.419	3.11
Within Groups	2.05	78	0.0263			
Total	2.1	80				

Table E-74: Summary of statistics used in single factor ANOVA comparing Pseudo-Nitzchia microscopy cell concentrations at different vertical positions during the cold finger procedure.

Groups	Count	Sum	Average	Variance
V1	27	6.68	0.248	0.0177
V2	27	8.67	0.321	0.0348
V3	27	6.34	0.235	0.0140

Table E-75: Summary of single factor ANOVA results comparing Pseudo-Nitzchia microscopy cell concentrations at different vertical positions during the cold finger procedure.

Source of Variation	SS	df	MS	F	P-value	F crit
Between Groups	0.117	2	0.0585	2.63	0.0781	3.11
Within Groups	1.73	78	0.0222			
Total	1.85	80				

F. Ethics Clearance

UNIVERSITY OF CAPE TOWN
IYUNIVESITHI YASEKAPA · UNIVERSITEIT VAN KAAPSTAD

PRE-SCREENING QUESTIONNAIRE OUTCOME LETTER

STU-EBE-2023-PSQ000376

2023/08/30

Dear James Van Niekerk,

Your Ethics pre-screening questionnaire (PSQ) has been evaluated by your departmental ethics representative. Based on the information supplied in your PSQ, it has been determined that you do not need to make a full ethics application for the research project in question.

You may proceed with your research project titled:

Investigation of the Interactions Between Sea Ice Algae from the Marginal Ice Zone of Antarctica and Artificial Sea Ice.

Please note that should aspect(s) of your current project change, you should submit a new PSQ in order to determine whether the changed aspects increase the ethical risks of your project. It may be the case that project changes could require a full ethics application and review process.

Regards,

Faculty Research Ethics Committee